ISBN - 978-989-35197-4-5
Volume 2 - Issue 1 - 2026

TRANSLATIONAL CHEMISTRY

AN INTERFACE JOURNAL

PROTEOMASS SCIENTIFIC SOCIETY

Translational Chemistry
An Interface Journal

EDITORIAL BOARD

TRANSLATIONAL CHEMISTRY
AN INTERFACE JOURNAL
HTTPS://WWW.TRANSLATIONALCHEMISTRY.COM/

EDITORIAL BOARD | DOI: 10.5584/translationalchemistry.v1i2.254

TRANSLATIONAL CHEMISTRY

AN INTERFACE JOURNAL

Associated Editors

EDITORIAL

TRANSLATIONAL CHEMISTRY
AN INTERFACE JOURNAL
HTTPS://WWW.TRANSLATIONALCHEMISTRY.COM/

EDITORIAL | DOI: 10.5584/translationalchemistry.v2i1.255

Let There Be Light: Chemical Signatures and Translational Impact. Illuminating Translational Chemistry

Carlos Lodeiro[1,2], Laura Mercolini[3], José Luis Capelo[1,2]

[1]BIOSCOPE Research Group, LAQV-REQUIMTE, Chemistry Department, NOVA School of Science and Technology, Universidade NOVA de Lisboa, 2829-516 Caparica, Portugal. [2]PROTEOMASS Scientific Society, 2825-466, Costa de Caparica, Portugal. [3]Research group of Pharmaco-Toxicological Analysis (PTA Lab), Department of Pharmacy and Biotechnology (FaBiT), Alma Mater Studiorum –University of Bologna, Via Belmeloro 6, 40126 Bologna, Italy Portugal.

Received: January 2025 **Accepted:** January 2025 **Available Online**: January 2025

Chemistry has always had a singular vocation: to make the invisible visible. Among all the languages it employs, light holds a privileged place - not only as a tool for observation, but as a rigorous metaphor for the scientific process itself. Light is both messenger and method: it carries information, reveals structure, measures energy, exposes impurities, and confirms identities. And when chemistry becomes translational, light also becomes a bridge, linking a fundamental understanding of the universe around us to the solutions we implement in the real world. This First Issue in 2026 of Translational Chemistry is born from that conviction: translation is not an 'after' of science; it is a way of organizing it. To translate means to convert principles into decisions, mechanisms into measurements, signatures into diagnoses, reactivity into technology, and knowledge into benefit.

At the heart of chemistry lies the dynamics of electrons, and light is often the most direct route to interact with them. When a molecule absorbs a photon, it changes state; when it emits, it returns energy; when it scatters, it reveals order, bonds, symmetry, and heterogeneity. From this grammar comes an extraordinary capacity: to read signatures - spectral lines, vibrational bands, Raman patterns, fluorescence, chemiluminescence - and to turn those signatures into useful variables. A well-measured signature becomes a trustworthy number; a trustworthy number becomes a test; a test becomes a procedure; and a procedure, when robust and accessible, becomes impact.

Light connects the very distant to the very near: the composition of stars, interstellar clouds, and planetary atmospheres is inferred because atoms and molecules leave unmistakable optical fingerprints; Earth's atmosphere is monitored through the absorption and emission of trace gases; life itself uses pigments and cofactors as natural photonic devices. The 'universe around us' includes a nebula and a drop of urine, a surface-water sample and a tumor tissue - and in all these cases, light can be a privileged path for translating chemistry into actionable information.

That is also why the image of a 'spark' - an instant when energy and matter meet - remains so powerful for thinking about the origin and translation of chemical knowledge. Modern science studies, for example, how bursts of energy (light, electrical discharges, radiation, thermal gradients) can drive out-of-equilibrium chemistry and generate complexity: a 'flash' that is not myth, but a way of describing fast and decisive events in reaction networks. In the laboratory, synthetic chemistry has increasingly recreated plausible prebiotic scenarios and built minimal systems capable of generating or amplifying organization - not because life 'begins' in a single blaze, but because certain energetic regimes, however brief, can open reaction pathways and select products. In this view, light is no longer only what we observe: under certain conditions, it is also what makes things happen.

At a different scale, but with the same fascination, sonoluminescence reminds us that energy can be concentrated in extreme ways within a microscopic volume and manifest as light emission: a bubble collapses, a pulse emerges, a signal appears where we did not expect to 'see' light. The point is not to force simplistic parallels with cosmology; it is to recognize a common and profoundly chemical principle: local conditions can create excited states, generate reactive species, produce optical signatures, and convert energy into measurable information. In that sense, sonoluminescence functions as an echo - not literal, but conceptual - of the great questions about the origin of the universe: how energy organizes, how matter emerges in distinguishable states, and how physical information becomes inscribed in signals we can detect.

Translational chemistry thrives precisely here: in the ability to harness these principles and convert them into tools, from sensors and diagnostics to functional materials and sustainable processes.

It is at this point that an ancient cultural formulation - 'let there be light' - unexpectedly becomes a fertile editorial frame. Not as a scientific explanation, but as a metaphor that spans centuries: light as beginning, as revelation, as the separation between what is indis-

tinct and what is measurable. Science does not replace the symbolic dimension; it dialogues with it by offering an operational language: Light → Signature → Interpretation → Decision/Intervention. Light is the interaction (absorption, emission, scattering) or the energy that triggers reaction; the signature is the measured signal; interpretation is the model that turns signal into concentration, structure, chemical state, phenotype, or risk; and decision/intervention is the destination of knowledge - diagnosis, environmental control, process optimization, therapeutic action, functional materials.

This translational line - from photon to impact - defines the spirit of this second year of Translational Chemistry: An interface Journal, and specially its firts Issue.

The thematic spectrum is broad, yet coherent. In health, we welcome optical and spectrometric methodologies applied to biomarkers and the exposome, rapid assays based on fluorescence or chemiluminescence, vibrational spectroscopies (IR/Raman) for screening and stratification, chemical imaging, and validation strategies in biofluids and tissues. In environment and safety, we invite portable platforms and sensors for emerging pollutants, screening approaches with analytical confirmation, solutions for sample pretreatment and interference mitigation, and integration with risk assessment. In energy and materials, we are interested in photocatalysis, energy conversion, green processes, and molecular design guided by optical properties. We also value contributions that explore fundamental mechanisms underpinning applications - fast dynamics, excited states, reactivity under locally intense conditions - because translationality here lies in explaining the 'why' that enables the 'how'. Increasingly, we also emphasize the critical step that often determines the fate of a technology: moving from signature to meaning, where chemometrics, machine learning, mechanistic and hybrid models, cross-validation, and generalization across instruments and laboratories become essential.

This Issue is, above all, an invitation to think of chemistry as a discipline that both discovers and translates. Light - as tool, as phenomenon, as symbol - helps us bring physical chemistry, analytical chemistry, biochemistry, materials science, environmental science, engineering, and data into a shared narrative. By assembling diverse contributions under this guiding thread, we hope to stimulate unlikely dialogues and productive collaborations.

To authors, we ask for work that brings novelty, but also structure: clear hypotheses, reproducible methods, solid validation, and a narrative that explains not only what works, but why it works and what it is for.

To reviewers and readers, we thank you for sustaining the standard that makes science truly translational: the commitment to rigor, clarity, and usefulness. May this Issue contribute to a chemistry that illuminates - in the literal and the broadest sense - the universe around us, from questions of origins to the solutions the present requires.

REVIEW ARTICLE

TRANSLATIONAL CHEMISTRY
AN INTERFACE JOURNAL
HTTPS://WWW.TRANSLATIONALCHEMISTRY.COM/

REVIEW ARTICLE | DOI: 10.5584/translationalchemistry.v2i1.252

Synthetic Cathinones: Analytical Strategies, Pitfalls and Priorities for Forensic and Clinical Toxicology

Michele Protti[1], Chiara Pia Iattoni[1], Roberto Mandrioli[2], Laura Mercolini[1]

[1]Research group of Pharmaco-Toxicological Analysis (PTA Lab), Department of Pharmacy and Biotechnology (FaBiT), Alma Mater Studiorum – University of Bologna, Via Belmeloro 6, 40126 Bologna, Italy. [2]Department of Pharmacy and Biotechnology (FaBiT), Alma Mater Studiorum – University of Bologna, Corso d'Augusto 237, Rimini, Italy.

Received: December 2025 **Accepted:** January 2026 **Available Online**: January 2026

Abstract

Synthetic cathinones are β-keto analogues within the broader class of β-phenethylamine amphetamine-type stimulants and represent a persistent analytical challenge due to their structural variability and rapid analogue turnover. Their frequent misrepresentation as other stimulants, together with the limited clinical and toxicological data available for many compounds, complicate both interpretation and risk assessment. This review examines the pharmaco-toxicological context of synthetic cathinones, with a primary focus on analytical strategies for their detection and interpretation in clinical and forensic settings. Methodological considerations are discussed across blood/plasma, urine, oral fluid and hair, highlighting the strengths and limitations of current screening, confirmatory and quantitative approaches. Attention is given to issues affecting analytical reliability, including compound instability, matrix effects, availability of reference materials and the impact of evolving sampling and microsampling formats on specimen handling. Emphasis is also placed on the interpretive integration of analytical data with patterns of use and potential co-exposures. Overall, this paper aims to bridge analytical methodology and translational application, supporting robust and adaptable testing practices in response to changing stimulant profiles.

Keywords: Cathinone analogues, Liquid chromatography, High-resolution mass spectrometry, Metabolism-based markers, Microsampling, Stability.

1. Introduction

Over the past fifteen years, synthetic cathinones (β-keto analogues of amphetamine-type stimulants, ATS) have become a defining challenge for forensic and clinical toxicology. Their market dynamics are characterised by rapid analogue turnover after scheduling actions, regional heterogeneity in what is circulating at any given time and misrepresentation (*i.e.*, products sold or consumed as 'classic' stimulants that contain distinct cathinone analogues) [1-5]. This situation strains routine testing procedures and creates coverage gaps between what laboratories monitor and what is actually present in casework, emergency department samples, post-mortem specimens and population indicators such as wastewater-based epidemiology (WBE) data [6]. A suitable response could be based on three pillars. First, HRMS-based suspect screening (triage-level matching against curated suspect lists, with defined confidence tiers) can expand scope and allow retrospective mining as new analogues appear [7,8]; second, shared criteria for reporting-grade LC-MS/MS confirmation can help solve isomer-related ambiguities and include metabolite targeting, especially in urine [9]; third, matrix-aware pre-analytical steps (sampling, storage, sample treatment) are critical to analysis success, also because β-keto stability tends to be analogue- and matrix-specific and can bias quantitative and even qualitative outcomes if unmanaged [10,11]. The scientific rationale behind this strategy is clear: relatively small structural changes (ring substitutions, side-chain homologation, amine cyclisation) preserve stimulant pharmacology while changing chromatographic retention behaviour, MS fragmentation and metabolic patterns, thereby invalidating common routine conditions when reused uncritically [12-14]. Complementing clinical and casework evidence, WBE and event-focused investigations can help identify the analogues that will later dominate analytical findings, making them valuable foresight tools for suspect lists and library updates [15-17].

This review outlines a practice-oriented approach, organised around: chemical space with analytical consequences; screening and confirmation strategies that can be applied to tackle changes in illicit market compound availability; matrix-specific approaches to solve identification/quantitation problems and to mitigate analyti-

***Corresponding author:** Laura Mercolini, laura.mercolini@unibo.it

cal pitfalls. Throughout, we highlight open questions that remain critical for analytical success, such as immunoassay cross-reactivity, cut-off transfer across matrices (liquid / dried blood; blood / urine / oral fluid), reference material availability and clinical correlations for new analogues. This review is primarily written for routine and reference analysis laboratories operating in forensic and clinical toxicology. The decision frameworks are also applicable to public health and research laboratories involved in early-warning activities and population indicators (*e.g.*, WBE), where analytical governance and menu refresh are critical.

2. Chemical space and its analytical importance

Cathinone analogues represent a relatively large group of structurally closely related compounds and isomers sharing the β-keto phenethylamine scaffold. For analytical method developers and toxicologists, the most important subgroups are:

- **Pyrrolidinophenones** (*e.g.*, MDPV, α-PVP, MDPHP, α-PBP, α-PHP, α-PiHP, 5-PPDi, α-PCyP, 3,4-EtPV, α-PVT, **Figure 1a – 1j**).

These tend to be potent and rich in isomers, with lots of near-isobaric compounds and fragments, and in-source artefacts; their analysis relies largely on accurate-mass MS and metabolite confirmation in urine, but could also benefit from the orthogonality of GC-EI fingerprints and chiral LC to confirm identification in difficult cases [7,18-29].

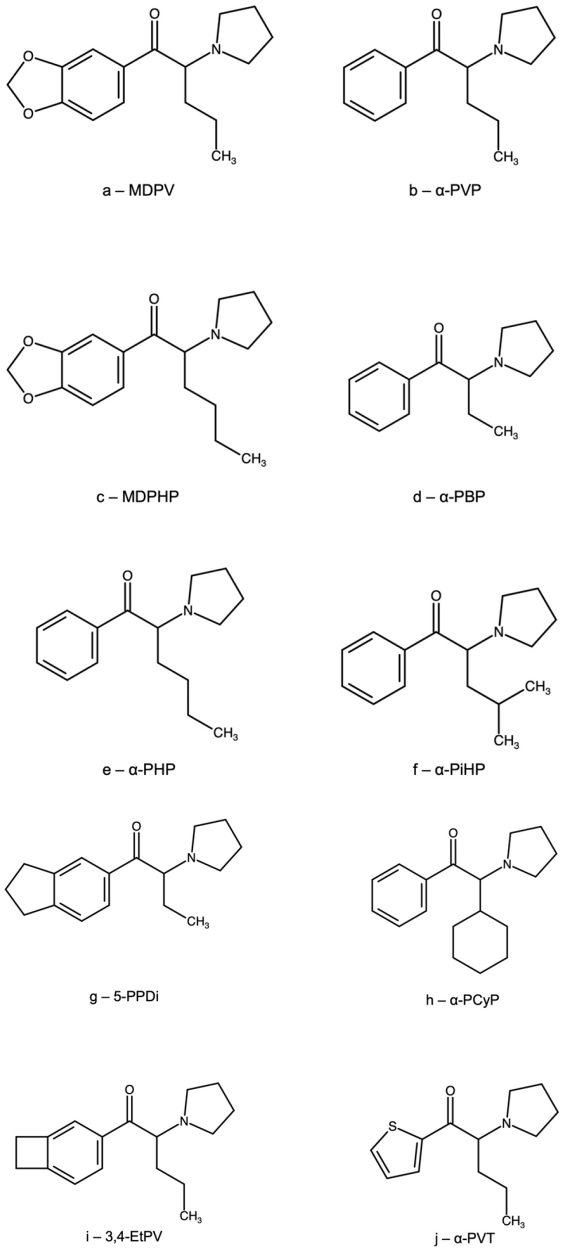

Figure 1 (1a - 1j) | Chemical structures of 10 representative pyrrolidinophenone cathinones.

Minimum ID Criteria

LC–MS/MS: two or more MRM transitions (quantifier + qualifier) with ion-ratio tolerance ≤20% absolute; RT window ≤±0.1–0.15 min vs calibrators; IS co-elution if labelled standard available [30-34]. HRMS: exact mass tolerance (*e.g.*, ≤5 ppm) on precursor + two or more diagnostic product ion; isotope fit within method bounds [7,35-39]. Urine metabolite co-evidence (recommended default for α-PVP/α-PHP families): include at least one phase-I metabolite established by hepatocytes/HRMS or case series; accept metabolite-only positives as screening-level, mandating HRMS re-interrogation for parent compounds [23,25,40-49]. Orthogonality triggers: Borderline ion ratios or co-eluting interferences → GC-EI spectrum with retention index match [9].

Positional/side-chain isomer ambiguity at reportable levels → GC-FTIR (solid-deposition if needed) or chiral LC when evidentiary defensibility is required [11,40,50-52]. An example of FTIR application is reported in **Figure 2**.

- **Methcathinones** (*e.g.*, 3-CMC/4-CMC; 2/3/4-MMC, 4-BMC, **Figure 3a - 3f**).

Positional isomerism is the main problem; coupling LC-(HR)MS retention orthogonality with diagnostic MS/MS fragments is the accepted best practice, with solid-deposition GC-FTIR providing additional information when necessary (*post-mortem*; contested forensic interpretation) [9,24,35,37,53–58].

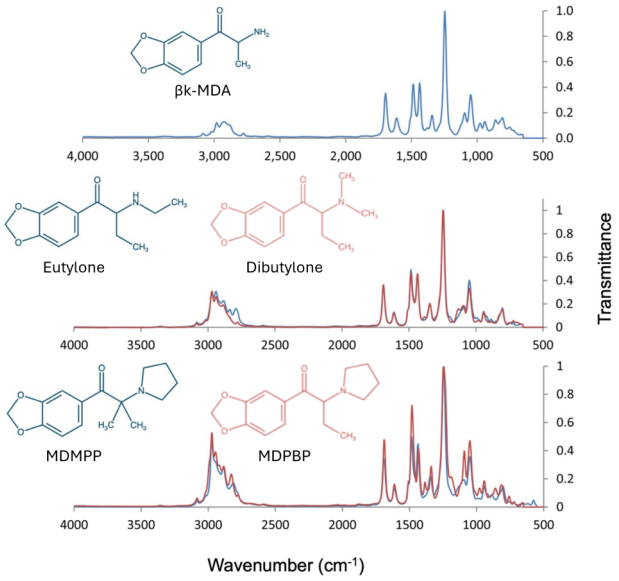

Figure 2 | FTIR spectra of some representative cathinone derivatives. Adapted with permission [17].

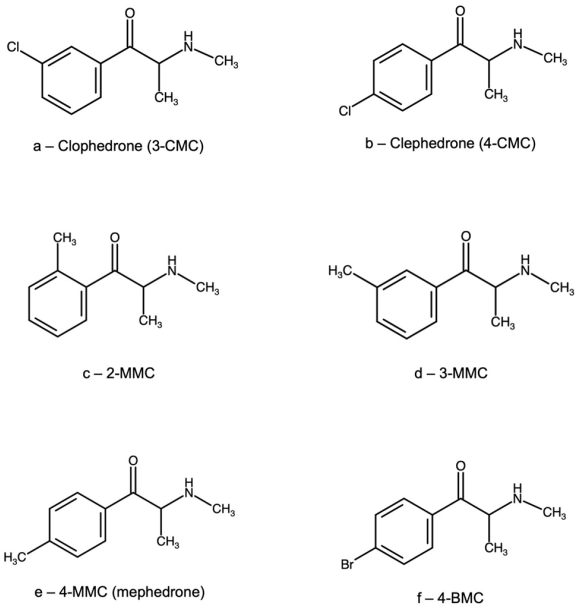

Figure 3 (3a - 3f) | Chemical structures of 6 representative methcathinones.

Minimum ID Criteria

Tight RT separation (optimise stationary phase and gradient) + two or more diagnostic transitions; where ΔRT <0.05-0.08 min, do not report without orthogonal evidence [30-34]. HRMS diagnostic product ions and fragment ratio patterns documented in method files for each positional isomer [7,35–38]. Orthogonality triggers (practically mandatory in contentious contexts): GC-FTIR with reference library for MMC/CMC resolution (document solid-deposition parameters if used) [15,37,55,57,67]. Chiral LC is optional if jurisdiction or question requires stereochemical assignment [34, 59-62].

- **N-ethylated derivatives** (*e.g.*, *N*-ethylhexedrone, NEH; *N*-ethylpentedrone, NEP, **Figure 4a - 4b**). Parent detectability can be limited; selected metabolites identified in hepatocytes/microsomes or controlled studies should be integrated into routine analytical panels to increase detection rates [8,14,39,40,46,48,53,57,63].

Minimum ID Criteria

Parent + metabolite confirmation preferred; where parent is absent, two complementary metabolites (distinct biotransformation routes) may justify confirmation if method validation anticipates this logic [31-34,59-61,64-66]. HRMS suspect tiers include metabolite formulas; store raw data for retrospective queries [7,35-39]. Orthogonality triggers: Any discordance between expected and actual metabolite pattern → targeted HRMS library matching; if still ambiguous, seek GC-EI on parent in fortified extracts for structural corroboration [15,32-39,46].

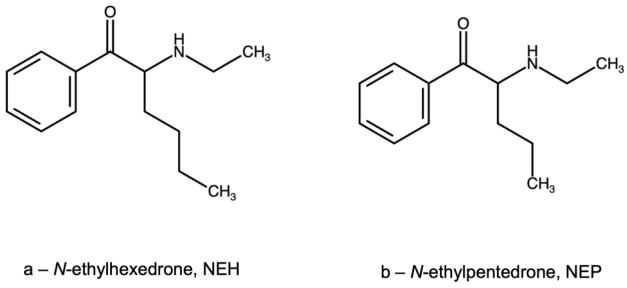

a – *N*-ethylhexedrone, NEH

b – *N*-ethylpentedrone, NEP

Figure 4 (4a - 4b) | Chemical structures of representative *N*-ethylated cathinones.

- **'One-Series' / newer homologues** (*e.g.*, eutylone, dipentylone, 4-MPD, 4-MEAP, 3,4-Pr-PipVP, **Figure 5a - 5e**). Minor side-chain modifications can produce significant chromatographic retention and fragment intensity ratio changes. For these reasons, frequent HRMS library and method updates must be applied, as well as metabolite inclusion where available [8,60,65-72].

Minimum ID Criteria

Refresh transitions and RT windows upon first WBE or casework signal; lock in diagnostic HRMS fragments in library before routine reporting [6,7,35-38]. Include at least one metabolite if available to confirm identifications in urine [32-34,49,59,60,62,64,66]. Orthogonality triggers: First 10-20 authentic positives post-onboarding → random GC-EI verification and second-operator HRMS review to qualify the menu update (documented in change-control log) [6,15,17, 35-37].

3. Screening and confirmation strategies

3.1. Screening

Immunoassays offer throughput and triage value but show uneven cross-reactivity across positional/side-chain isomers; negative immunoassays must not overrule clinical/investigative context [73-77]. This is particularly relevant when case history, setting (*e.g.*, nightlife/festival), or WBE intelligence suggest a newly rotated analogue. Modern screening workflows thus prioritise broad-scope MS-based screening (triage-level detection):

- HRMS (QTOF/Orbitrap) used for suspect screening with defined confidence tiers enables with suspect tiers enables retrospective mining when early-warning systems or seizures flag newcomers [16,35,36,78].
- Ion-mobility MS (when available) adds a gas-phase separation dimension that can reduce false positives/negatives for near-isomers at low levels [79].
- Matrix-tailored rapid MS (*e.g.*, multi-residue LC-MS for blood; CE-HRMS for urine) keeps throughput high while preserving essential selectivity [39].

Population indicators (WBE; pooled venue urinals; venue oral-fluid swabs) consistently anticipate analogue shifts, informing which suspects to add next and where to tighten ID criteria [17, 80-84]. In practice, labs that formally feed WBE and seizure intelligence into quarterly suspect refreshes report fewer surprise gaps downstream.

3.2. Confirmation

For reportable identifications (confirmation), targeted LC–MS/MS is foundational, provided that identification criteria (co-elution with IS; ion ratios within tolerance; S/N thresholds) are followed

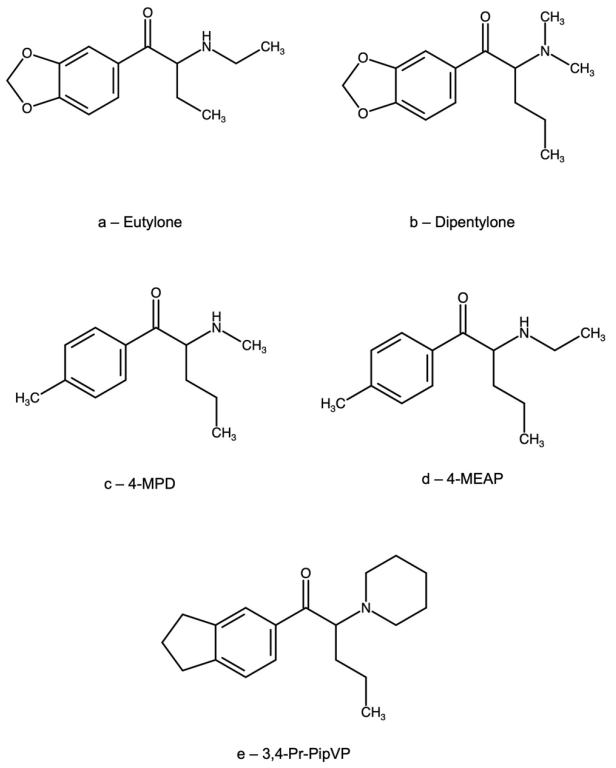

Figure 5 (5a - 5e) | Chemical structures of 5 representative 'one-series' and newer cathinones.

and library panels are renewed to reflect illicit market innovation [30,33,35,85]. When extreme selectivity is needed (positional isomers; near-isobars; low-level co-exposure), orthogonal evidence should be applied:

- GC-MS (EI) and GC-FTIR provide structural fingerprints and retention indexing; solid-deposition GC-FTIR markedly improves spectral quality and has proven decisive for MMC/CMC isomer resolution [9,16,86,87].
- Accurate-mass MS confirmation (exact mass + diagnostic product ions) resolves isomer-dense families and, importantly, allows retrospective re-interrogation of stored files when suspect lists change [57,88,89].
- Chiral LC is warranted for enantioselective questions and when evidentiary defensibility demands stereochemical resolution (selected ATS/cathinones) [51,61,62,90,91].

3.3. Metabolite-linked confirmation

Urine confirmations that include diagnostic metabolites substantially extend detection windows and increase specificity (*e.g.*, NEH/NEP; α-PVP; 3-CMC), reducing the risk of false negatives when parent compounds are unstable or poorly excreted [23,24,49,60,66,92,93]. Where metabolite hierarchies remain unsettled, method architecture should be modular (easy addition of new MRM transitions and cut-offs with limited re-validation), and suspect tiers in HRMS should be curated explicitly for new metabolites arising from hepatocyte and microsome models [25,55,94-96].

4. Matrix-specific approaches

4.1. Blood/plasma: strong and weak points

Strengths

Blood and plasma provide proximity to the effect site and are integral to clinical interpretation, pharmacokinetics, and evidentiary timelines. Validated LC-MS/MS methods demonstrate selective quantification with matrix-effect characterisation, carry-over control and well-defined ion-ratio tolerances [57,60,65,66]. When analogue density or low concentration challenges selectivity, accurate-mass confirmation and orthogonal EI/retention-index evidence enhance identifications [92,97,98].

Weaknesses

For β-keto stimulants, stability is not a class constant. Benchtop time, pH, temperature, preservatives (*e.g.*, NaF) and freeze-thaw cycles can compromise analyte integrity; re-injection windows matter (carry-over; adsorption; degradation) [10,66,71,99]. Parent levels can be transient, while conjugation/redistribution and post-collection metabolism continue in sub-optimally handled specimens.

Policy implication

Pre-analytical steps should be well-described and rigorously respected in SOPs, with the following critical points: (i) immediate cooling and pH control where indicated; (ii) limited benchtop-time; (iii) documented freeze-thaw behaviour; (iv) short, justified re-injection windows; and (v) mandatory QC acceptance rules that

discard batches showing drift in IS response consistent with instability. When parent decay is plausible, consider urine metabolite evaluation as a possible confirmation strategy.

4.2. Miniaturised dried blood matrices (DBS/VAMS) for cathinones

Dried formats shorten liquid residence time, potentially improving stability for labile cathinones, and simplify shipment/logistics (ambient shipping; reduced biohazard footprint) [51,57,60,100-103]. They can be especially helpful when serial sampling or field collection is required (*e.g.*, clinical toxicology in non-hospital settings; public health surveillance).

What to validate

- Device-specific calibration (do not borrow calibrations from liquid matrices).
- Extraction efficiency and substrate carry-over; check whether analyte/substrate interactions produces bias in recovery or ionisation.
- Haematocrit effects and spot inhomogeneity (DBS), or volumetric tip fill behaviour (VAMS) with real blood.
- Cut-off translation from liquid to dried matrices must be empirically verified with parallel collections in the same individuals/cases.

Analytical architectures

Methods for dried matrices include UHPLC–HRMS–QTOF for broad new psycoactive substance (NPS) panels and UPLC for targeted cathinone sets; both require recovery-focused validation and carefully designed IS panels [51,57,101]. When the target analogue is suspected to be labile (*e.g.*, α-PVP family), adding urine metabolite confirmation keeps overall case sensitivity high even if dried-blood parent is near LOQ.

4.3. Urine

Urine affords longer detection windows and generally higher concentrations of diagnostic metabolites, providing redundant axes when parent cathinones are unstable, transient, or weakly excreted (**Figure 6**).

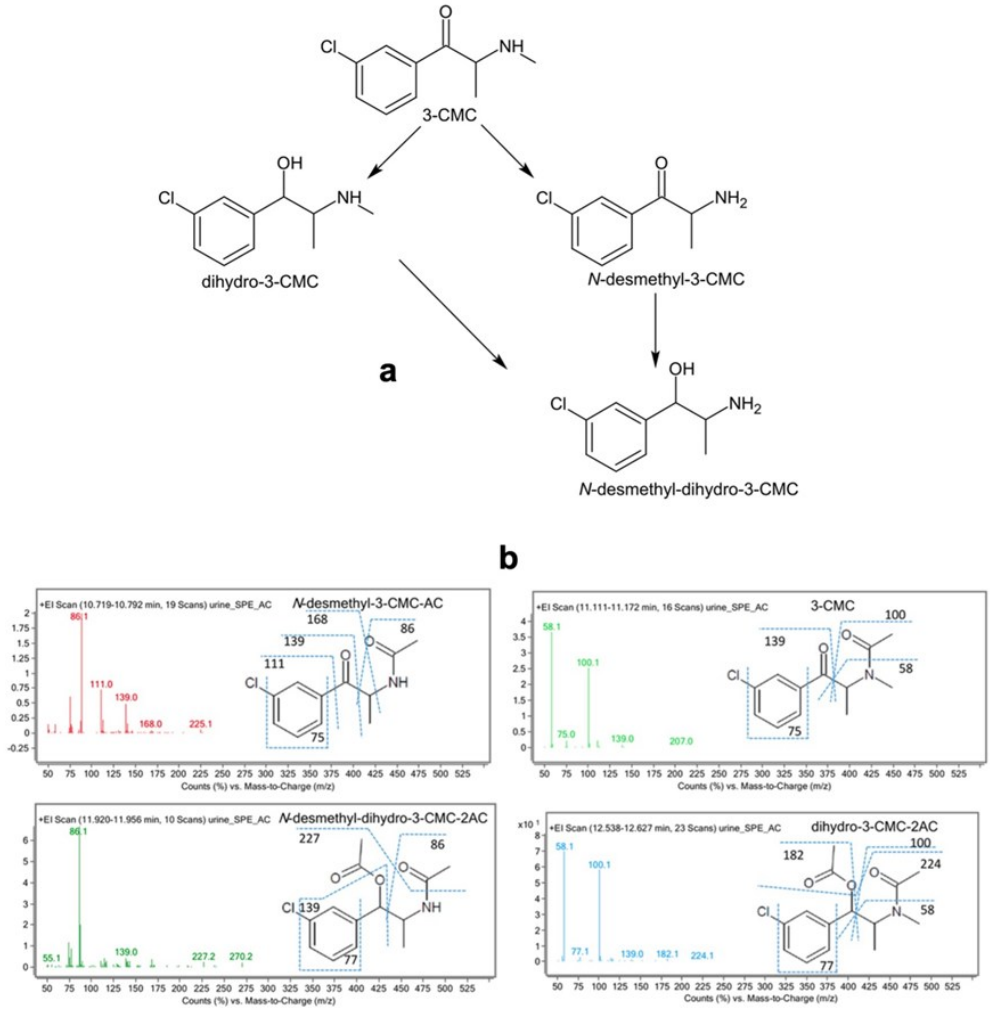

Figure 6 | (a) Proposed metabolism of 3-CMC and (b) experimental mass spectra of the acetyl derivatives of 3-CMC and its metabolites (acetylation was carried out to make the compounds suitable for GC separation). Adapted with permission [118].

For multiple families (*e.g.*, NEH/NEP, α-PVP/α-PHP, 3-CMC/4-CMC), determination of the parent drug plus at least one metabolite markedly increases specificity and practical sensitivity in real-world cases [32,44,46,49,77,100,104-106]. When blood/plasma show borderline parent levels or re-injection issues, a metabolite-linked urine confirmation increases the accuracy of case interpretation [63]. Actionable rule: for families with poor or variable parent excretion, reportable confirmation requires co-evidence of either parent + metabolite or two complementary metabolites with appropriate ion-ratio and retention windows.

4.3.1. Pre-analytical stability in urine

β-keto stability in urine depends on pH, temperature, preservatives and storage time. Conjugation/redistribution can shift profiles during storage. Several studies demonstrate compound-specific degradation and significant benefit from pH control and cold chain, including the use of NaF when justified by validation [47,66]. Re-injection windows and autosampler conditions also matter (carry-over; adsorption; hydrolysis). Suggested SOPs:

- Collection/Preservation: immediate cooling; pH documentation; add NaF if validated to slow degradation.
- Stability Files: per-analogue stability tables (benchtop, refrigerated, frozen; short- vs long-term; freeze-thaw cycles) referenced in batch plans; fail batch if IS drifts or QC trend suggests degradation.
- Re-injection Policy: specify maximum interval from extraction to analysis; specify autosampler temperature; require QC re-checks after delays.

4.3.2. Urine sample preparation

Urine method architectures span dilute-and-shoot (fast triage), SPE/μSPE, DLLME, PALME/EME and CE–HRMS screening; choice is based on throughput, matrix load and the need for orthogonality [35,42,107,108].

- Dilute-and-shoot LC-MS/MS: maximal throughput, acceptable for targeted sets with robust ion-ratio windows and good IS coverage; best when paired with HRMS suspect screening for scope and GC-FTIR fallback for isomers [16,57,63].
- SPE / μSPE: improved cleanliness/selectivity, compatible with metabolite panels; micro-formats (MIP–μSPE) add selectivity for problem families [45]. An example of advanced material that has been applied to MIP-μSPE for synthetic cathinone analysis in urine is shown in **Figure 7**, together with the corresponding sample preparation procedure.
- DLLME / PALME / EME: green(er) options with strong preconcentration; PALME is attractive for polar targets when coupled to LC-MS/MS [9,65,70].
- CE–HRMS: powerful for broad screening (including anionic metabolites) with high orthogonality; use as screening tier to precede LC-MS/MS confirmations [73].

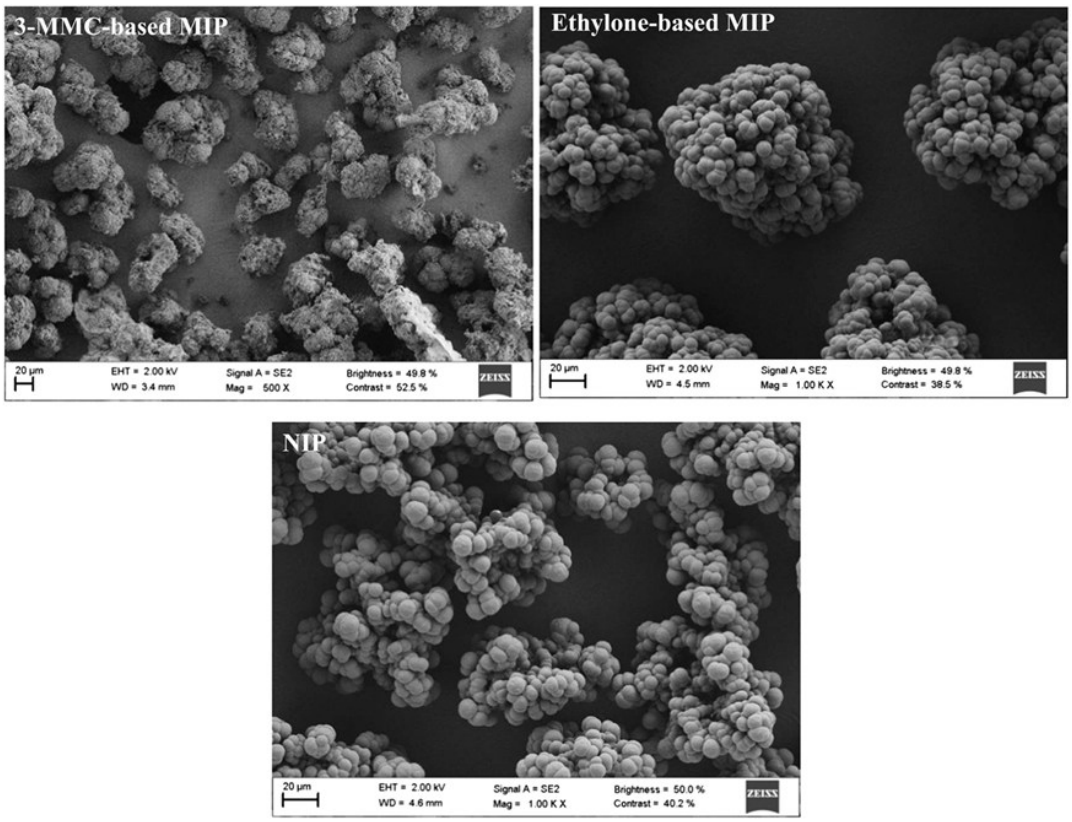

Figure 7 | Scanning electron microscope (SEM) images for, 3-MMC-based MIP, ethylone-based MIP and non-imprinted polymer (NIP). Used with permission [45].

Pragmatic SOP suggestion: use dilute-and-shoot (or µSPE) for daily throughput; route isomeric conflicts to GC-FTIR or HRMS supported by diagnostic fragments; embed metabolites for families with weak parent excretion.

4.4. Oral fluid

Oral fluid collection is overseen, non-invasive, and operationally compatible with rapid LC-MS/MS confirmation, making it valuable for time-proximal stimulant assessment (DUID, venue screening, ED intake) [78]. However, device chemistry, stimulation status, salivary flow, and oral contamination can skew concentrations and must be documented for interpretation [109,110]. SOP datapoints to capture: device brand/lot, stimulated vs unstimulated, collection time relative to alleged use/event, recent oral exposures (smoking, vaping, mouthwash), and internal volume controls where the device provides them [44,74,100].

4.4.1. Oral fluid extraction and screening options

Validated approaches include dilute-and-shoot LC–MS/MS with robust ion-ratio controls, µSPE or QuEChERS-style extractions (micro-QuEChERS shows a strong balance of speed and cleanup), and broad HRMS for non-targeted screening and presumptive identification [111]. Device eluates may contain salts and buffers that impact ionisation; matrix-matched calibration and IS mapping are mandatory.

4.4.2. Reporting and defensibility

- Cut-offs: align with device recovery properties and the lab's validated LLOQ/decision limits; report device brand and any collection-buffer dilution assumptions used in quantitation.
- Isomer issues: for positional isomers detected in oral fluid at low ng/mL, require HRMS diagnostic product ions or route to GC–FTIR confirmation if challenged.
- Contamination control: where recent oral use is suspected, pair with urine metabolite evidence to distinguish contamination from systemic exposure.

4.5. Hair

Hair provides long detection windows and information on patterns of use when segmental analysis is appropriate. It is especially useful for retrospective investigation and for contexts where frequent liquid sampling is impractical [6,22,30,56,112]. As an example, the frequency of NPS detected in postmortem hair samples per year between January 2008 and December 2020 are summarized in **Figure 8**.

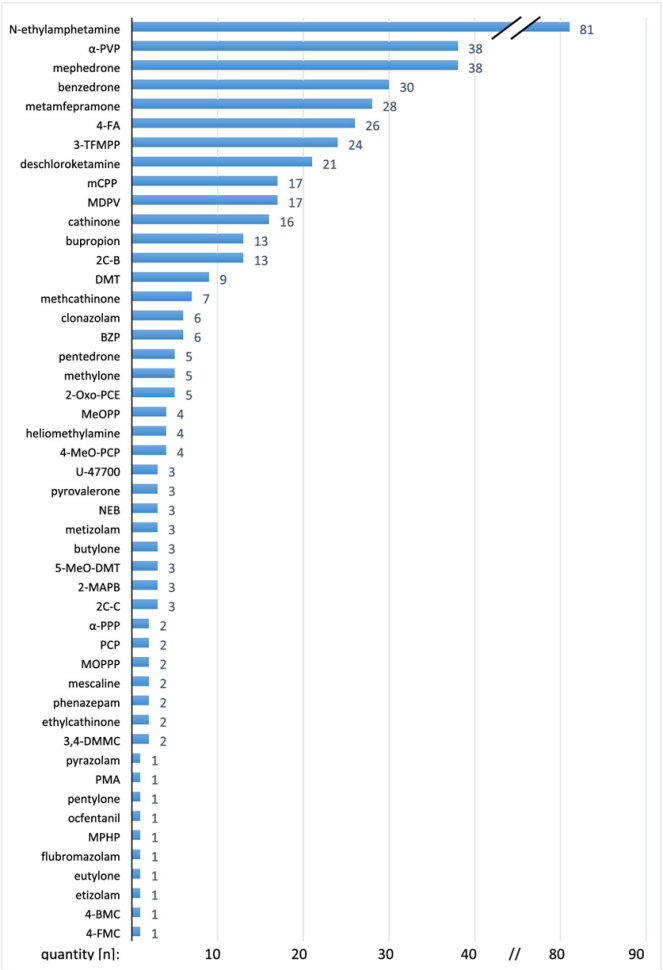

Figure 8 | Total number of detected NPS in postmortem hair samples (January 2008 - December 2020). Used with permission [115].

4.5.1. Challenges and opportunities of hair analysis

External contamination (smoke, powders), cosmetic treatments (bleaching, dyes), and hygiene impact interpretation. The literature converges on:

- Validated decontamination protocols (multi-solvent or aqueous/organic sequences) with procedural blanks [113].
- IS panels and matrix-matched calibrations.
- Segmental analysis guided by growth assumptions but reported conservatively due to inter-individual rate variation.

Key defensibility tactic: whenever parent compounds are detected in hair, seek metabolites in the same segment (where available) to strengthen the case for systemic exposure vs external contamination [114]. If metabolite presence is not supported by known biotransformation or isomeric doubt remains, escalate to GC-MS/TOF or HRMS with diagnostic product ions for structural confidence [115].

4.5.2. Reporting policy

- Decontamination statement (protocol steps, controls) is part of the analytical result.
- Cosmetic history (when available) should be documented in the case record.
- Matrix caveats: clearly separate pattern-of-use inference from dose/intoxication claims; avoid pharmacokinetic over-reach in hair unless supported by controlled studies.

5. Stability, Pre-Analytical Variables, and Degradation Pathways

Stability is one of the defining analytical challenges in the detection of synthetic cathinones. The β-keto substitution that characterises this class influences chemical reactivity across biological matrices, making these compounds more susceptible to degradation than amphetamines. This instability is neither uniform across analogues nor predictable from structural similarity alone. As a result, pre-analytical handling becomes integral to analytical validity, and even well-designed chromatographic and mass-spectrometric protocols can fail if sample integrity is compromised prior to extraction or analysis. Much of the instability observed in cathinones stems from the lability of the β-keto moiety. In aqueous media, this functional group undergoes reduction, hydrolysis, and rearrangement, often at rates that increase dramatically with temperature, pH variation, or prolonged exposure to enzymes [33,66,99]. Blood and plasma exemplify this vulnerability: degradation begins almost immediately after collection and can progress substantially within a few hours if samples remain at room temperature [116]. Several pyrrolidinophenones, as well as mephedrone- and methylone-type analogues, are particularly affected [41]. Their degradation not only reduces parent concentrations, but can lead to the appearance of transformation products that may interfere with interpretation, especially in clinical settings where early concentration data guide management decisions. Pre-analytical variables are bound to amplify or mitigate degradation. Temperature exerts the strongest influence; immediate cooling and prompt freezing slow decomposition substantially. pH exerts matrix-dependent effects. Acidification may stabilise some analogues but accelerate decomposition of others, and the addition of preservatives such as sodium fluoride (NaF) provides partial protection but cannot fully prevent β-keto reduction or oxidative pathways. Benchtop time is another critical determinant: even short delays between collection, centrifugation, and freezing can alter analyte profiles. Autosampler residence presents a further, often overlooked, risk. Some cathinones degrade measurably during overnight autosampler sequences, leading to downward drift in quality control results or unexpected discrepancies between first and last injections in a batch [88].

Urine offers improved stability for certain metabolites but not necessarily for parent compounds. In this matrix, pH once again plays a central role. Degradation accelerates in alkaline conditions, and repeated freeze-thaw cycles can modify both parent and metabolite concentrations. Because metabolites often serve as the primary targets for confirmation, mismanaging these pre-analytical steps may distort the relative abundance of phase I products and thereby complicate interpretive judgments. The risk is not limited to quantitative shifts: for some compounds, metabolite formation may occur ex vivo, leading to apparent 'metabolic signatures' that do not accurately reflect in vivo biotransformation [66]. Dried matrices such as DBS and VAMS offer partial mitigation against aqueous instability but introduce their own complexities. Drying typically slows degradation yet does not eliminate it, as the β-keto group may still undergo slow conversion even in the absence of liquid water [59]. Moreover, substrate interactions and differences in drying kinetics across devices can lead to inconsistent measurable concentrations. The effect of haematocrit on spot homogeneity and analyte distribution remains a notable concern, particularly for cathinones that partition unevenly between plasma and red blood cells [60]. Recently, dried urine spots (DUS) have been evaluated and showed good analyte stability (**Figure 9**) [117].

A further dimension of stability focus arises in processed samples. Extracts prepared for LC-MS/MS analysis may degrade in autosampler vials, especially at ambient temperatures or when stored for extended periods. Buffer composition, solvent ratio, and the presence of formic acid all influence degradation rates. Choosing appropriate storage conditions and limiting injection delays are essential to avoid artefactual decreases in analyte signal [71]. These pre-analytical and stability challenges extend beyond routine operations and directly affect confirmatory workflows. When parent compounds degrade rapidly, the detection window narrows, and metabolite-based confirmation becomes crucial. In some cases, such as with *N*-ethyl analogues or pyrrolidinophenones, the apparent absence of the parent alongside strong metabolite signals is not a paradox but an expected consequence of instability. Analytical frameworks must therefore integrate stability profiles into interpretation, ensuring that qualitative and quantitative findings are harmonised within the known degradation behaviour of each analogue [118]. Collectively, these observations emphasise that stability is not a peripheral concern but a central determinant of analytical success. Accurate measurement of cathinones requires a pre-analytical policy that codifies acceptable time windows, temperature controls, preservative use, and storage conditions for each matrix.

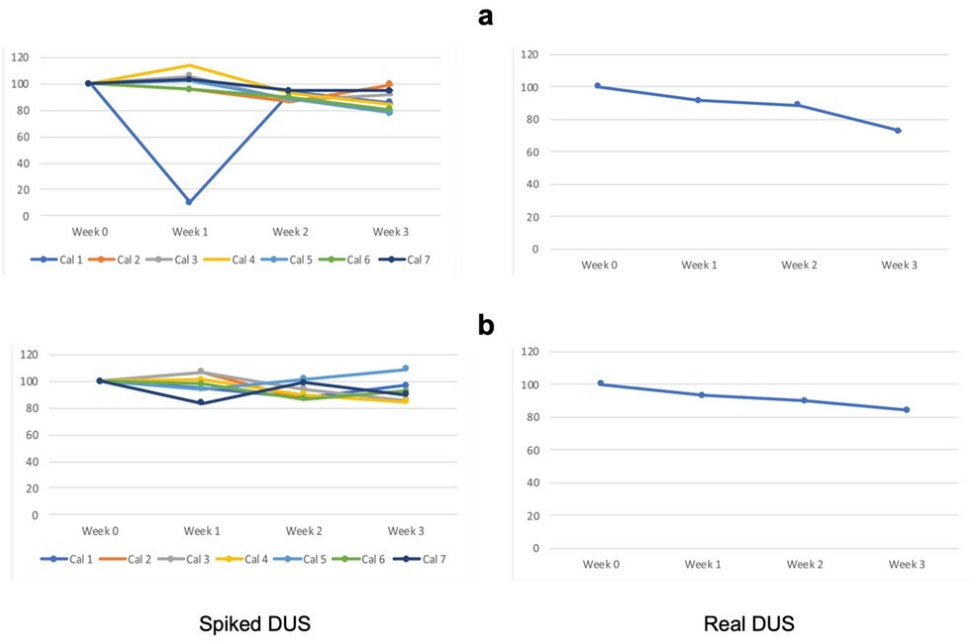

Figure 9 | Three-week stability of (a) MDPHP and (b) MDPV in spiked dried urine spots (DUS) and in a real DUS from a user. Used with permission [117].

Without such measures, degradation may outpace detection, compromising not only quantitative reliability but also the fundamental ability to confirm exposure. As new analogues continue to emerge, establishing compound-specific stability data (preferably harmonised across laboratories) will be essential for maintaining the integrity of cathinone testing in both forensic and clinical domains. A graphical summary of this section is shown in **Figure 10**.

6. Population Indicators, Early-Warning Systems, and Menu Refresh Strategy

Surveillance of synthetic cathinones increasingly depends on a constellation of population-level indicators that together offer a view of emerging substances far earlier than traditional casework alone. These external information streams, such as seizure intelligence, clinical toxicology alerts, poison centre enquiries, wastewater -based epidemiology (WBE), and coordinated early-warning systems, form a valuable counterpart to laboratory analytics.

In a drug class defined by rapid structural evolution, they allow laboratories to anticipate analogue turnover, update methods before widespread circulation, and validate analytical priorities with real -world evidence [119,120]. Among these indicators, seizure monitoring remains the most immediate source of intelligence on cathinone emergence. National forensic laboratories frequently record abrupt shifts in seized materials, with one analogue replacing another in a matter of weeks. This pattern has been well documented in Europe, North America and Asia, where cathinones regularly appear as substitutes in counterfeit MDMA or cocaine products or as the dominant component of powder mixtures sold through local networks [60,121,122]. Seizure data often demonstrate geographical specificity: certain metropolitan regions exhibit high circulation of pyrrolidinophenones, while others experience waves of methcathinone isomers or eutylone-type compounds [1,83]. Such heterogeneity reflects both regional supply lines and the operational behaviour of illicit manufacturers. From an analytical perspective, these observations show the limitations of fixed LC-MS/MS panels or static target lists; instead, laboratories require dynamic, evidence-driven menus shaped by current circulation rather than historical prevalence [123]. Clinical and emergency department presentations add a complementary dimension to this picture. Hospitals frequently detect new cathinones in symptom-driven testing before they appear in formal seizure datasets. The clinical profiles associated with sympathomimetic toxicity (tachycardia, agitation, hyperthermia, psychosis) are not specific to cathinones, yet temporal clustering of such cases can signal the introduction of a new analogue into local drug markets [6,17]. Poison centre enquiries play a similar role: spikes in calls related to unusual stimulant-like symptoms often precede systematic toxicology confirmation. These early clinical signals guide laboratories toward compounds that may require immediate expansion of HRMS suspect lists or targeted method development, particularly when reference standards are not yet available. In practice, laboratories that integrate clinical intelligence into their menu strategy are better positioned to detect analogues that initially circulate in low volumes or within specific user communities [36,84]. WBE further strengthens this surveillance ecosystem by providing near-real-time evidence of stimulant use at the population level. Several studies demonstrate that cathinone concentrations in wastewater can rise sharply within days following the introduction of a new analogue, often well before its identification in seized materials or clinical samples [54]. Because WBE reflects aggregate consumption rather than the behaviour of isolated individuals, it serves as a sensitive barometer for market shifts.

Peaks, declines and analogue replacements observed in wastewater frequently correspond to the manufacturing cycles that drive cathinone availability. By feeding these insights into analytical workflows, laboratories can identify which analogues merit inclu-

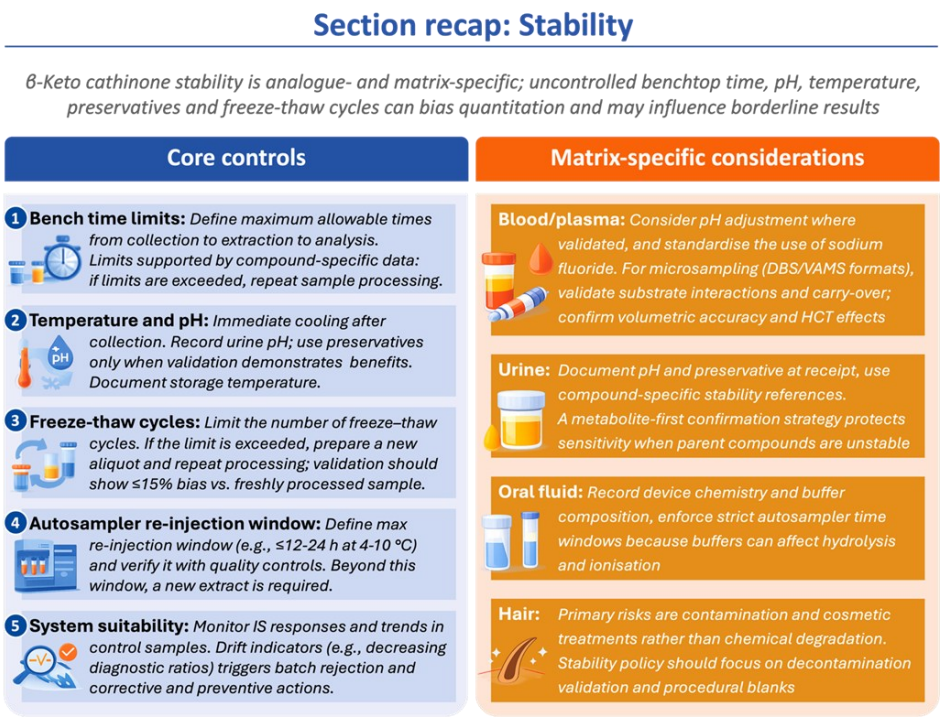

Figure 10 | Graphical recap of Section 5. Stability.

sion in suspect lists, which require new transitions or metabolite targets, and which have fallen below relevant prevalence thresholds [38]. Coordinated early-warning systems such as those operated by the EUDA (formerly EMCDDA), UNODC and national public-health agencies unify these disparate streams into structured alerts. These systems issue formal notifications when new analogues are detected, when toxic clusters emerge, or when severe adverse events occur. Importantly, early-warning bulletins often precede the availability of certified reference materials; therefore, HRMS laboratories must rely on predicted exact masses, class-informed fragmentation patterns, and retention-time heuristics to achieve preliminary detection [39,124]. This underscores the need for broad-scope HRMS acquisition rather than narrow targeted panels, as suspect-screening workflows allow laboratories to identify new analogues even before standards arrive. Retrospective data mining is particularly valuable in this context: once reference spectra or standards become available, LC-HRMS datasets collected weeks or months earlier can be interrogated again for previously unassigned features, thereby accelerating analytical readiness. The integration of these population indicators into routine toxicology practice directly informs the concept of menu refresh. In contrast to classical drug-testing paradigms where analyte lists remain stable for years, cathinone panels require continuous maintenance. A rational refresh strategy combines three elements: prevalence, risk and analytical feasibility. Prevalence is dictated by population indicators such as seizures, WBE and clinical case clusters [16,78,125]. Risk is informed by documented toxicity, frequency of severe presentations, and evidence of adulteration or substitution in high-use drug markets. Analytical feasibility reflects whether a compound can be detected and confirmed reliably with available technology, including the availability of standards, validated transitions and metabolic markers. When these three criteria intersect, a compound should be incorporated into LC–MS/MS confirmation panels and added to HRMS suspect screens. Conversely, analogues that disappear from circulation may be deprioritised but retained in retrospective-analysis libraries to ensure interpretive completeness. This population-driven approach has several advantages. It allows laboratories to keep pace with structural innovation in cathinone synthesis, reduces the risk of false negatives caused by outdated menus, and aligns analytical capacity with real-world harm. It also creates a feedback loop: toxicology findings contribute to early-warning alerts, which in turn shape the analytical priorities of laboratories across regions. In this cyclical framework, cathinone surveillance becomes a collaborative process between forensic laboratories, clinicians, epidemiologists and regulatory agencies. A graphical summary of this section is shown in **Figure 11**.

7. Conclusions and Expert Opinion: Future Directions and Analytical Priorities

Synthetic cathinones represent one of the most rapidly shifting and analytically demanding domains in forensic and clinical toxicology. Their ongoing structural diversification and 'chemical plasticity' ensure that new analogues will continue to emerge, often designed to exploit analytical blind spots and to challenge existing workflows. Consequently, laboratories must move from reactive method updates to a posture of continuous, intelligence-informed stewardship, combining structural awareness, predictive screening, and rapid implementation of fit-for-purpose confirmation routes. A recurring message across the evidence reviewed is that no single strategy is sufficient in isolation. Broad-scope HRMS remains crucial to detect emerging cathinones before reference materials are available and to support retrospective data mining, while targeted LC-MS/MS still provides the quantitative and confirmatory robus-

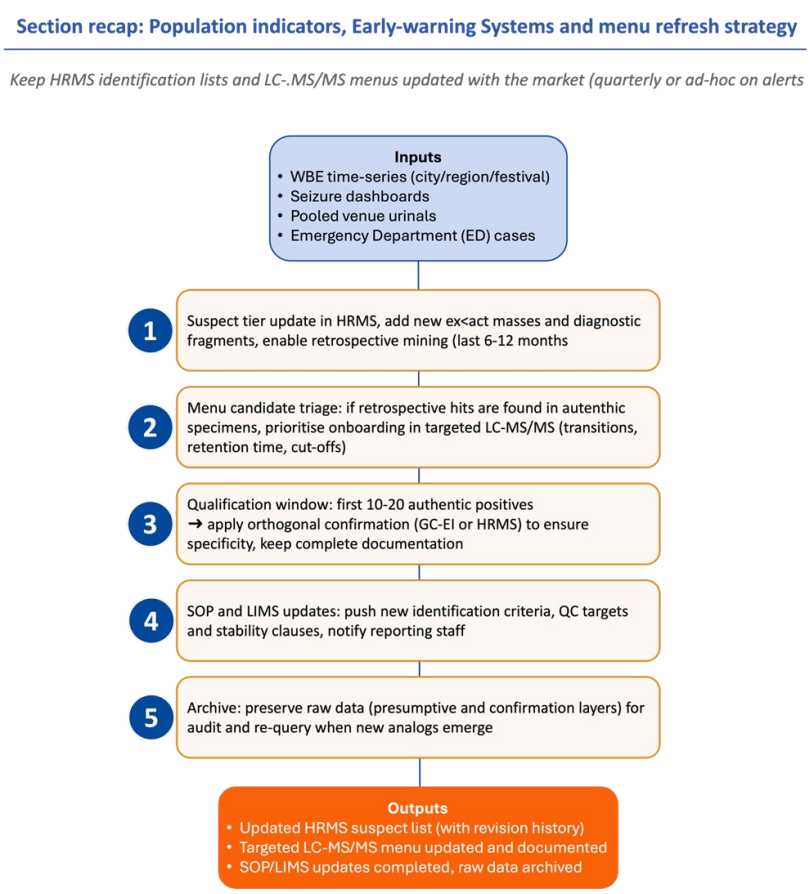

Figure 11 | Graphical recap of Section 6. Population Indicators.

tness required for defensible reporting. Orthogonal approaches (*e.g.*, GC-EI, GC-FTIR, accurate-mass MS/MS and, where appropriate, chiral LC) remain necessary whenever isomerism, interpretive ambiguity, or evidentiary thresholds require higher structural certainty. Rather than being viewed as 'specialty' options, these orthogonal tools should be embedded into decision trees with predefined triggers for escalation in high-suspicion or high-impact contexts. Matrix-specific constraints fundamentally shape detectability and interpretation and cannot be handled with legacy assumptions borrowed from classical stimulants. Blood/plasma often carry the highest interpretive value but are frequently most vulnerable to degradation; urine extends detection windows but increasingly shifts confirmation logic from parent compounds to metabolites; oral fluid narrows temporal coverage and introduces device- and contamination-related variability; hair provides longitudinal insight but requires stringent control of contamination and incorporation pathways. Microsampling platforms offer clear logistical advantages, but their deployment at scale will require systematic resolution of substrate interactions, drying kinetics, haematocrit-related effects, and long-term stability in dried formats. Analytical conclusions are only robust when these matrix-dependent uncertainties are explicitly acknowledged and addressed. A concise practice-oriented summary of recommended workflows by matrix is provided in **Table 1**. Cathinone instability is a defining analytical variable rather than a secondary technical nuisance. The β-keto motif confers chemical lability across matrices, and temperature, pH, preservatives, freeze-thaw cycles, autosampler residence, and extract longevity can all introduce substantial bias in parent and metabolite signals. Harmonised stability protocols, aligned across laboratories and matrices, would markedly improve interpretive confidence, reduce the risk of artefactual negatives, and strengthen comparability of clinical and forensic datasets. A shared, compound-specific stability resource (even if incremental) would be particularly valuable for newer analogues where handling uncertainty is currently high. In parallel, systematic characterisation of cathinone metabolism remains a high-priority gap. For many newly emerging substances, comprehensive biotransformation data are still missing, yet metabolite-informed confirmation is increasingly necessary because parent-only strategies are already unreliable for several families. Coordinated use of hepatocytes, liver microsomes, and complementary in vivo or case-based evidence can accelerate the identification of robust metabolite markers that extend detection windows, clarify interpretive boundaries, and reduce false negatives. Where metabolite hierarchies remain unsettled, laboratories should adopt conservative reporting logic and explicitly state uncertainty rather than over-interpreting parent-metabolite discordance. Finally, cathinone toxicology increasingly depends on integrating external intelligence streams into analytical governance. Seizure intelligence, WBE, clinical clusters and coordinated early-warning networks can reveal market changes earlier than conventional casework and should directly inform rolling updates of targeted panels, HRMS suspect lists, metabolite targets and spectral resources. Static LC–MS/MS menus cannot keep pace with the turnover rate of cathinones; a defined schedule for 'menu refresh'

Table 1 | Recommended analytical workflows by matrix.

Matrix	Primary screening (typical)	Confirmation / escalation (typical)	Key pitfalls to control (high-impact)
Blood / plasma	Targeted LC-MS/MS for panel coverage; HRMS when analogue turnover is suspected	LC-MS/MS under validated reporting criteria; escalate to accurate-mass MS/MS and/or GC-EI / GC-FTIR when isomerism or low-level ambiguity occurs; consider metabolite-linked urine confirmation when parent decay is plausible	Pre-analytical stability (pH/temperature/preservatives), re-injection windows, carry-over/adsorption, post-collection metabolism
Dried blood (DBS / VAMS)	Targeted LC-MS/MS or UHPLC-HRMS for broad NPS panels	Confirm with validated LC–MS/MS criteria; use urine metabolite evidence to preserve sensitivity when parent is near LOQ or suspected labile	Device-specific calibration, extraction efficiency/substrate interactions, haematocrit (DBS) or volumetric fill behaviour (VAMS), comparability vs liquid matrices
Urine	HRMS suspect screening to track market turnover; targeted LC-MS/MS for routine reporting	Reporting is strengthened by parent + ≥1 diagnostic metabolite (family-dependent) and/or orthogonal confirmation for isomers/challenged cases	Pre-analytical and autosampler stability; choice of preparation (dilute-and-shoot *vs* SPE/µSPE *vs* microextractions); ion suppression control; metabolite selection
Oral fluid	Dilute-and-shoot LC-MS/MS for rapid time-proximal assessment; HRMS when needed	LC-MS/MS with robust ion-ratio/RT criteria; escalate to HRMS diagnostic ions and/or GC-FTIR if positional isomers are critical; pair with urine metabolites when contamination vs systemic exposure is uncertain	Device chemistry/buffers and dilution assumptions, oral contamination, stimulated vs unstimulated collection, documentation of collection conditions
Hair	Targeted LC-MS/MS after validated decontamination; segmental strategy when appropriate	Defensibility can be strengthened by seeking metabolites in the same segment when supported; escalate to HRMS or GC-MS/TOF when structural confidence is challenged	External contamination and cosmetic treatments, decontamination controls/blanks, conservative interpretation (avoid PK over-reach)

with documented versioning is becoming an essential quality element rather than an optional organisational practice. In summary, analytical resilience against synthetic cathinones will not be achieved through any single technology, but through coordinated evolution of detection tools, shared reference and spectral resources, metabolite and stability knowledge, matrix-aware interpretation and intelligence-driven method stewardship. Alignment of these pillars enables laboratories to address cathinone innovation while maintaining accuracy, timeliness and defensibility in forensic and clinical decision-making. A graphical summary of this section is shown in **Figure 12**.

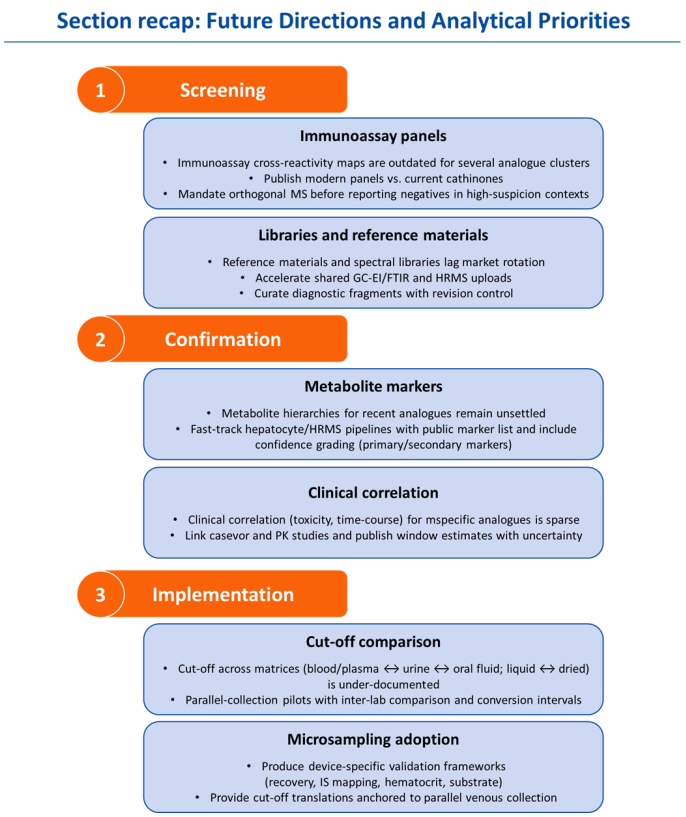

Figure 12 | Graphical recap of Section 7. Future Directions.

Acknowledgements

The Authors acknowledge the financial contribution from the Department of Pharmacy and Biotechnology (FaBiT), Alma Mater Studiorum – University of Bologna through Fundamental Oriented Research (RFO) funds.

References

[1] J.J. Palamar, A. Salomone, Am J Addict 30 (2021) 49–54. DOI: 10.1111/ajad.13086.

[2] H.-H. Chou, C.-H. Hsieh, C.-H. Chaou, C.-K. Chen, T.-H. Yen, S.-C. Liao, C.-J. Seak, H.-Y. Chen, Hum. Exp. Toxicol. 40 (2021) 1403–1412. DOI: 10.1177/0960327121996043.

[3] European Union Drugs Agency (EUDA). European Drug Report 2025: Trends and Developments. 2025. ISBN: 978-92-9408-074-5. ISSN: 2314-9086.

[4] United Nations Office on Drugs and Crime (UNODC). World Drug Report 2025: Contemporary Issues on Drugs. United Nations publication; 2025. ISBN: 978-921-159485-0. ISSN: 2411-8338.

[5] E. Ferrari Júnior, B.H.M. Leite, E.B. Gomes, T.M. Vieira, P. Sepulveda, E.D. Caldas, Front. Toxicol. 4 (2022) 1033733. DOI: 10.3389/ftox.2022.1033733.

[6] I.A. Larabi, N. Fabresse, I. Etting, L. Nadour, G. Pfau, J.H. Raphalen, P. Philippe, Y. Edel, J.C. Alvarez, Drug Alcohol Depend. 204 (2019) 107508. DOI: 10.1016/j.drugalcdep.2019.06.011.

[7] M.A.B. Axelsson, H. Lövgren, R. Kronstrand, H. Green, M.A. Bergström, Basic Clin. Pharmacol. Toxicol. 131 (2022) 420–434. DOI: 10.1111/bcpt.13786.

[8] A.J. Krotulski, S.J. Varnum, B.K. Logan, J. Forensic Sci. 65 (2020) 550–562. DOI: 10.1111/1556-4029.14184.

[9] G. Mercieca, S. Odoardi, M. Cassar, S. Strano Rossi, J. Pharm. Biomed. Anal. 149 (2018) 494–501. DOI: 10.1016/j.jpba.2017.11.024.

[10] A.A. Aldubayyan, E. Castrignanò, S. Elliott, V. Abbate, Forensic Toxicol. 41 (2023) 81–93. DOI: 10.1007/s11419-022-00634-w.

[11] A.A. Aldubayyan, E. Castrignanò, S. Elliott, V. Abbate, Talanta 253 (2023) 123986. DOI: 10.1016/j.talanta.2022.123986.

[12] M. Protti, in: A. Dasgupta (Ed.), Critical Issues in Alcohol and Drugs of Abuse Testing, Academic Press, Elsevier; London (2019) pp. 259-271.

[13] N. Nadal-Gratacós, M.D. Pazos, D. Pubill, J. Camarasa, E. Escubedo, X. Berzosa, R. López-Arnau, ACS Pharmacol. Transl. Sci. 7 (2024) 2588–2603. DOI: 10.1021/acsptsci.4c00299.

[14] J.L. Costa, K.F. Cunha, R. Lanaro, R.L. Cunha, D. Walther, M.H. Baumann, Drug Test. Anal. 11 (2019) 461–471. DOI: 10.1002/dta.2502.

[15] N. La Maida, V. Aquilina, F. Vaiano, M. Cavallo, C.A. Locatelli, G. Mannaioni, D. Arillotta, S. Pichini, A. Di Trana, S. Graziano, J. Anal. Toxicol. 49 (2025) 417–421. DOI: 10.1093/jat/bkaf024.

[16] G. Frison, F. Zancanaro, S. Frasson, L. Quadretti, M. Agnati, F. Vlassich, G. Gagliardi, T.M.G. Salerno, P. Donato, L. Mondello, Front. Chem. 8 (2021) 618339. DOI: 10.3389/fchem.2020.618339.

[17] A. Carlsson, V. Sandgren, S. Svensson, P. Konradsson, S. Dunne, M. Josefsson, J. Dahlén, Drug Test. Anal. 10 (2018) 1076–1098. DOI: 10.1002/dta.2366.

[18] P. Wachholz, R. Celiński, B. Bujak-Giżycka, R. Skowronek, N. Pawlas, J. Anal. Toxicol. 47 (2023) 547–551. DOI: 10.1093/jat/bkad026.

[19] S. Casati, A. Ravelli, M. Dei Cas, R.F. Bergamaschi, S. Vanerio, L. Sicuro, C. Faraone, M. Rossi, N. Galante, L. Mollica, G. Roda, P. Rota, A. Battistini, J. Anal. Toxicol. 49(6) (2025) 384–393. DOI: 10.1093/jat/bkaf048.

[20] M. Bassi, S. Bilel, M. Tirri, G. Corli, F. Di Rosa, A. Gregori, A.M. Alkilany, O. Rachid, E. Roda, F. De Luca, P. Papa, E. Buscaglia, G. Zauli, C.A. Locatelli, M. Marti, Neurotoxicology 103 (2024) 230–255. DOI: 10.1016/j.neuro.2024.06.014.

[21] E. Gerace, D. Caneparo, F. Borio, A. Salomone, M. Vincenti, J. Sep. Sci. 42 (2019) 1577–1584. DOI: 10.1002/jssc.201801249.

[22] N. La Maida, G. Mannocchi, S. Pichini, G. Basile, A. Di Giorgi, F.P. Busardò, E. Marchei, Eur. Rev. Med. Pharmacol. Sci. 26 (2022) 5033–5042. DOI: 10.26355/eurrev_202207_29289.

[23] Z. Li, S. Xiang, T. Zheng, G. Wu, L. Wu, Curr. Drug Metab. 25 (2025) 742–753. DOI: 10.2174/0113892002348484250309011657.

[24] J. Czerwinska, M.C. Parkin, C. George, A.T. Kicman, P.I. Dargan, V. Abbate, Drug Test. Anal. 14 (2022) 741–746. DOI: 10.1002/dta.3214.

[25] D. Fabregat-Safont, M. Mardal, J.V. Sancho, F. Hernández, K. Linnet, M. Ibáñez, J. Pharm. Anal. 10 (2020) 147–156. DOI: 10.1016/j.jpha.2019.12.006.

[26] A.A. Aldubayyan, E. Castrignanò, S. Elliott, V. Abbate, Forensic Toxicol. 42 (2024) 172–180. DOI: 10.1007/s11419-024-00684-2.

[27] P. Kavanagh, M. Gofenberg, V. Shevyrin, O. Dvorskaya, G. Dowling, A. Grigoryev, Drug Test. Anal. 12 (2020) 1442–1451. DOI: 10.1002/dta.2891.

[28] M. Grapp, C. Kaufmann, H.M. Schwelm, M.A. Neukamm, J.

Anal. Toxicol. 47 (2023) 162–174. DOI: 10.1093/jat/bkac057.

[29] E.B. Croce, A. Dimitrova, M.G. Di Milia, S. Pierotti, D. Arillotta, M. Barbaresi, M. Focardi, F. Vaiano, J. Anal. Toxicol. 49 (2025) 137–141. DOI: 10.1093/jat/bkae092.

[30] F. Freni, S. Bianco, C. Vignali, A. Groppi, M. Moretti, A.M.M. Osculati, L. Morini, Forensic Sci. Int. 298 (2019) 115–120. DOI: 10.1016/j.forsciint.2019.02.036.

[31] Y.-T. Yen, S.-L. Zhou, D.-Y. Huang, S.-H. Tseng, C.-F. Wang, S.-C. Chyueh, Forensic Sci. Int. 360 (2024) 112074. DOI: 10.1016/j.forsciint.2024.112074.

[32] S.-Y. Fan, C.-Z. Zang, P.-H. Shih, Y.-C. Ko, Y.-H. Hsu, M.-C. Lin, S.-H. Tseng, D.-Y. Wang, Forensic Sci. Int. 315 (2020) 110429. DOI: 10.1016/j.forsciint.2020.110429.

[33] B.P. dos Santos, L. Birk, V.C. Pôrto, S.N. Nascimento, V.C. Sebben, S. Eller, T.F. de Oliveira, J. Mass Spectrom. 60 (2025) e5178. DOI: 10.1002/jms.5178.

[34] D. Loganathan, R. Yi, B. Patel, J. Zhang, N. Kong, Anal. Bioanal. Chem. 413 (2021) 2147–2161. DOI: 10.1007/s00216-021-03182-1.

[35] J. Ji, Y. Zhang, J. Wang, Rapid Commun. Mass Spectrom. 35 (2021) e9136. DOI: 10.1002/rcm.9136.

[36] T.-I. Weng, L.-Y. Chen, J.-Y. Chen, P.-S. Chen, H.-L. Hwa, C.-C. Fang, J. Formos. Med. Assoc. 119 (2020) 1827–1834. DOI: 10.1016/j.jfma.2020.01.005.

[37] A. Giorgetti, R. Barone, G. Pelletti, M. Garagnani, J. Pascali, B. Haschimi, V. Auwärter, Drug Test. Anal. 14 (2022) 202–223. DOI: 10.1002/dta.3170.

[38] T.-T. Ting, P.-C. Chen, Y.-C. Chang, P.-J. Chiang, H.-C. Li, S.-H. Chen, P.-C. Chen, H.-T. Chu, P.-Y. Chuang, Y.-H. Liu, P.-S. Chen, J. Hazard. Mater. 476 (2024) 135020. DOI: 10.1016/j.jhazmat.2024.135020.

[39] H.H.-H. Lin, Y.-H. Wang, J.I.W.W. Liu, M.-C. Hsieh, S.-J. Huang, E. Lien, L.-W. Huang, A.Y.-C. Lin, Sci. Total Environ. 934 (2024) 173313. DOI: 10.1016/j.scitotenv.2024.173313.

[40] D. Rouxinol, D. Dias da Silva, J.P. Silva, F. Carvalho, M. de Lourdes Bastos, H. Carmo, Toxicol. Lett. 320 (2020) 113–123. DOI: 10.1016/j.toxlet.2019.10.003.

[41] K.A. Alsenedi, C. Morrison, J. Chromatogr. B 1076 (2018) 91–102. DOI: 10.1016/j.jchromb.2018.01.027.

[42] K.-W. Cheng, C.-M. Hsieh, H.-W. Chen, P.-C. Chi, D.-P. Yang, S.-H. Chan, J.-Y. Chen, H.-L. Hwa, C.-C. Fang, T.-I. Weng, P.-S. Chen, Rapid Commun. Mass Spectrom. 34 (2020) e8579. DOI: 10.1002/rcm.8579.

[43] C. Bouzoukas, P. Nikolaou, S. Athanaselis, A. Dona, C. Spiliopoulou, I. Papoutsis, Forensic Sci. Int. 370 (2025) 112469. DOI: 10.1016/j.forsciint.2025.112469.

[44] A. Di Trana, N. La Maida, G. de la Rosa, A. Di Giorgi, S. Graziano, K. Aldhaehri, E. Papaseit, O. Hladun, M. Farré, C. Pérez, S. Pichini, AAPS J. 27 (2025) 25. DOI: 10.1208/s12248-024-01012-7.

[45] J. Sánchez-González, S. Odoardi, A.M. Bermejo, P. Bermejo-Barrera, F.S. Romolo, A. Moreda-Piñeiro, S. Strano-Rossi, Drug Test. Anal. 11 (2019) 33–44. DOI: 10.1002/dta.2448.

[46] Y.-L. Yeh, C.-L. Hsieh, Y.-J. Huang, Y.-H. Chang, S.-M. Wang, J. Food Drug Anal. 33 (2025) 132–149. DOI: 10.38212/2224-6614.3543.

[47] H.-W. Chen, H.-T. Liu, Y.-N. Kuo, D.-P. Yang, T.-T. Ting, J.-H. Chen, J.-Y. Chiu, Y.-C. Jair, H.-C. Li, P.-J. Chiang, W.-R. Chen, M.-C. Lin, Y.-H. Hsu, P.-S. Chen, J. Pharm. Biomed. Anal. 233 (2023) 115443. DOI: 10.1016/j.jpba.2023.115443.

[48] S. Lee, J. Lee, D. Jang, H.J. Cho, S. Choi, E. Ryu, W. Koo, J. Song, J.S. Pyo, N.Y. Lim, C.H. Kwon, K. Jung, J.Y. Kim, S. Suh, Y. Hong, E. Han Simultaneous analysis of 203 drugs of abuse and metabolites in urine samples using liquid chromatography-tandem mass spectrometry. J Chromatogr B Analyt Technol Biomed Life Sci. 1256 (2025) 124524. DOI: 10.1016/j.jchromb.2025.124524.

[49] M. Grapp, C. Kaufmann, H.M. Schwelm, M.A. Neukamm, S. Blaschke, A. Eidizadeh, Drug Test. Anal. 12 (2020) 1320–1335. DOI: 10.1002/dta.2869.

[50] N. Bithi, S.D. Merrigan, G.A. McMillin, J. Addict. Med. 17 (2023) e209–e210. DOI: 10.1097/ADM.0000000000001117.

[51] M. Protti, I. Varfaj, A. Carotti, D. Tedesco, M. Bartolini, A. Favilli, S. Gerli, L. Mercolini, R. Sardella, Talanta 257 (2023) 124332. DOI: 10.1016/j.talanta.2023.124332.

[52] A. Pérez-Alcaraz, F. Borrull, C. Aguilar, M. Calull, F. Benavente, Talanta 225 (2021) 121994. DOI: 10.1016/j.talanta.2020.121994.

[53] D. Berardinelli, O. Taoussi, G. Daziani, F. Tavoletta, G. Ricci, L.P. Tronconi, P. Adamowicz, F.P. Busardò, J. Carlier, AAPS J. 26 (2024) 70. DOI: 10.1208/s12248-024-00940-8.

[54] I. Langa, R. Gonçalves, M.E. Tiritan, C. Ribeiro, Forensic Sci. Int. 325 (2021) 110873. DOI: 10.1016/j.forsciint.2021.110873.

[55] C. Feliu, E. Hattat, Y. Tholance, S. Hodin, J. Pipet, T. Panther, C. Bidat, X. Delavenne, Forensic Sci. Int. 367 (2025) 112364. DOI: 10.1016/j.forsciint.2025.112364.

[56] G. Musile, M. Mazzola, K. Shestakova, S. Savchuk, S. Appo-

lonova, F. Tagliaro, J. Chromatogr. B 1152 (2020) 122263. DOI: 10.1016/j.jchromb.2020.122263.

[57] M. Massano, M. Nuñez-Montero, E. Papaseit, O. Hladun, C. Pérez-Maña, M. Ventura, E. Marchei, E. Alladio, E. Gerace, S. Pichini, M. Farrè, A. Salomone, J. Pharm. Biomed. Anal. 241 (2024) 115994. DOI: 10.1016/j.jpba.2024.115994.

[58] X. Li, S. Zhang, Z. Xu, S. Huang, M. Guo, J. Ying, Y. Pan, D. Zhang, T. Lü, J. Chromatogr. A 1761 (2025) 466343. DOI: 10.1016/j.chroma.2025.466343.

[59] M. Massano, C. Incardona, E. Gerace, P. Negri, E. Alladio, A. Salomone, M. Vincenti, Talanta 241 (2022) 123265. DOI: 10.1016/j.talanta.2022.123265.

[60] Y. Wang, Y. Shi, Y. Yu, L. Chen, J. Jiang, J. Long, P. Xiang, G. Duan, J. Anal. Toxicol. 45 (2021) 633–643. DOI: 10.1093/jat/bkaa106.

[61] J. Czerwinska, M.C. Parkin, A. Cilibrizzi, C. George, A.T. Kicman, P.I. Dargan, V. Abbate, Pharmaceuticals (Basel) 14 (2020) 5. DOI: 10.3390/ph14010005.

[62] R. Alremeithi, M.A. Meetani, A.A. Alaidaros, A. Lanjawi, K. Alsumaiti, J. Anal. Methods Chem. 2018 (2018) 4396043. DOI: 10.1155/2018/4396043.

[63] Y. Li, R. Lian, F. Yang, Z. Xu, F. Cao, R. Wang, C. Liang, Y. Zhang, Anal. Methods 13 (2021) 5048–5055. DOI: 10.1039/D1AY01280K.

[64] A.D. Giachetti, J.H. Kahl, M.E. Zaney, G.W. Hime, D.M. Boland. Method Validation of Seven Synthetic Cathinones by LC-MS/MS Analysis and the Prevalence of N-Ethylpentylone in Postmortem Casework. J Anal Toxicol. 46 (2022) 122–127. DOI: 10.1093/jat/bkaa194.

[65] A.L. Fabris, S. Pedersen-Bjergaard, E.L. Øiestad, G.N. Rossi, J.E.C. Hallak, R.G. dos Santos, J.L. Costa, M. Yonamine, Anal. Chim. Acta 1301 (2024) 342387. DOI: 10.1016/j.aca.2024.342387.

[66] P. Adamowicz, A. Malczyk, Forensic Sci. Int. 295 (2019) 36–45. DOI: 10.1016/j.forsciint.2018.12.001.

[67] S.K. Manier, F. Schwermer, L. Wagmann, N. Eckstein, M.R. Meyer, Metabolites 11 (2021) 3. DOI: 10.3390/metabo11010003.

[68] M.F. Fogarty, A.J. Krotulski, D.M. Papsun, S.E. Walton, M. Lamb, M.T. Truver, C.W. Chronister, B.A. Goldberger, B.K. Logan, J. Anal. Toxicol. 47 (2023) 753–761. DOI: 10.1093/jat/bkad037.

[69] T. Lau, M. Concheiro, G. Cooper, J. Anal. Toxicol. 44 (2020) 679–687. DOI: 10.1093/jat/bkaa071.

[70] A.L. Fabris, R. Lanaro, J.L. Costa, M. Yonamine, J. Anal. Toxicol. 47 (2023) 353–365. DOI: 10.1093/jat/bkad003.

[71] H.L. Ciallella, L.R. Rutter, L.A. Nisbet, K.S. Scott, Front. Chem. 8 (2020) 597726. DOI: 10.3389/fchem.2020.597726.

[72] K.F. da Cunha, K.D. Oliveira, J.L. Costa, Forensic Toxicol. 42 (2024) 18–30. DOI: 10.1007/s11419-023-00671-z.

[73] R. Gottardo, D. Sorio, G. Soldati, M. Ballotari, N.M. Porpiglia, F. Tagliaro, Electrophoresis 42 (2021) 450–459. DOI: 10.1002/elps.202000304.

[74] K.F. da Cunha, K.D. Oliveira, M.A. Huestis, J.L. Costa, J. Anal. Toxicol. 44 (2020) 697–707. DOI: 10.1093/jat/bkaa089.

[75] M. Protti, E. Milandri, R. Di Lecce, L. Mercolini, R. Mandrioli, Adv. Sample Prep. 13 (2025) 100161. DOI: 10.1016/j.sampre.2025.100161.

[76] A.A. Aldubayyan, E. Castrignanò, S. Elliott, V. Abbate, Pharmaceuticals (Basel) 15 (2022) 510. DOI: 10.3390/ph15050510.

[77] N. Ayala-Lopez, J.M. Colby, J.J. Hughey, J. Anal. Toxicol. 46 (2022) 99–102. DOI: 10.1093/jat/bkaa179.

[78] M. Dei Cas, E. Casagni, S. Arnoldi, V. Gambaro, G. Roda, Forensic Sci. Int.: Synergy 1 (2019) 71–78. DOI: 10.1016/j.fsisyn.2019.04.003.

[79] A. Yanini, F.A. Esteve-Turrillas, M. de la Guardia, S. Armenta, J. Chromatogr. A 1574 (2018) 91–100. DOI: 10.1016/j.chroma.2018.09.006.

[80] J.R.H. Archer, F. Mendes, S. Hudson, K. Layne, P.I. Dargan, D.M. Wood, Br. J. Clin. Pharmacol. 86 (2020) 517–527. DOI: 10.1111/bcp.14239.

[81] A. Power, M. Gardner, R. Andrews, G. Cozier, R. Kumar, T.P. Freeman, I.S. Blagbrough, P. Sunderland, J. Scott, A. Frinculescu, T. Shine, G. Taylor, C. Norman, H. Ménard, N.N. Daéid, O.B. Sutcliffe, S.M. Husbands, R.W. Bowman, T.S.F. Haines, C.R. Pudney, Anal. Chem. 97 (2025) 10163–10172. DOI: 10.1021/acs.analchem.4c05247.

[82] D. Florou, V.A. Boumba, Toxicol. Rep. 8 (2021) 1699–1720. DOI: 10.1016/j.toxrep.2021.09.003.

[83] M. Deville, R. Fedorowicz, F. Grandjean, M. Simon, C. Charlier, J. Anal. Toxicol. 46 (2023) e291–e295. DOI: 10.1093/jat/bkac092.

[84] H.-T. Yeh, H.-Y. Chen, S.-W. Liu, T.-I. Weng, C.-C. Fang, J.-H. Yu, Y.-C. Chen, Y.-J. Su, S.-Y. Gao, C.-C. Lin, Toxics 10 (2022) 386. DOI: 10.3390/toxics10070386.

[85] N. La Maida, V. Aquilina, F. Vaiano, M. Cavallo, C.A. Loca-

telli, G. Mannaioni, D. Arillotta, S. Pichini, A. Di Trana, S. Graziano, J. Anal. Toxicol. 49 (2025) 417–421. DOI: 10.1093/jat/bkaf024.

[86] J.L. Bonetti, R.F. Kranenburg, S. Hokanson, M. Pothier, S. Samanipour, A.C. van Asten, Forensic Chem. 41 (2024) 100619. DOI: 10.1016/j.forc.2024.100619.

[87] Y. Abiedalla, J. DeRuiter, C.R. Clark, J. Chromatogr. B 1048 (2017) 38–48. DOI: 10.1016/j.jchromb.2017.01.045.

[88] S. Hemmer, L. Wagmann, B. Pulver, F. Westphal, M.R. Meyer, Metabolites 12 (2022) 1209. DOI: 10.3390/metabo12121209.

[89] F. Aknouche, A. Ameline, L. Gheddar, C. Maruejouls, P. Kintz, J. Anal. Toxicol. 46 (2022) 949–955. DOI: 10.1093/jat/bkac048.

[90] M.A. Meetani, R.H. Alremeithi, M.K. Mousa, J. Chromatogr. Sci. 57 (2019) 361–368. DOI: 10.1093/chromsci/bmz008.

[91] H.M. Schwelm, C. Grumann, V. Auwärter, M.A. Neukamm, Drug Test. Anal. 12 (2020) 1354–1365. DOI: 10.1002/dta.2886.

[92] A. Alexandridou, T. Mouskeftara, N. Raikos, H.G. Gika, J. Chromatogr. B 1156 (2020) 122308. DOI: 10.1016/j.jchromb.2020.122308.

[93] J. Carrola, N. Duarte, P. Florindo, S. Henriques, G. da Silva, L. Bijlsma, R. Moreira, C. Correia, M. de Jesus Perry, Á. Lopes, C. de Mello-Sampayo, M. do Rosário Bronze, J. Chromatogr. B 1159 (2020) 122340. DOI: 10.1016/j.jchromb.2020.122340.

[94] Y.-L. Yeh, C.-Y. Wen, C.-L. Hsieh, Y.-H. Chang, S.-M. Wang, Forensic Sci. Int. 361 (2024) 112134. DOI: 10.1016/j.forsciint.2024.112134.

[95] J. Carlier, X. Diao, R. Giorgetti, F.P. Busardò, M.A. Huestis, Int. J. Mol. Sci. 22 (2021) 230. DOI: 10.3390/ijms22010230.

[96] L. Wagmann, F. Frankenfeld, Y.M. Park, J. Herrmann, S. Fischmann, F. Westphal, R. Müller, V. Flockerzi, M.R. Meyer, Front. Chem. 8 (2020) 539. DOI: 10.3389/fchem.2020.00539.

[97] Y.A. Bin Jardan, K. Mohamed, N. Abbas, M. El-Gendy, N. Alsaif, M. Alanazi, M. Mohammed, M. Abounassif, M. Hefnawy, J. Pharm. Biomed. Anal. 194 (2021) 113798. DOI: 10.1016/j.jpba.2020.113798.

[98] M. Antunes, M. Sequeira, M. de Caires Pereira, M.J. Caldeira, S. Santos, J. Franco, M. Barroso, H. Gaspar, J. Anal. Toxicol. 45 (2021) 233–242. DOI: 10.1093/jat/bkaa074.

[99] L.D. Paul, J. Welter-Luedeke, S. Penzel, A. Zangl, M. Graw, Forensic Sci. Int. 321 (2021) 110721. DOI: 10.1016/j.forsciint.2021.110721.

[100] L. Mercolini, M. Protti, M.C. Catapano, J. Rudge, A.E. Sberna, J. Pharm. Biomed. Anal. 123 (2016) 186–194. DOI: 10.1016/j.jpba.2016.02.015.

[101] M. Protti, R. Mandrioli, L. Mercolini, Anal. Chim. Acta 1046 (2019) 32–47. DOI: 10.1016/j.aca.2018.09.004.

[102] M. Protti, R. Mandrioli, H.M. Santos, C. Lodeiro, J.L. Capelo-Martínez, L. Mercolini, Bioanalysis 17 (2025) 997–1009. DOI: 10.1080/17576180.2025.2546782.

[103] M. Protti, L. Mercolini, R. Mandrioli, Anal. Chim. Acta 1359 (2025) 344018. DOI: 10.1016/j.aca.2025.344018.

[104] E. Ferrari Júnior, E.D. Caldas, Forensic Toxicol. 40 (2022) 88–101. DOI: 10.1007/s11419-021-00600-y.

[105] H.M. Schwelm, M. Persson, B. Pulver, M.V. Huß, H. Gréen, V. Auwärter, Drug Test. Anal. 16 (2024) 277–288. DOI: 10.1002/dta.3538.

[106] Y.-L. Yeh, S.-M. Wang, Drug Test. Anal. 14 (2022) 1325–1337. DOI: 10.1002/dta.3258.

[107] L. Borovcová, V. Pauk, K. Lemr, J. Sep. Sci. 41 (2018) 2288–2295. DOI: 10.1002/jssc.201800006.

[108] L.-Y. Zhao, M. Qin, T. Zheng, G.-P. Wu, T. Lu, J. Chromatogr. A 1737 (2024) 465464. DOI: 10.1016/j.chroma.2024.465464.

[109] A. Sorribes-Soriano, F.A. Esteve-Turrillas, S. Armenta, P. Amorós, J.M. Herrero-Martínez, Anal. Chim. Acta 1052 (2019) 73–83. DOI: 10.1016/j.aca.2018.11.046.

[110] R. Rocchi, M.C. Simeoni, C. Montesano, G. Vannutelli, R. Curini, M. Sergi, D. Compagnone, Drug Test. Anal. 10 (2018) 865–873. DOI: 10.1002/dta.2330.

[111] E. Ferrari Júnior, V.S. Bitencourt, Á.B.M. de Souza, E.D. Caldas, J. Pharm. Biomed. Anal. 244 (2024) 116139. DOI: 10.1016/j.jpba.2024.116139.

[112] F.K. Nzekoue, M. Agostini, M. Verboni, C. Renzoni, L. Alfieri, S. Barocci, M. Ricciutelli, G. Caprioli, S. Lucarini, J. Pharm. Biomed. Anal. 205 (2021) 114310. DOI: 10.1016/j.jpba.2021.114310.

[113] V. Longo, G. Stocchero, M. Lucchiari, G.M. Marchio, F. Donini, F. Ingenito, L. Bertoldi, L. Pecoraro, A. Anesi, D. Favretto, Drug Test. Anal. 17 (2025) 56–74. DOI: 10.1002/dta.3675.

[114] A. Niebel, F. Krumbiegel, S. Hartwig, M.K. Parr, M. Tsokos, Forensic Sci. Med. Pathol. 16 (2020) 32–42. DOI: 10.1007/s12024-019-00209-z.

[115] A. Niebel, L. Westendorf, F. Krumbiegel, S. Hartwig, M.K. Parr, M. Tsokos, Drug Test. Anal. 14 (2022) 110–121. DOI: 10.1002/dta.3150.

[116] S. Hemmer, L. Wagmann, B. Pulver, F. Westphal, M.R. Meyer, Metabolites 12 (2022) 1209. DOI: 10.3390/metabo12121209.

[117] B. Rossi, F. Freni, C. Vignali, S. Ortu, L. Morin, Forensic Sci. Int. 377 (2025) 112622. DOI: 10.1016/j.forsciint.2025.112622.

[118] A. Romańczuk, S. Rojek, K. Synowiec, M. Maciów-Głąb, K. Kula, E. Rzepecka-Woźniak, J. Anal. Toxicol. 47 (2023) 470–480. DOI: 10.1093/jat/bkad010.

[119] United Nations Office on Drugs and Crime (UNODC). UNODC Early Warning Advisory (EWA) on New Psychoactive Substances (NPS). https://www.unodc.org/LSS/Home/NPS

[120] European Union Drugs Agency (EUDA). The EU Early Warning System on new psychoactive substances (NPS). https://www.euda.europa.eu/activities/eu-early-warning-system-on-nps_en

[121] J. Schram, M. Parrilla, N. Sleegers, F. Van Durme, J. van den Berg, A.L.N. van Nuijs, K. De Wael, Drug Test. Anal. 13 (2021) 1282–1294. DOI: 10.1002/dta.3018.

[122] P. Engelgardt, M. Krzyżanowski, P. Piotrowski, M. Borkowska-Sztachańska, A. Wasilewska, Int. J. Occup. Med. Environ. Health 35 (2022) 485–495. DOI: 10.13075/ijomeh.1896.01863.

[123] S. Casati, A. Ravelli, M. Dei Cas, R.F. Bergamaschi, S. Vanerio, L. Sicuro, C. Faraone, M. Rossi, N. Galante, L. Mollica, G. Roda, P. Rota, A. Battistini, J. Anal. Toxicol. 49 (2025) 384–393. DOI: 10.1093/jat/bkaf048.

[124] E.J. Vogel, M. Neyra, D.A. Larsen, T. Zeng, Environ. Sci. Technol. 58 (2024) 8518–8530. DOI: 10.1021/acs.est.4c01251.

[125] P.O.M. Gundersen, D. Pasin, L. Slørdal, O. Spigset, M. Josefsson, Forensic Sci. Int. 361 (2024) 112131. DOI: 10.1016/j.forsciint.2024.112131.

ORIGINAL ARTICLE

TRANSLATIONAL CHEMISTRY
AN INTERFACE JOURNAL
HTTPS://WWW.TRANSLATIONALCHEMISTRY.COM/

ORIGINAL ARTICLE | DOI: 10.5584/translationalchemistry.v2i1.253

Reactivity of palladacycles with phosphorus donor nucleophiles. The first crystal and molecular structure of a mixed-bridged acetate/phosphine dinuclear species

Juan M. Ortigueira [2], Fátima Lucio-Martínez [1], M. Luz Durán [1], José M. Vila [1,*]

[1]Departamento de Química Inorgánica, Universidade de Santiago de Compostela, Campus Vida E-15782 Santiago de Compostela, Spain. [2]Campus Terra E-27002 Lugo, Spain.

Received: December 2025 **Accepted:** February 2026 **Available Online**: April 2026

ABSTRACT

Treatment of 2,4-(MeO)C_6H_3C(H)=N-[3,5-$Cl_2C_6H_3$] **1** with palladium(II) acetate in toluene at 60 °C under argon gave the dinuclear acetate-bridged palladacycle **2** as an air-stable solid. Reaction of **2** with the diphosphine $Ph_2PCH_2PPh_2$ (dppm) in 1:1 molar ratio and NH_4PF_6 yielded complex **3** where only one of the acetate ligands was exchanged by a diphosphine to give a mixed-bridged dinuclear palladacycle bearing charged and neutral linkers spanning between the metal centers, with the organic ligands in a *cis* fashion. The first crystal structure of one such complex, **3**, is now reported herein. This innovation highlights the unique ability of palladacycles to yield novel structures; more often than not, through a process of sheer serendipity. Complex **2** could be converted into the corresponding halide-bridged analogues by treatment in acetone with aqueous sodium chloride or sodium bromide to give the chloride-bridged **4**, or bromide-bridged **5**, compounds, respectively, as air-stable solids. The metallated moieties show a *trans* conformation of the Schiff base ligands, as opposed to the *cis* arrangement in **3**. Treatment of **4** and **5** with the small bite diphosphine $Ph_2PCH_2PPh_2$ in 1:1 ratio gave the dinuclear compounds **6** and **7**, likewise with two distinct bridging ligands; whereas the large bite diphosphine *trans*-$Ph_2PCH=CHPPh_2$ (*trans*-dppe) yielded **8** and **9** that are symmetric complexes across the C=C double bond as shown by the appearance of only one set of signals in the ^{1}H NMR spectrum, and by a singlet resonance in the ^{31}P-{^{1}H} spectrum for the two equivalent phosphorus nuclei. Reaction of **4** and **5** with $Ph_2PCH_2PPh_2$, $Ph_2P(CH_2)_2PPh_2$ (dppe) *cis*-$Ph_2PCH=CHPPh_2$ (*cis*-dppe), $Ph_2P(CH_2)_3PPh_2$ (dppp) or $Ph_2P(CH_2)_4PPh_2$ (dppb), and with PPh_3 in the appropriate molar ratio gave the complexes **10**-**19** as mono- or dinuclear species. All the compounds in this report were adequately characterized by microanalytical and spectroscopic measurements; the crystal molecular structures of **2**, **3**, **9** and **12** are reported.

1. Introduction

The most noticeable feature that distinguishes metallacycles is the covalent C-M bond, which was first achieved by Cope and Siekman by the reaction of aromatic azo compounds and potassium tetrachloroplatinate(II) or palladium chloride(II). [1] This milestone marked the starting point for cyclometallated compounds [2,3], which presently constitute an important branch of organometallic chemistry. In the specific case of palladium, the ensuing palladacycles [4] show considerable stability with the five- and six-membered metallacycle [5] rings being the most favoured, although studies in search for four-membered metallacycle rings [6] have recently appeared. They have numerous applications among which the following are noteworthy: metallomesogens [7,8], phosphorescent compounds [9-12], antineoplastic species [13-18], catalysts [19-23] inclusive of the Suzuki-Miyaura [24,25] and Mizoroki-Heck cross-coupling reactions [26,27], and organic synthesis intermediates [2,28]. One of the most suitable ligands for the preparation of palladacycles are the Schiff bases of variable denticity [C,N], [C,N,N], [C,N,S], [C,N:C,N] which are readily available and at times they can lead to unexpected, yet innovative reactivity. [29] The synthesis sequence usually begins with the preparation of the acetate-bridged complexes in solution, starting materials for a long series of palladacyles; notwithstanding, a ball mill mechanosynthesis method has been depicted. [30] One of the more pressing questions was to determine whether the acetate-bridged metallacycles were polymeric or dinuclear species, which was difficult to assert solely on the basis spectroscopic and microanalytical measurements, an issue that was settled with the advent of X-ray structural analysis, in favor of the dinuclear nature, at least in the solid state. [31] After a straightforward metathesis reaction with sodium chloride or bromide the subsequent halide-bridged dinuclear complexes are the starting point for a vast quantity and variety of products resulting from reactions with neutral and anionic nucleophiles, such as tertiary

***Corresponding author:** José M. Vila, josemanuel.vila@usc.es

mono-, di-and triphosphines, and thallium acetylacetonate, respectively; in particular, the reactions with phosphorus donors may yield single- and dinuclear compounds with mono- or bidentate phosphines, as appropriate. Herein, we describe the synthesis, characterization and structural analysis (in part) of single and dinuclear palladacycles inclusive of mixed dinuclear μ-diphosphine/μ-acetate and μ-diphosphine/μ-halide complexes; the first molecular structural analysis of the former type is also given.

2. Materials and Methods

2.1. General procedures

Solvents were purified by standard methods. Chemicals palladium (II) acetate, 2,4-dimethoxybenzaldehyde, 3,5-dichloroaniline, ammonium hexafluorophosphate and the phosphines PPh_3, $Ph_2PCH_2PPh_2$ (dppm), $Ph_2PCH=CHPPh_2$ (*trans*- and *cis*-dppe), $Ph_2P(CH_2)_nPPh_2$, (n = 2, dppe, n = 3 dppp, n = 4 dppb) were used as supplied from commercial sources. Microanalyses were carried out at the Servicio de Análisis Elemental at the University of Santiago using a FISONS elemental analyzer, Model 1108. IR spectra were recorded as KBr pellets or polythene discs on ABB Bomen model MB102 (equipped with vacuum purge and with GOLDENGATE equipment for pure solid samples) and on JASCO FT/ IR-4600 (equipped with an ATR, model ATR-PRO ONE) spectrophotometers. NMR spectra were obtained as $CDCl_3$, DMSO-d_6 or Me_2CO-d_6 solutions as appropriate and referenced to $SiMe_4$ (^1H) or 85 % H_3PO_4 (^{31}P–{^1H}) and were recorded on BRUKER DPX 250 and Varian Inova 400 spectrometers. All chemical shifts, in ppm, were reported downfield from the standards.

2.2. Synthesis

Preparation of the ligand

2,4-$(MeO)_2C_6H_3C(H)=N(3,5\text{-}Cl_2C_6H_3)$ 1. The aldehyde 2,4-dimethoxybenzaldehyde (1.0 g, 4.366 mmol) and 3,5-dichlorobenzenamine (450 mg, 4.537 mmol) were added together in chloroform (*ca.* 40 cm^3) in a round-bottom flask to give a yellow solution which was refluxed in a modified Dean-Stark apparatus for 8 h, after which the resulting solution was cooled to room temperature and the solvent was removed under reduced pressure. Yield 866.7 mg 64 %. Anal. Calc. for $C_{15}H_{13}Cl_2NO_2$ (310.18): C, 58.1, H, 4.2, N, 4.5 %. Found: C, 57.9, H, 4.4, N, 4.6 %. IR (cm^{-1}): ν(C=N): 1617 m sh. ^1H NMR ($CDCl_3$, δ ppm, J Hz): 3.87 (s, 3H, MeO); 3.88 (s, 3H, MeO); 6,46 (d, 1H, H3, ^3J(H3H5) = 2.2); 6.58 (dd, 1H, H5, ^3J(H5H6) = 8.8, ^4J(H3H5) = 2.2); 7,06 (d, 2H, H8, H12, ^4J(H8H10) = ^4J(H10H12) = 1.8); 7.16 (t, 1H, H10, ^4J(H8H10) = ^4J(H10H12) = 1.8): 8.05 (d, 1H, H6, ^{3}JH5H6) = 8.8; 8.73 (s, 1H, HC=N); ^{13}C–{^1H} NMR: 164.6 (C=N); 157.7 (C7); 161.6, 155.4 (C2, C4); 135.3 (C1); 129.5 (C6); 125.1 (C5); 120.0 (C3); 113.4 (C9, C11); 106.2 (C10); 98.2 (C8, C12); 55.8, 55.7 (MeO).

Preparation of the complexes

[Pd{2,4-$(MeO)_2C_6H_2C(H)=N(3,5\text{-}Cl_2C_6H_3)$}(μ-$O_2CMe$)]$_2$ 2. A mixture of 2,4-$(MeO)_2C_6H_3C(H)=N(3,5\text{-}Cl_2C_6H_3)$ (552 mg, 1.778 mmol) and palladium(II) acetate (400 mg, 1.782 mmol) in toluene (40 cm^3) was stirred for 12 h at 60 ºC under argon. After cooling to room temperature, the precipitate was filtered off and the solid residue was chromatographed on a column packed with silica gel. Elution with a mixture of CH_2Cl_2:EtOH (97:3, *v/v*) afforded the final product which after concentration, was recrystallized from chloroform/n-hexane to give an orange solid. Yield 802 mg 95 %. Anal. Calc. for $C_{34}H_{30}Cl_4N_2O_8Pd_2$ (949.26): C, 43.0, H, 3.2, N, 2.9 %. Found: C, 42.9, H, 3.3, N, 2.7 % IR (cm^{-1}): ν (C=N): 1593 m sh; ν_{as} (COO): 1563 s; ν_s(COO): 1412 s. ^1H NMR ($CDCl_3$, δ ppm, J Hz): 2.06 (s, 6H, $MeCO_2$); 3.63 (s, 6H, MeO); 3.84 (s, 6H, MeO); 5.65 (d, 2H, H3, ^4J(H3H5) = 1.9); 6.05 (d, 2H, H5, ^4J(H3H5) = 1.9); 6.87 (d, 4H, H8, H12, ^4J(H8H10) = ^4J(H10H12) = 1.8); 7.09 (t, 2H, H10, ^4J(H8H10) = ^4J(H10H12) = 1.8); 7.96 (s, 2H, HC=N). ^{13}C–{^1H} NMR: 180.8 ($MeCO_2$); 168.7 (C=N); 160.3 (C7); 160.3, 160.3 (C2, C4); 134.2 (C1); 150.4 (C6); 126.2 (C5); 121.8 (C3), 126.6 (C9, C11); 108.3 (C10); 95.3 (C8, C12); 55.6, 55.4 (MeO); 24.4 ($MeCO_2$).

[{Pd[2,4-$(MeO)_2C_6H_2C(H)=N$-(3,5-$Cl_2C_6H_3$)]}$_2$(μ-$Ph_2PCH_2PPh_2$)(μ-O_2CMe)][PF_6] 3. $Ph_2PCH_2PPh_2$ (dppm) (8.7 mg, 0.023 mmol) was added to a suspension of **2** (22.0 mg, 0.023 mmol) in acetone (*ca*. 25 cm^3). The mixture was stirred for 2 h at room temperature and then NH_4PF_6 (3.8 mg, 0.023 mmol) was added. The mixture was stirred for a further 24 h at room temperature after which the solution was filtered off and after concentration the residue was chromatographed on a column packed with silica gel. Elution with a mixture of CH_2Cl_2:EtOH (97:2, *v/v*) afforded the final product which after concentration, was recrystallized from chloroform/n-hexane to give a brown solid. Yield 31.9 mg 97.8 %. Anal. Calc. for $C_{57}H_{49}Cl_4F_6N_2O_6P_3Pd_2$ (1419.53): C, 48.2, H, 3.5, N, 2.0 %. Found: C, 48.1, H, 3.7, N, 1.7 %. IR (cm^{-1}): ν(C=N): 1586 m, ν_{as}(COO), 1561 s; ν_s(COO), 1424 s; ν_{as}(PF) = 834 vs, ν_{as}(PF2) = 556 m. ^1H NMR ($CDCl_3$, δ ppm, J Hz): 2.18 (s, 3H, $MeCO_2$); 3.00 (s, 6H, MeO); 3.76 (s, 6H, MeO); 5.32 (m, 2H, PCH_2P); 5.39 (dd, 2H, H5, ^4J(H3H5) = 1.9, ^4J(H5P) = 7.2); 5.96 (d, 2H, H3, ^4J(H3H5) = 1.9; 6.98 (d, 4H, H8, H12, ^4J(H8H10) = ^4J(H10H12) = 1.8); 7.25 (t, 2H, H10, ^4J(H8H10) = ^4J(H10H12) = 1.8); 8.64 (s, 2H, HC=N). ^{31}P-{^1H} NMR (CDCl3, δ ppm, J Hz): 30.81 (s, 2P). Specific molar conductivity Λ_M = 176 Ω^{-1} cm^2 mol^{-1}.

[Pd{2,4-$(MeO)_2C_6H_2C(H)=N(3,5\text{-}Cl_2C_6H_3)$}(μ-Cl)]$_2$ 4. An aqueous solution of NaCl (*ca.* 10^{-2} M) was added dropwise to a solution of **2** (670 mg, 0.723 mmol) in acetone (25 cm^3) and the mixture was stirred for 24 h at 40 ºC, after which time complex **4** precipitated out as an orange solid, which was filtered off and dried *in vacuo* over P_2O_5. Yield 442.8 mg 67,89 %. Anal. Calc. for $C_{30}H_{24}Cl_6N_2O_4Pd_2$ (902.08): C, 39.9, H, 2.7, N, 3.1 %. Found: C, 39.7, H, 2.9, N, 3.3 %. IR (cm^{-1}): ν(C=N): 1591 m; ν(Pd-Cl): 312, 268 m. ^1H NMR (d_6-DMSO, d ppm, J Hz): 3.88 (s, 6H, MeO); 3.91 (s, 6H, MeO); 6.25 (d, 2H, H3); 7.01 (d, 2H, H5); 1.8); 8.30 (s, 2H, HC=N).

[Pd{2,4-$(MeO)_2C_6H_2C(H)=N(3,5\text{-}Cl_2C_6H_3)$}(μ-Br)]$_2$ 5. An aqueous solution of NaBr (*ca.* 10^{-2} M) was added dropwise to a solution of **2** (165 mg, 0.174 mmol) in acetone (25 cm^3) and the mixture was stirred for 24 h at 40 ºC, after which time complex **5**

precipitated out as an orange solid, which was filtered off and dried *in vacuo* over P_2O_5. Yield 163.8 mg 95 %. Anal. Calc. for $C_{30}H_{24}Br_2Cl_4N_2O_4Pd_2$ (990.97): C, 36.4, H, 2.4, N, 2.8 %. Found: C, 36.6, H, 2.4, N, 2.6 %. IR (cm^{-1}): ν(C=N): 1590 m; ν(Pd-Br): 183, 172 m. ^1H NMR (d_6-DMSO, δ ppm, J Hz): 3.77 (s, 6H, MeO); 3.78 (s, 6H, MeO); 6.46 (d, 2H, H3, ^3J(H3H5) = 1.4); 7.09 (d, 2H, H5, ^4J (H3H5) = 1.4); 7.38 (d, 4H, H8, H12, ^4J(H8H10) = ^4J(H10H12) = 1.8); 7.47 (t, 2H, H10, ^4J(H8H10) = ^4J(H10H12) = 1.8); 8.30 (s, 2H, HC=N).

[{Pd[2,4-$(MeO)_2C_6H_2C(H)$=N-(3,5-$Cl_2C_6H_3$)]}$_2$(μ-Cl)(μ-$Ph_2PCH_2PPh_2$)]Cl 6. To a stirred suspension of compound **4** (50.0 mg, 0.053 mmol) in acetone (*ca.* 25 cm^3), $Ph_2PCH_2PPh_2$ (dppm) (21.0 mg, 0.053 mmol) was added. The mixture was stirred for 24 h at room temperature. The resulting yellow precipitate was filtered off and dried *in vacuo*. Yield 58.4 mg 85.6 %. Anal. Calc. for $C_{55}H_{46}Cl_6N_2O_4P_2Pd_2$ (1286.47): C, 51.4, H, 3.6, N 2.2 %. Found: C, 50.9, H 3.3, N, 2.6 %. IR (cm^{-1}): ν(C=N): 1586 m; ν(Pd-Cl): 291 m. ^1H NMR ($CDCl_3$, δ ppm, J Hz): 2,98 (s, 6H, MeO); 3.73 (s, 6H, MeO); 4.30 (t, 2H, PCH_2P, ^2J(PH) =11.5; 5,35 (dd, 2H, H5, ^4J (H3H5) = 1.9, ^4J(H5P) = 6.6); 5,91 (d, 2H, H3, ^4J(H3H5) = 1.9); 7,00 (d, 4H, H8, H12, ^4J(H8H10) = ^4J(H10H12) = 1.8); 7,21 (t, 2H, H10); 8.45 (d, 2H, HC=N, ^4J(H5P) = 7.1). ^{31}P-{^1H} NMR ($CDCl_3$, δ ppm, J Hz): 31,9 (s, 2P). Specific molar conductivity Λ_M = 146 Ω^{-1} cm^2 mol^{-1}.

[{Pd[2,4-$(MeO)_2C_6H_2C(H)$=N-(3,5-$Cl_2C_6H_3$)]}(μ-Br)(μ-$Ph_2PCH_2PPh_2$)]Br 7. To a stirred suspension of compound **5** (60.0 mg, 0.062 mmol) in acetone (*ca.* 25 cm^3), $Ph_2PCH_2PPh_2$ (dppm) (24.0 mg, 0.062 mmol) was added. The mixture was stirred for 24 h at room temperature. The resulting yellow precipitate was filtered off and dried *in vacuo*. Yield 69.7 mg 81.7 %. Anal. Calc. for $C_{55}H_{46}Br_2Cl_4N_2O_4P_2Pd_2$ (1375.37): C, 48.0, H, 3.4, N, 2.0 %. Found: C, 48.0, H, 2.3, N, 3.5 %. IR (cm^{-1}): ν(C=N): 1588 m; ν(Pd-Br): 177 m. ^1H NMR ($CDCl_3$, δ ppm, J Hz): 2,98 (s, 6H, MeO); 3.73 (s, 6H, MeO); 5.03 (t, 2H, PCH_2P, ^2J(PH)=11.5; 5,38 (dd, 2H, H5, ^4J(H3H5) = 1.8, ^4J(H5P) = 7.1); 5,91 (d, 2H, H3, ^4J(H3H5) = 1.8); 7,00 (d, 4H, H8, H12, ^4J(H8H10) = ^4J(H10H12) = 1.8); 7,24 (t, 2H, H10); 8.14 (d, 2H, HC=N, ^4J(H5P) = 6.6). ^{31}P-{^1H} NMR ($CDCl_3$, δ ppm, J Hz): 26,0 (s, 2P). Specific molar conductivity Λ_M = 170 Ω^{-1} cm^2 mol^{-1}.

[{Pd[2,4-$(MeO)_2C_6H_2C(H)$=N-(3,5-$Cl_2C_6H_3$)]}$_2$(μ-*trans*-Ph_2PCH=$CHPPh_2$)(Cl_2)] 8. To a stirred suspension of **4** (27.0 mg, 0.020 mmol) in acetone (*ca.* 25 cm^3), *trans*-Ph_2PCH=$CHPPh_2$ (*trans*-dppe) (8.1 mg, 0.020 mmol) was added. The mixture was stirred for 24 h at room temperature. The resulting yellow precipitate was filtered off and dried *in vacuo*. Yield 20.1 mg 77.3 %. Anal. Calc. for $C_{56}H_{46}Cl_6N_2O_4P_2Pd_2$ (1298.48): C, 51.8, H, 3.6, N, 2.2. Found: C, 48.5, H, 3.2, N, 2.2. IR (cm^{-1}): ν(C=N): 1611 m; ν(Pd-Cl): 291 m. ^1H NMR ($CDCl_3$, δ ppm, J Hz): 2.88 (s, 6H, MeO); 3.73 (s, 6H, MeO); 5,59 (br, 2H, H5); 5,93 (d, 2H, H3, ^4J(H3H5) = 1.8); 6.51 (m, 2H, PCH=CHP); 7,20 (s, 4H, H8, H12); 8.50 (d, 2H, HC=N); ^4J (H5P) = 7.0). ^{31}P-{^1H} NMR ($CDCl_3$, δ ppm, J Hz): 37,5 (s, 2P).

[{Pd[2,4-$(MeO)_2C_6H_2C(H)$=N-(3,5-$Cl_2C_6H_3$)]}$_2$(μ-*trans*-Ph_2PCH=$CHPPh_2$)(Br_2)] 9. To a stirred suspension of **4** (27.0 mg, 0.027 mmol) in acetone (*ca.* 25 cm^3), *trans*-Ph_2PCH=$CHPPh_2$ (*trans*-dppe) (11 mg, 0.028 mmol) was added. The mixture was stirred for 24 h at room temperature. The resulting yellow precipitate was filtered off and dried *in vacuo*. Yield 34.7 mg 89.4 %. Anal. Calc. for $C_{56}H_{46}Br_2Cl_4N_2O_4P_2Pd_2$ (1387.38): C, 48.5, H, 3.3, N, 2.0. Found: C, 48.5, H, 3.2, N, 2.2. IR (cm^{-1}): ν(C=N): 1612 m; ν(Pd-Br): 176 m. ^1H NMR ($CDCl_3$, δ ppm, J Hz): 2.89 (s, 6H, MeO); 3.73 (s, 6H, MeO); 5,61 (br, 2H, H5); 5,93 (d, 2H, H3, ^4J(H3H5) = 1.7); 6.54 (m, 2H, PCH=CHP); 7,24 (s, 4H, H8, H12); 8.48 (br, 2H, HC=N). ^{31}P-{^1H} NMR ($CDCl_3$, δ ppm, J Hz): 39,3 (s, 2P).

[Pd{2,4-$(MeO)_2C_6H_2C(H)$=N(3,5-$Cl_2C_6H_3$)}(Cl)(PPh_3)] 10. To a stirred suspension of **4** (50.0 mg, 0.055 mmol) in acetone (*ca.* 25 cm^3), PPh_3 (29.0 mg, 0.111 mmol) was added. The mixture was stirred for 24 h at room temperature and after which the solution was filtered off and after concentration afforded the final product which was recrystallized from chloroform/n-hexane. The resulting orange precipitate was filtered off and dried *in vacuo*. Yield 42.7 mg 54 %. Anal. Calc. for $C_{33}H_{27}Cl_3NO_2PPd$ (713.33): C, 55.6, H, 3.8, N, 2.0 %. Found: C, 55.6, H, 3.5, N, 2.2 %. IR (cm^{-1}): ν(C=N): 1585 m sh; ν(Pd-Cl): 294 m. ^1H NMR ($CDCl_3$, δ ppm, J Hz): 3.76 (s, 3H, MeO); 2.94 (s, 3H, MeO); 5,67 (dd, ^1H, H5, ^4J(H3H5) = 1.8, ^4J(H5P) = 6.7); 5,96 (d, 1H, H3, ^4J(H3H5) = 1.8); 7,18 (t, 1H, H10, ^4J (H8H10) = ^4J(H10H12) = 1.9); 7,27 (d, 2H, H8, H12, ^4J(H8H10) = ^4J(H10H12) = 1.9); 8.52 (d, 1H, HC=N, ^4J(HP) = 7.0); ^{31}P-{^1H} NMR ($CDCl_3$, δ ppm, J Hz): 23.78 (s, 1P).

[Pd{2,4-$(MeO)_2C_6H_2C(H)$=N(3,5-$Cl_2C_6H_3$)}(Br)(PPh_3)] 11. To a stirred suspension of **5** (29.0 mg, 0.029 mmol) in acetone (*ca.* 25 cm^3), PPh_3 (15.0 mg, 0.057 mmol) was added. The mixture was stirred for 24 h at room temperature and after which the solution was filtered off and after concentration afforded the final product which was recrystallized from chloroform/n-hexane. The resulting orange precipitate was filtered off and dried *in vacuo*. Yield 40.9 mg 93 %. Anal. Calc. for $C_{33}H_{27}BrCl_2NO_2PPd$ (757.78): C, 52.3, H, 3.6, N, 1.8 %. Found: C, 52.1, H, 3.6, N, 1.8 %. IR (cm^{-1}): ν(C=N): 1584 m sh; ν(Pd-Br): 204 m. ^1H NMR ($CDCl_3$, δ ppm, J Hz): 3.76 (s, 3H, MeO); 2.94 (s, 3H, MeO); 5,64 (dd, 1H, H5, ^4J(H3H5) = 2.0, ^4J (H5P) = 6.9); 5,96 (d, 1H, H3, ^4J(H3H5) = 2.0); 7,18 (t, 1H, H10, ^4J (H8H10) = ^4J(H10H12) = 1.8); 7,25 (d, 2H, H8, H12, ^4J(H8H10) = ^4J(H10H12) = 1.8); 8.53 (d, 1H, HC=N, ^4J(HP) = 7.0). ^{31}P-{^1H} NMR ($CDCl_3$, δ ppm, J Hz): 44.57 (s, 1P).

[Pd{2,4-$(MeO)_2C_6H_2C(H)$=N(3,5-$Cl_2C_6H_3$)}(Br)(PPh_3)$_2$] 12. Compound **12** was prepared analogously from **5** (30.0 mg, 0.031 mmol) and PPh_3 (40.0 mg, 0.124 mmol). Yield 65.9 mg 52.1 %. Anal. Calc. for $C_{51}H_{42}BrCl_2NO_2P_2Pd$ (1020.06): C, 60.1, H, 4.2, N, 1.4. Found: C, 60.1, H, 4.3, N, 1.4 %. IR (cm^{-1}): ν(C=N): 1556 m; ν (Pd-Br) 203 m. ^1H NMR ($CDCl_3$, δ ppm, J Hz): 3.76 (s, 3H, MeO); 2.94 (s, 3H, MeO); 5,65 (d, 1H, H5, ^4J(H3H5) = 1.9); 5,96 (d, 1H, H3, ^4J(H3H5) = 1.9); 8.53 (s, 1H, HC=N); 7,25 (d, 2H, H8, H12, ^4J (H8H10) = ^4J(H10H12) = 1.8); 7,18 (t, 1H, H10, ^4J(H8H10) = ^4J (H10H12) = 1.9);. ^{31}P-{^1H} NMR ($CDCl_3$, δ ppm, J Hz): 23.66 (s, P).

[{Pd[2,4-$(MeO)_2C_6H_2C(H)$=N-(3,5-$Cl_2C_6H_3$)]}$_2$(μ-$Ph_2P(CH_2)_3PPh_2$)(Cl_2)] 13. To a stirred suspension of **4** (39.0 mg, 0.045 mmol)

in acetone (*ca.* 25 cm^3), $Ph_2P(CH_2)_3PPh_2$ (dppp) (22 mg, 0.045 mmol) was added. The mixture was stirred for 24 h at room temperature. The resulting orange precipitate was filtered off and dried *in vacuo*. Yield 20.1 mg 78.3 %. Anal. Calc. for $C_{57}H_{50}Cl_6N_2O_4P_2Pd_2$ (1314.52): C, 52.1, H, 3.8, N, 2.1 %. Found: C, 52.5, H, 3.7, N, 2.2 %. IR (cm^{-1}): ν(C=N): 1585 m sh; u(Pd-Cl) 287 m. ^{1}H NMR ($CDCl_3$, δ ppm, J Hz): 3.00 (s, 6H, MeO); 3.75 (s, 6H, MeO); 5,68 (dd, 2H, H5, ^{4}J(H3H5) = 1.9, ^{4}J(H5P) = 6.7); 5,66 (d, 2H, H3, ^{4}J(H3H5) = 1.9); 7,27 (br, 4H, H8, H12); 8.45 (d, 2H, HC=N); ^{4}J(H5P) = 6.8). ^{31}P-{^{1}H} NMR ($CDCl_3$, δ ppm, J Hz): 36,5 (s, 2P).

[{Pd[2,4-$(MeO)_2C_6H_2C(H)$=N-(3,5-$Cl_2C_6H_3$)]}$_2$(μ-$Ph_2P(CH_2)_3PPh_2$)(Br_2)] 14. The diphosphine dppp (7.0 mg, 0.017 mmol) was added to a suspension of **5** (17.0 mg, 0.017 mmol) in acetone (*ca.* 25 cm^3). The mixture was stirred for 24 h at room temperature after which the solution was filtered off and after concentration was recrystallized from acetone/n-hexane to give a yellow solid witch was filtered off and dried *in vacuo*. Yield 20.1 mg 84.1 %Anal. Calc. for $C_{57}H_{50}Br_2Cl_4N_2O_4P_2Pd_2$ (1403.42): C, 48.8, H, 3.6, N, 2.0. Found: C, 49.1, H, 3.3, N, 2.0 %. IR (cm^{-1}): ν(C=N): 1588 m; ν(Pd-Br): 201 m. ^{1}H NMR ($CDCl_3$, δ ppm, J Hz): 3.74 (s, 6H, MeO); 2.98 (s, 6H, MeO) 5,65 (dd, 2H, H5, ^{4}J(H3H5) = 1.9, ^{4}J(H5P) = 6.3); 5,94 (d, 2H, H3, ^{4}J(H3H5) = 1.9); 7,18 (d, 4H, H8, H12, ^{4}J(H8H10) = ^{4}J(H10H12) = 1.9); 7,25 (t, 2H, H10, ^{4}J(H8H10) = ^{4}J(H10H12) = 1.9); 8.44 (d, 2H, HC=N, ^{4}J(H5P) = 6.7). ^{31}P-{^{1}H} NMR ($CDCl_3$, δ ppm, J Hz): 35,9 (s, 2P).

[Pd{2,4-$(MeO)_2C_6H_2C(H)$=N-(3,5-$Cl_2C_6H_3$)}$_2$(μ-$Ph_2P(CH_2)_4PPh_2$)(Cl_2)] 15. To a stirred suspension of **4** (50.0 mg, 0.055 mmol) in acetone (*ca.* 25 cm^3), $Ph_2P(CH_2)_3PPh_2$ (dppb) (24 mg, 0.056 mmol) was added. The mixture was stirred for 24 h at room temperature. The resulting yellow precipitate was filtered off and dried *in vacuo*. Yield 49.6 mg 67.0 %. Anal. Calc. for $C_{58}H_{52}Cl_6N_2O_4P_2Pd_2$ (1328.55): C, 52.4, H, 4.0, N, 2.1 %. Found: C, 52.1, H, 3.7, N, 2.1 %. IR (cm^{-1}): ν(C=N): 1611 w; ν(Pd-Cl) 293: m. ^{1}H NMR ($CDCl_3$, δ ppm, J Hz): 3.00 (s, 6H, MeO); 3.74 (s, 6H, MeO); 5,69 (br, 2H, H5); 5,95 (br, 2H, H3); 6,55 (d, 4H, H8, H12, ^{4}J(H8H10) = ^{4}J(H10H12) = 1.8); 6,73 (t, 2H, H10, ^{4}J(H8H10) = ^{4}J(H10H12) = 1.9); 8.47 (br, 2H, HC=N); ^{31}P-{^{1}H} NMR ($CDCl_3$, d ppm, J Hz): 33,1 (s, 2P).

[Pd{2,4-$(MeO)_2C_6H_2C(H)$=N-(3,5-$Cl_2C_6H_3$)}($Ph_2PCH_2CH_2$)PPh_2-P,P)][PF_6] 16. $Ph_2PCH_2CH_2PPh_2$ (dppe) (45.0 mg, 0.112 mmol) was added to a suspension of **4** (50.0 mg, 0.055 mmol) in acetone (*ca.* 25 cm^3). The mixture was stirred for 2 h at room temperature and then NH_4PF_6 (6.9 mg, 0.042 mmol) was added. The mixture was stirred for a further 20 h at room temperature after which the solution was filtered off and after concentration was recrystallized from chloroform/n-hexane to give a yellow solid witch was filtered off and dried *in vacuo*. Yield 80.0 mg 81.2 %. Anal. Calc. for $C_{41}H_{36}Cl_2F_6NO_2P_3Pd$ (958.97): C, 51.4, H, 3.8, N, 1.5 %. Found: C, 51.7, H, 3.6, N, 1.4 %. IR (cm^{-1}): ν(C=N): 1585 m. ^{1}H NMR ($CDCl_3$, δ ppm, J Hz): 3.20 (s, 3H, MeO); 3.78 (s, 3H, MeO); 5,88 (ddd, 1H, H5, ^{4}J(H3H5) = 2.0, ^{4}J(H5Pc) = 5.8, ^{4}J(H5Pt) = 8.2); 6,08 (d, 1H, H3, ^{4}J(H3H5) = 2.0); 6,61 (d, 2H, H8, H12, ^{4}J(H8H10) = ^{4}J(H10H12) = 1.8); 6,86 (t, 1H, H10, ^{4}J(H8H10) = ^{4}J(H10H12) = 1.8); 8.36 (dd, 1H, HC=N, ^{4}J(HPc) = 1.8, ^{4}J(H5Pt) = 6.9). ^{31}P-{^{1}H} NMR ($CDCl_3$, δ ppm, J Hz): 45.6 (d, 1P, J(PP) = 27.6); 63.1 (d, 1P, J(PP) = 27.6). Specific molar conductivity Λ_M = 230 Ω^{-1} cm^2 mol^{-1}.

[Pd{2,4-$(MeO)_2C_6H_2C(H)$=N-(3,5-$Cl_2C_6H_3$)}($Ph_2P(CH_2)_4PPh_2$-*P,P*)][PF_6] 17. Compound **17** was prepared similarly from **4** (50.0 mg, 0.055 mmol) and dppb (48.0 mg, 0.112 mmol). Yield 97.0 mg 81.2 %. Anal. Calc. for $C_{43}H_{40}Cl_2F_6NO_2P_3Pd$ (987.02): C, 52.3, H, 4.1, N, 1.4 %. Found: C, 51.9, H, 4.3, N, 1.6 %. IR (cm^{-1}): ν(C=N): 1591 d. ^{1}H NMR ($CDCl_3$, δ ppm, J Hz): 3.11 (s, 3H, MeO); 3.75 (s, 3H, MeO); 5,80 (ddd, 1H, H5, ^{4}J(H3H5) = 1.9, ^{4}J(H5Pc) = 6.2, ^{4}J(H5Pt) = 8.9); 6,02 (d, 1H, H3, ^{4}J(H3H5) = 1.9); 6,29 (d, 2H, H8, H12, ^{4}J(H8H10) = ^{4}J(H10H12) = 1.8); 6,83 (t, 1H, H10, ^{4}J(H8H10) = ^{4}J(H10H12) = 1.8; 8.23 (dd, 1H, HC=N, ^{4}J(HPc) = 1.1, ^{4}J(H5Pt) = 6.6)). ^{31}P-{^{1}H} NMR ($CDCl_3$, δ ppm, J Hz): 0.5 (d, 1P, J(PP) = 57.2); 27.3 (d, 1P, J(PP) = 57.2). Specific molar conductivity Λ_M = 176 Ω^{-1} cm^2 mol^{-1}.

[Pd{2,4-$(MeO)_2C_6H_2C(H)$=N-(3,5-$Cl_2C_6H_3$)}($Ph_2PCH_2PPh_2$-*P,P*)][PF_6] 18. Compound **18** was prepared similarly to from $Ph_2PCH_2PPh_2$ (32.0 mg, 0.083 mmol) and **5** (42.0 mg, 0.042 mmol). Yield 39.2 mg 97.5 %. Anal. Calc. for $C_{40}H_{34}Cl_2F_6NO_2P_3Pd$ (944.94): C, 50.8, H, 3.6, N, 1.5 %. Found: C, 50.9, H, 3.3, N, 1.8 %. IR (cm^{-1}): ν(C=N): 1591 m. ^{1}H NMR ($CDCl_3$, δ ppm, J Hz): 3.22 (s, 3H, MeO); 3.76 (s, 3H, MeO); 4.18 (dd, 2H, PCH_2P, ^{2}J(HP) = 11.3, ^{2}J(HP) = 8.7); 5,79 (ddd, 1H, H5, ^{4}J(H3H5) = 2.0, ^{4}J(H5Pc) = 8.3, ^{4}J(H5Pt) = 9.9); 6,03 (d, 1H, H3, ^{4}J(H3H5) = 2.0); 8.38 (d, 1H, HC=N, ^{4}J(HP) = 5.5); 6,91 (d, 2H, H8, H12, ^{4}J(H8H10) = ^{4}J(H10H12) = 1.9); 7,01 (t, 1H, H10, ^{4}J(H8H10) = ^{4}J(H10H12) = 1.9). ^{31}P-{^{1}H} NMR ($CDCl_3$, δ ppm, J Hz): -8.4 (d, 1P, J(PP) = 68.3); -32.5 (d, 1P, J(PP) = 68.3). Specific molar conductivity Λ_M = 123 Ω^{-1} cm^2 mol^{-1}.

[Pd{2,4-$(MeO)_2C_6H_2C(H)$=N-(3,5-$Cl_2C_6H_3$)}$_2$(*cis*-Ph_2PCH=$CHPPh_2$-*P,P*)][Br] 19. *cis*-Ph_2PCH=$CHPPh_2$ (40.0 mg, 0.101 mmol) was added to a suspension of **5** (50.0 mg, 0.050 mmol) in acetone (*ca.* 25 cm^3). The mixture was stirred for 22 h at room temperature after which the solution was filtered off and after concentration was recrystallized from chloroform/n-hexane to give a yellow solid witch was filtered off and dried *in vacuo*. Yield 68.3 mg 76.6 %. Anal. Calc. for $C_{41}H_{34}BrCl_2NO_2P_2Pd$ (891.89): C, 55.2, H, 3.8, N, 1.6 %. Found: C, 55.6, H, 3.5, N, 1.5 %. IR (cm^{-1}): ν(C=N): 1608 w. ^{1}H NMR ($CDCl_3$, δ ppm, J Hz): 3.41 (s, 3H, MeO); 3.71 (s, 3H, MeO); 6,50 (ddd, 1H, H5, ^{4}J(H3H5) = 2.0, ^{4}J(H5Pc) = 4.7, ^{4}J(H5Pt) = 7.9); 6,03 (d, 1H, H3, ^{4}J(H3H5) = 2.0); 6,29 (d, 2H, H8, H12, ^{4}J(H8H10) = ^{4}J(H10H12) = 1.8); 6,90 (t, 1H, H10, ^{4}J(H8H10) = ^{4}J(H10H12) = 1.8); 8.13 (d, 1H, HC=N, ^{4}J(HP) = 1.4). ^{31}P-{^{1}H} NMR ($CDCl_3$, δ ppm, J Hz): 51.2 (d, 1P, J(PP) = 16.7); 59.5 (d,1P, J (PP) = 16.7) Specific molar conductivity Λ_M = 163 Ω^{-1} cm^2 mol^{-1}.

3. Results and Discussion

The complexes and reaction patterns are shown in **Schemes 1** and **2**. The compounds described in this paper were characterized by microanalytical measurements (C, H, N; the error being an absolute

0.3 %) by IR and by ^{1}H and ^{31}P-{^{1}H} NMR spectroscopy, and (in part) by X-ray diffraction analysis; crystallographic data are in **Table 1**. Treatment of the ligand **1** with palladium(II) acetate in toluene at 60 °C for 12 h and work up of the mixture gave complex **2** as an orange solid (see Experimental). The IR spectrum showed the band for the ν (C=N) stretch at lower frequency than in the ligand spectrum [32] and an up-field shift of the *H*C=N the resonance in the ^{1}H NMR spectrum; these data concur with Pd-N bond formation. [33] The ν_{as}(COO) and ν_{s}(COO) values were in agreement with bridging acetate groups; [34] the proton NMR spectrum showed a singlet resonance *ca.* 2.00 ppm (6H) which was ascribed to the equivalent methyl acetate protons, reflecting a *trans* geometry of the cyclometallated moieties, and absence of the H6 resonance consequent upon metallation of the ligand.

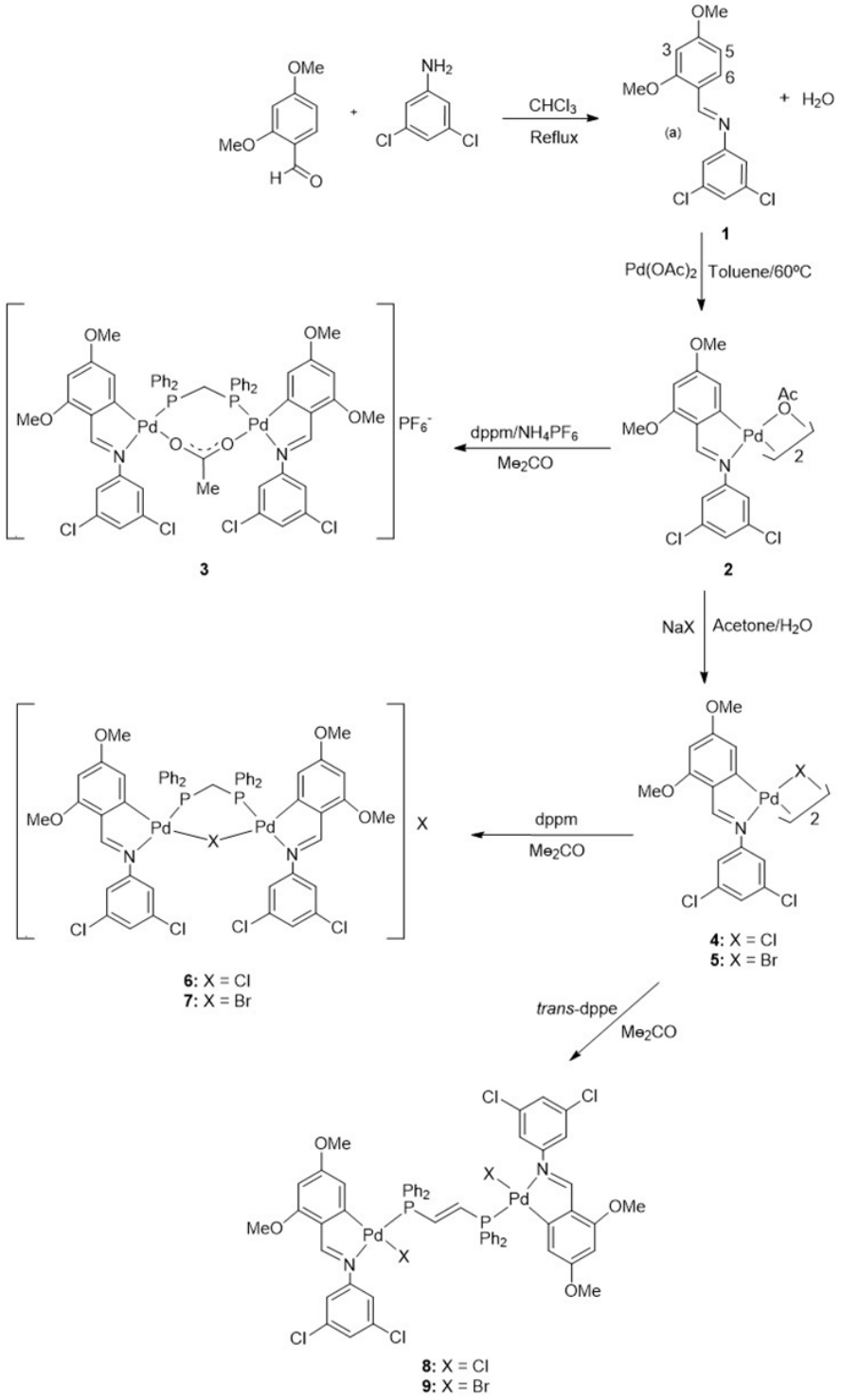

Scheme 1 | Reaction sequence leading to the syntheses of the compounds **2-9**.

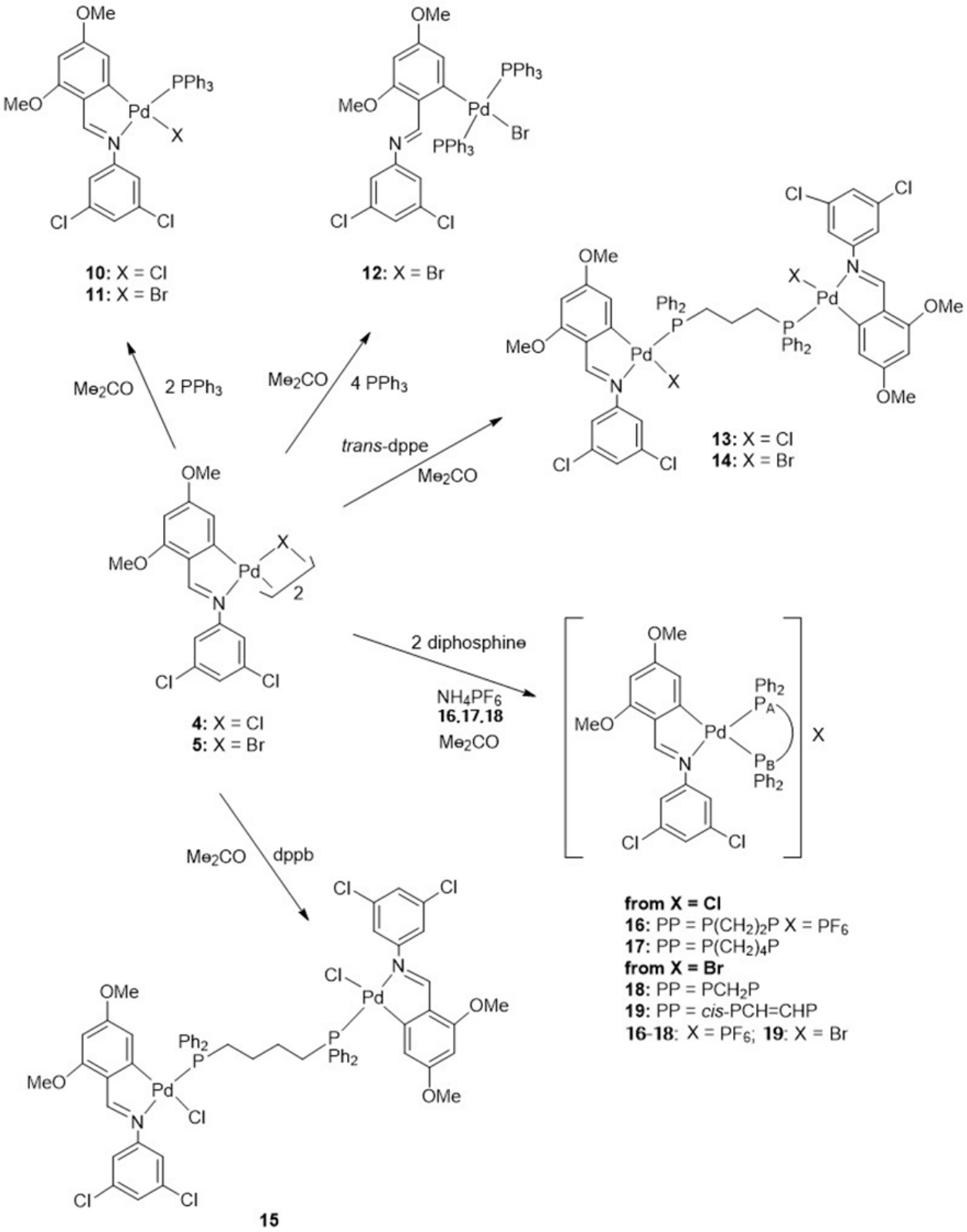

Scheme 2 | Reactivity of the dinuclear halide-bridged complexes.

Table 1 | Crystallographic data for **2**, **3**, **9** and **12**.

Compound	**2**	**3**	**9**	**12**
Empirical formula	$C_{68}H_{60}Cl_8N_4O_{16}Pd_4$	$C_{58.25}H_{50.25}Cl_{7.75}F_6N_2O_6P_3Pd_2$	$C_{60}H_{50}Br_2Cl_{16}N_2O_4P_2Pd_2$	$C_{52}H_{43}BrCl_5NO_2P_2Pd$
Formula weight	1898.40	1568.70	1864.78	1139.3
Temperature/K	100(2)	100.0	293(2)	293(2)
Crystal system	triclinic	monoclinic	triclinic	monoclinic
Space group	P-1	c2/c	P-1	P2(1)/C
a/Å	9.5409(13)	21.057(2)	9.125(5)	13.0621(4)
b/Å	14.8059(18)	20.817(2)	12.412(5)	35.3990(12)
c/Å	26.074(3)	32.852(3)	16.598(5)	12.3864(4)
α/°	97.798(2)	90	96.758(5)	90
β/°	92.009(2)	97.016(2)	96.150(5)	117.9930(10)
γ/°	93.866(2)	90	94.181(5)	90
Volume/Å^3	3637.3(8)	14292(3)	1849.1(14)	5057.2(3)
Z	2	8	1	4
ρ_{calc}g/cm^3	1.733	1.458	1.675	1.496
μ/mm^{-1}	1.335	0.921	2.232	1.525
F(000)	1888	6276	920	2296
Crystal size/mm^3	0.28 × 0.14 × 0.08	0.32 x 0.19 x 0.15	0.33 x 0.15 x 0.10	0.44 x 0.30 x 0.21
Radiation	Mo Kα (λ = 0.71073)	Mo Kα (λ = 0.71073)	Mo Kα (λ = 0.71073)	Mo Kα (λ = 0.71073)
2θ /°	1.69 to 28.28	1.25 to 28.30	1.24 to 28.29	1.15 to 28.29
Index ranges	-12 ≤ h ≤ 12, -19 ≤ k ≤ 19, -34 ≤ l ≤ 34	-28 ≤ h ≤ 26, -23 ≤ k ≤ 27, -43 ≤ l ≤ 23	-12 ≤ h ≤ 10, -16 ≤ k ≤ 16, -22 ≤ l ≤ 22	-17 ≤ h ≤ 10, -46 ≤ k ≤ 47, -16 ≤ l ≤ 16
Reflections collected	66916	52294	18238	49417
Independent reflections	17756 [R_{int} = 0.0351]	17676 [R_{int} = 0.1983]	8920 [R(int) = 0.0227]	12517 [R(int) = 0.0357]
Data/restraints/parameters	17756 / 0 / 901	17676 / 30 / 826	8920 / 48 / 455	12517 / 48 / 607
Goodness-of-fit on F^2	1.076	0.990	1.140	1.067
Final R indexes [I>=2σ (I)]	R_1 = 0.0561, wR_2 = 0.1328	R_1 = 0.0634, wR_2 = 0.1682	R_1 = 0.0338, wR_2 = 0.0902	R_1 = 0.0391, wR_2 = 0.1075
Final R indexes [all data]	R_1 = 0.1033, wR_2 = 0.1650	R_1 = 0.1436, wR_2 = 0.2059	R_1 = 0.0542, wR_2 = 0.1234	R_1 = 0.0645, wR_2 = 0.1368
Largest diff. peak/hole/e Å^{-3}	2.667/-1.463	1.262/-0660	0.643/-0.744	1.63/-1.91

Crystal structure of 2

Appropriate crystals of **2** were precipitated by recrystallization from a dichloromethane-*n*-hexane solution. The structure of **2** is given in **Figure 1** and the caption contains selected interatomic distances and angles for **2**. Crystallographic data are given in **Table 1**. The crystals consist of discrete molecules separated by normal van der Waals distances. The asymmetric unit comprises two molecules of **2**. The molecular configuration is a dinuclear anti isomer with the cyclopalladated moieties in an open book geometry supported by two acetate-bridging ligands linking the palladium atoms. [35] The Pd-Pd distances of 2.8937(7) and 2.9050(7) may be regarded as nonbonding given the covalent radius of square-planar Pd(II) of 1.31 Å. [36] Nevertheless, in view of the palladium van der Waals radius of 1.61 Å some interaction may exist. [37] The geometry around palladium is slightly distorted square-planar with coordination to a nitrogen atom of the imine group, an *ortho* carbon of the phenyl ring, and two oxygen atoms, one from each of the bridging acetates. The two [C,N] metallacycles are in an open book disposition with the close-to-parallel ligands lying above one another consequent on the geometry of the two mutually *cis* acetate ligands. The ensuing ligand repulsions on the *trans* side of each molecule originates tilting of the palladium coordination planes at angles of 26.0 and 25.5°.

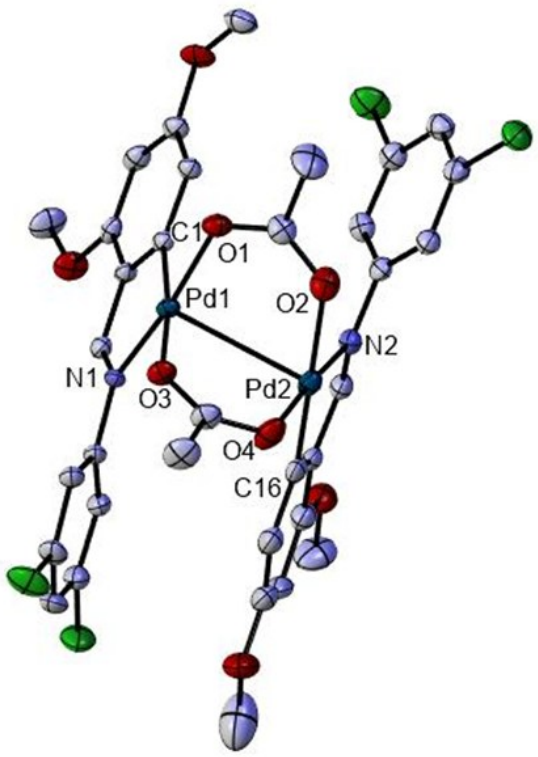

Figure 1 | ORTEP drawing of compound **2** with thermal ellipsoid plot shown at 50 % probability level. Hydrogen atoms and solvent molecules have been omitted for clarity. Selected bond lengths (Å) and angles (°): C(1)-Pd(1) 1.971(5); N(1)-Pd(1) 2.055(4); O(1)-Pd(1) 2.033(4); O(3)-Pd(1) 2.162(4); C(16)-Pd(2) 1.928(6); N(2)-Pd(2) 2.018(5); O(2)-Pd(2) 2.138(4); O(4)-Pd(2) 2.042(4). C(1)-Pd(1)-N(1) 81.1(2); C(1)-Pd(1)-O(5) 164.6(2); N(1)-Pd(1)-O(5) 88.91(17); C(1)-Pd(1)-P(1) 102.23(17); N(1)-Pd(1)-P(1) 166.07(13); O(5)-Pd(1)-P(1) 90.27(12); C(16)-Pd(2)-O(6) 172.79(19); C(16)-Pd(2)-N(2) 81.2(2); O(6)-Pd(2)-N(2) 92.07(16); C(16)-Pd(2)-P(2) 94.42(16); O(6)-Pd(2)-P(2) 92.51(12); N(2)-Pd(2)-P(2) 173.27(13).

The palladium-nitrogen bonds of Pd(1)-N(1) 2.055(4), Pd(2)-N(2) 2.018, Pd(3)-N(3) 2.027(5) and Pd(4)-N(4) 2.046(4) Å, concur with the value based on the covalent radii for both atoms, 1.31 Å and 0.701 Å, respectively, whilst the palladium-carbon bonds Pd(1)-C(1) 1.971(5), Pd(2)-C(16) 1.928(6), Pd(3)-C(35) 1.072(6) and Pd(4)-C(50) 1.972(5) show lower values than expected 2.081 Å [C(sp^2) 0.771 Å], pointing to an important amount of multiple bonding. As for the bonds to oxygen each metal atom shows two distinct Pd-O distances consequent on the differing *trans* influence of the aromatic carbon atom and the imine nitrogen giving lengthening of the Pd-O band *trans* to carbon; *e.g.*, Pd(1)-O(1) 2.033(4) Å and Pd(1)-O(3) 2.162(4) Å, the latter *trans* to carbon. The sum of angles at each palladium is *ca.* 360°, with moderate divergence form the ideal square-planar environment in the aftermath of chelation by the metallacycle, as shown by the diminished N-Pd-C bond angles, *e.g.*, C(1)-Pd(1)-N(1) 81.05(19) Å. Treatment of compound **2** with the diphosphine $Ph_2PCH_2PPh_2$ (dppm) in 1:1 molar ratio and NH_4PF_6 yielded complex **3**. Two different ligands, *i.e.*, an acetate anion and a tertiary diphosphine span across the two metal centers with the oxygen and phosphorus donors *trans* to the aryl carbon and imine nitrogen atoms, respectively. The values for the ν_{as}(COO) and ν_s(COO) bands in the IR spectrum concur with its bridging coordination. Only one collection of signals was observed in the ^{1}H and ^{31}P NMR (a singlet resonance) spectra in compliance with the symmetric nature of the compound. The resonances at 3.76 and 3.00 ppm were assigned to the MeO groups, the latter high-field shifted due to the shielding effect of the phosphine phenyl rings; this concurs with a phosphorus trans to nitrogen geometry. The signal at 5.32 ppm was assigned as a multiplet to the PCH_2P protons owing to the AA´XX´ spin system. The conductivity measurement in dry acetonitrile, Λ_M = 176 W^{-1} cm^2 mol^{-1}, indicates a 1:1 electrolyte species. [38]

Crystal structure of 3

Suitable crystals of **3** were grown from a chloroform solution. The crystal structure of **3** and selected interatomic distances and angles for **3** are depicted in **Figure 2**. The asymmetric unit comprises one molecule of **3**, and the structure consists of discrete molecules with the palladium(II) atoms bonded in a slightly distorted square-planar environment to two mutually perpendicular pairs of [O,O] and [P,P] donors, pertaining to bridging acetate and bis (diphenylphosphino)methane ligands, respectively; the former are both *trans* to the phenyl carbons and the latter to the imine nitrogens, with an angle between the [Pd(1)Pd(2)O(5)O(6)] and [Pd(1) Pd(2)P(1)P(2)] planes of 89.91°. The bond distances and angles are within the predicted values (*vide supra*); but it should be noted that as opposed to the structure of **2** the two oxygen donors are *trans* to

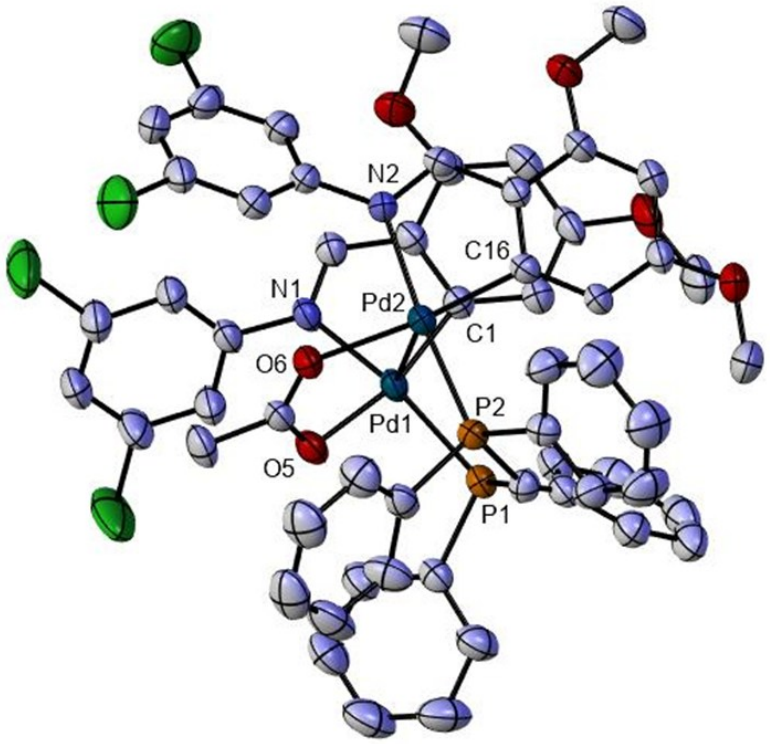

Figure 2 | ORTEP drawing of compound **3** with thermal ellipsoid plot shown at 50 % probability level. Hydrogen atoms and solvent molecules have been omitted for clarity. Selected bond lengths (Å) and angles (°): C(1)-Pd(1) 2.006(5); N(1)-Pd(1) 2.054(5); O(5)-Pd(1) 2.131(4); P(1)-Pd(1) 2.2724(17); C(16)-Pd(2) 2.023(5); N(2)-Pd(2) 2.119(4); O(6)-Pd(2) 2.108(4); P(2)-Pd(2) 2.2595(15). C(1)-Pd(1)-O(1) 89.82(19); C(1)-Pd(1)-N(1) 81.05(19); O(1)-Pd(1)-O(3) 88.32(15); N(1)-Pd(1)-O(3) 100.46(16); O(1)-Pd(1)-N(1) 170.62(16); C(1)-Pd(1)-O(3) 172.60(18); C(16)-Pd(2)-N(2) 82.2(2); C(16)-Pd(2)-(4) 92.8(2); N(2)-Pd(2)-O(2) 96.80(17); O(4)-Pd(2)-O(2) 88.21(18); N(2)-Pd(2)-O(4) 174.83(18; C(16)-Pd(2)-O(2) 178.9(2).

phenyl carbons, hence the lengthening of both Pd-O linkages Pd(1) -O(5) and Pd(2)-O(6) of 2.131(4) and 2.108(4) Å, respectively. Likewise, similar elongated Pd-N distances should be assumed from the theoretical value of 2.011 Å (*vide supra*), yet only one is significantly longer, *i.e.*, Pd(2)-N(2) of 2.119(4) Å. We trust this to be due to the somewhat reduced N-Pd-N angle at Pd(1) which hinders the phosphorus *trans* influence sufficiently so as to diminish the Pd(1)-N(1) length to only a minor extent of 2.054(5) Å; *cf.* N(1) -Pd(1)-P(1) 166.07(13)° and N(2)-Pd(2)-P(2) 173.27°. Furthermore, the bonding assembly of the bridging ligands sets the Schiff base ligands in a "*cis*" nature, *i.e.*, with the metallated rings pointing in the same direction; in contrast to the structure of **2** with a '*trans*' arrangement of the palladated ligands. Reaction of **2** in acetone with aqueous sodium chloride or bromide readily gave *via* metathesis the ensuing halide-bridged compounds **4** and **5**, respectively, which were fully characterized. The spectroscopic data are like the parent compound **1**, save for the Pd-X bonds resulting from exchange of the bridging units, and they are in agreement with the absence of the acetate ligands (see Experimental). The IR spectra showed two ν(Pd-X) bands, consistent with an asymmetric Pd_2X_2 bridging unit: υ(Pd-Cl) 312, 268 cm^{-1}, 4; υ(Pd-Br) 183, 172 cm^{-1}, **5**; the higher frequency stretch was assigned to the Pd-X bond *trans* to the nitrogen atom because of the disparate *trans* influence of the C (aryl) and N(imine) atoms consistent with an asymmetric Pd_2X_2 bridging unit. Reaction of dppm or with (*trans*-dppe) in 1:1 molar ratios gave **6** and **7**, on the one hand (**Scheme 1**), and **8** and **9**, on the other (**Scheme 1**), respectively. Likewise, treatment of **4** and **5** with $Ph_2P(CH_2)_3PPh_2$ (dppp) or $Ph_2P(CH_2)_4PPh_2$ (dppb), gave compounds **13-14** and **15** (X = Cl) (**Scheme 2**), also respectively; all compounds were fully characterized. The ^{31}P NMR showed a singlet resonance for the two equivalent phosphorus nuclei; accordingly, for symmetry reasons only one set of signals for the proton resonances was present. The phosphorus donors are *trans* to the nitrogen atoms (*vide supra*). The *H*C=N resonance was a doublet (except for **9** and **15**) due to coupling to the nucleus with $^4J(PH)$ *ca.* 6-7 ppm. The PCH=CHP signals were assigned as multiplets for the AA´XX´ spin systems in both cases. The IR spectra showed the υ (Pd-X) stretches at slightly lower frequencies due to the *trans* influence of the aryl carbon atom, υ(Pd-Cl) 291 cm^{-1}, **6**; υ(Pd-Br) 177 cm^{-1}, **7**; υ(Pd-Cl) 291 cm^{-1}, **8**; υ(Pd-Br) 176 cm^{-1}, **9**; υ(Pd-Cl) 287 cm^{-1}, **13**; υ(Pd-Br) 201 cm^{-1}, **14**; υ(Pd-Cl) 293 cm^{-1}, **15**. The conductivity measurement in dry acetonitrile Λ_M = 146 and 170 Ω^{-1} cm^2 mol^{-1}, for **6** and **7**, respectively, suggest 1:1 electrolyte species. Treatment of **4** and **5** with triphenylphosphine in 1:2 or 1:4 ratio in acetone yielded the mononuclear complexes compounds **10-11** and **12**, respectively as air-stable solids, characterized accordingly. The spectroscopic data for **10-11** point towards a *trans* arrangement of the nitrogen and phosphorus atoms giving a $^4J(PH)$ of 7 Hz; the C

(4)-MeO resonance was shifted to higher field in a similar fashion as for the compounds with the diphosphine ligands (*vide supra*). As for complex **12** the incoming second phosphine ligand cleaves the Pd-N bond with opening of the metallacycle ring, but keeping the halide ligand bonded to the metal, in non-electrolyte species, shown by the presence of the corresponding υ(Pd-X) stretches in the IR spectra. The phosphorus resonance in the ^{31}P NMR spectrum was a singlet resonance in accordance with a *trans* P-Pd-P geometry and in the ^{1}H NMR the *H*C=N resonance was also a singlet. It has been argued that in such compounds some interaction between the nitrogen and palladium atoms may exist (*vide infra*, structure of **12**); nevertheless, absence of any ^{4}J(PH) coupling seems to preclude this possibility. This coincides with the angle between the metallated phenyl ring plane and the palladium coordination plane close to 90° and may be tentatively taken as an extension of the Karplus correlation relative to the influence of the dihedral angle on the coupling constant. [39] Yet, the phosphorus NMR indicates the phosphine phenyl rings still exert some shielding influence on the phenyl protons, their resonances and that of the C(4)-methoxy group being high-field shifted.

Crystal structure of 9

Satisfactory crystals of **9** were obtained by recrystallization from a dichloromethane-hexane solution. The structure of **9** is given in **Figure 3** inclusive of the caption containing selected interatomic distances and angles. The molecule is a centrosymmetric dinuclear complex, incorporating two square-planar palladium(II) atoms related by an inversion center, both being linked to a bromide ligand, a bidentate N-(2,4-dimethoxybenzylidene)-3,5-dichloroaniline-*C,N* (C *trans* to bromide), and finally a centrosymmetric *trans*-1,2-bis(diphenylphosphino)ethene which bridges the two palladium centers; thus, the asymmetric unit consists of half of the molecule of **9**. The observed bond dsistances and angles are within the predicted values (*vide supra*), displaying somewhat larger values for the elongated Pd-Br and Pd-N bond distances caused by the *trans* influence of the phenyl carbon and phosphorus atoms, respectively.

Unlike the previous structures the phenyl ring on nitrogen is quite tilted away from the metallacycle plane with an angle between the [Pd(1)C(1)C(6)C(7)N(1)] and [C(8)C(9)C(10)C(11)C(12)C(13)] planes of 73.58°; *cf.* complexes **2** and **3** where the analogous angles are at 40.90 and 56.51°, respectively. Treatment of **4** and **5** with diphosphines in 1:1 ratio and NH_4PF_6 gave complexes where the two phosphorus donors were linked by a carbon chain, as opposed to the monophosphine situation in compound **12**, with removal of the halide-ligand from the palladium coordination sphere, but preserving the metallacycle ring, yielding 1:1 electrolytes; therefore, only compounds **16-19** are obtained regardless of the starting dinuclear compound. The corresponding metallacycle ring has a varied number of links depending on the number of carbons joining the phosphorus atoms. The H5 resonance in the ^{1}H NMR was a *ddd* coupled to H3 and to the two phosphorus nuclei with ^{4}J(HP_B), *pseudo-trans*, greater than ^{4}J(HP_A), *pseudo-cis*. The phosphorus nuclei resonances were doublets; the higher field doublet was ascribed to the nucleus *trans* to the aryl carbon, P_B, whilst the lower field one to the nucleus *trans* to the imine nitrogen, P_A.

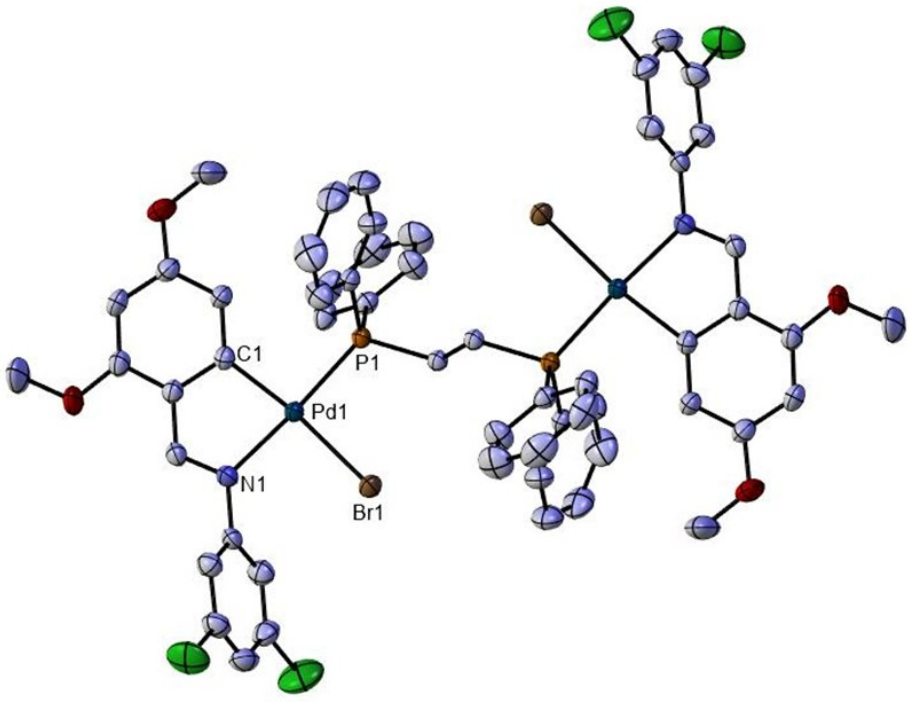

Figure 3 | ORTEP drawing of compound **9** with thermal ellipsoid plot shown at 50 % probability level. Hydrogen atoms and solvent molecules have been omitted for clarity. Selected bond lengths (Å) and angles (°): C(1)-Pd(1) 2.025(3); N(1)-Pd(1) 2.097(3); Br(1)-Pd(1) 2.5074(9); P(1)-Pd(1) 2.2553(10). C(1)-Pd(1) 2.025(3); N(1)-Pd(1) 2.097(3); Br(1)-Pd(1) 2.5074(9); Pd(1)-P(1) 2.2553(10). C(1)-Pd(1)-N(1) 80.99(12); C(1)-Pd(1)-P(1) 93.88(10); N(1)-Pd(1)-Br(1) 92.63 (8); P(1)-Pd(1)-Br(1) 92.94(3); N(1)-Pd(1)-P(1) 172.43(8); C(1)-Pd(1)-Br(1) 171.91(10).

This is inferred on the premise that a ligand of greater *trans* influence shifts the phosphorus resonance trans to itself to higher field. [40-42] Coupling of the imine resonance to phosphorus was detected in all cases, albeit only for **16** and **17** could coupling to both ^{31}P nuclei be disclosed. The PCH=CHP proton resonances could not be clearly assigned (compound **19**); we suggest they were shifted to lower field due to shielding of the phosphine phenyls and hence occluded by them.

Structure of complex 12

Proper crystals of **12** were obtained by recrystallization from a dichloromethane-*n*-hexane solution. The structure of **12** is given in **Figure 4** together with selected interatomic distances and angles. The crystal structure consists of discrete molecules. The palladium atom is in a square-planar environment bonded to the aryl carbon, the bromide and the two phosphorus atoms. The angles between adjacent atoms in the coordination sphere lie in the range 86.35(8)º [C(1)-Pd(1)-P(1)] to 95.24(2)º [P(2)-Pd(1)-Br(2)]. The distances at palladium are similar to previous reported values (*vide supra*). The dihedral angles between the metalated ring and the coordination and aniline ring plane are 85.05° and 44.93°, respectively. Pd(II) complexes, with trimethyl-, triethyl-, and triphenylphosphine, as well as with bis(diphenylphosphino)methane (dppm), showing Pd···N weak interactions in the range 2.576(4)-2.805(5) have been reported suggesting five-coordinate complexes; [43,44] and we have shown even shorter distances of 2.359 Å and 2.338 Å for complexes with $(Ph_2PCH_2CH_2)_2PPh$ (triphos), the latter being the shortest one reported to date. [45] In the present case the Pd-N distance, 2.785 Å, certainly precludes any covalent interaction, albeit given the palladium van der Waals radius of 1.61 Å (*vide supra*) some interaction may be predicted pointing towards an occupied apical site of the square planar palladium coordination plane by the imine nitrogen atom.

4. Conclusions

In this work, we have shown that the reaction of a particular Schiff base with palladium acetate produces a dinuclear palladium complex with bridging acetate ligands; these may be easily replaced by a diphosphine or halide ions. In the first case, compounds with mixed bridging ligands are produced, and in the second, the corresponding metathesis reaction gives rise to the ensuing dinuclear complexes with bridging chloride or bromide ligands. The latter are excellent starting reagents for treatment with nucleophiles, such as tertiary phosphines literally giving rise to a huge score of derivatives, some of which are presented here. Thus, depending on the number of phosphorus donor atoms, dinuclear and mononuclear

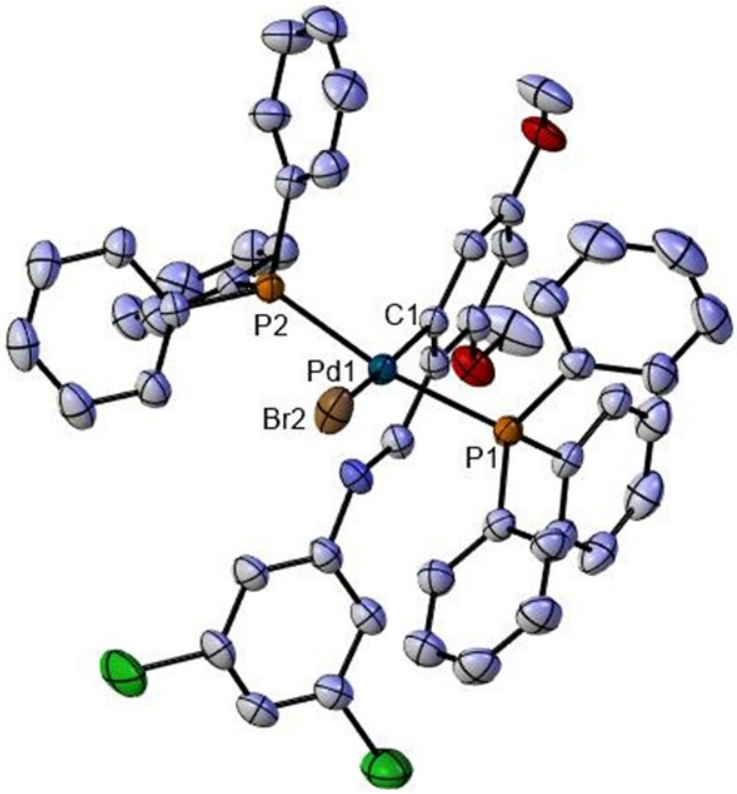

Figure 4 | ORTEP drawing of compound **12** with thermal ellipsoid plot shown at 50 % probability level. Hydrogen atoms and solvent molecules have been omitted for clarity. Selected bond lengths (Å) and angles (°): C(1)-Pd(1) 1.996(3); Br(2)-Pd(1) 2.5131(4); P(1)-Pd(1) 2.3353(7); P(2)-Pd(1) 2.3464(7). C(1)-Pd(1)-P(1) 86.35(8); C(1)-Pd(1)-P(2) 86.54(8); P(1)-Pd(1)-P(2) 170.17(3); C(1)-Pd(1)-Br(2) 169.30(9); P(1)-Pd(1)-Br(2) 90.53(2); P(2)-Pd(1)-Br(2) 95.24(2).

complexes can be obtained. In the former case, the metal centers are joined by a) two distinct bridging ligands, diphosphine and halide; b) two identical halide ions; c) only one bridging diphosphine. In the latter case the metal is bonded, a) to one phosphorus donor and a terminal halide; b) to two phosphines, inducing cleavage of the Pd-N and thus losing its palladacycle character; c) to a chelating diphosphine and absence of the halide ion. Four crystal structures have been described, that for compound **3** being the first crystal and molecular structure depicting a dinuclear palladacycle with mixed diphosphine and acetate linkers, whose arrangement seems to resemble that of the parent compound **2**; notwithstanding, the orientation of the metallated ligands adopt a *cisoid* geometry, as opposed to the *transoid* fashion in the structure of **2**.

Supplementary Materials

ACESION Codes: CCDC 2529548 (**2**), CCDC 2529549 (**3**), CCDC 25295550 (**9**), and CCDC 2530054 (**12**), contain the supplementary crystallographic data for this paper. These data can be obtained free of charge via www.ccdc.cam.ac.uk/data_request/cif, or by emailing data_ request@ccdc.cam.ac.uk, or by contacting The Cambridge Crystallographic Data Centre, 12 Union Road, Cambridge CB2 1EZ, UK; fax: +44 1223 336033.

Author Contributions

Conceptualization, J.M.V. and J.M.O.; methodology, J.M.O.; software, F.L.M.; validation, J.M.V., J.M.O. and M.D.; formal analysis, J.M.O.; investigation J.M.V. and J.M.O.; resources, J.M.O.; data curation, F.L.M. and M.D.; writing—original draft preparation, J.M.V. and J.M.O.; writing—review and editing, J.M.V.; visualization, J.M.V., J.M.O. and F.L.M.; supervision, J.M.V. and M.D.; project administration, J.M.O.; funding acquisition, J.M.O. All authors have read and agreed to the published version of the manuscript.

Conflict of Interests

The authors declare no conflict of interest.

References

[1] A. C. Cope and R. W. Siekman, J. Am. Chem. Soc., 1965, **87**, 3272–3273.

[2] M. Albrecht, Chem. Rev., 2010, **110**, 576–623.

[3] I. Omae, Cyclometallation reactions, 2014.

[4] J. M. Pereira, M.T.; Vila, in Palladacycles. Synthesis, Characterization and Applications, ed. M. Dupont, J; Pfeffer, Wiley-VCH, 2008, pp. 87–108.

[5] P. S. Zhou, K. M. Sanders, I. A. Guzei, D. G. Musaev and S. S. Stahl, J. Am. Chem. Soc., 2025, **147**, 26091–26096.

[6] M. T. Chicote, D. Bautista, J. Vicente and I. Saura-Llamas, Eur. J. Inorg. Chem., DOI:10.1002/ejic.202400719.

[7] M. Marcos, Metallomesogens. Synthesis, Properties and Applications ed. Serrano, J.L., 1996.

[8] A. Ionescu, N. Godbert, A. Crispini, R. Termine, A. Golemme and M. Ghedini, J. Mater. Chem., 2012, **22**, 23617–23626.

[9] M. V. Kashina, K. V. Luzyanin, D. V. Dar'in, S. I. Bezzubov and M. A. Kinzhalov, Inorg. Chem., 2024, **63**, 5315–5319.

[10] M. Sun, H. Yu, K. Zhang, S. Wang, T. Hayat, A. Alsaedi and D. Huang, ACS Sensors, 2018, **3**, 285–289.

[11] D. Dalmau, O. Crespo, J. M. Matxain and E. P. Urriolabeitia, Inorg. Chem., 2023, **62**, 9792–9806.

[12] M. S. Lowry and S. Bernhard, Chem. - A Eur. J., 2006, **12**, 7970 –7977.

[13] J. Albert, R. Bosque, M. Cadena, L. D'Andrea, J. Granell, A. González, J. Quirante, C. Calvis, R. Messeguer, J. Badía, L. Baldomà, T. Calvet and M. Font-Bardia, Organometallics, 2014, **33**, 2862–2873.

[14] M. Clemente, I. H. Polat, J. Albert, R. Bosque, M. Crespo, J. Granell, C. López, M. Martínez, J. Quirante, R. Messeguer, C. Calvis, J. Badía, L. Baldomà, M. Font-Bardia and M. Cascante, Organometallics, 2018, **37**, 3502–3514.

[15] N. Cutillas, G. S. Yellol, C. De Haro, C. Vicente, V. Rodríguez and J. Ruiz, Coord. Chem. Rev., 2013, **257**, 2784–2797.

[16] C. Navarro-Ranninger, I. López-Solera, V. M. González, J. M. Pérez, A. Alvarez-Valdés, A. Martín, P. R. Raithby, J. R. Masaguer and C. Alonso, Inorg. Chem., 1996, **35**, 5181–5187.

[17] F. Reigosa-Chamorro, L. R. Raposo, P. Munín-Cruz, M. T. Pereira, C. Roma-Rodrigues, P. V. Baptista, A. R. Fernandes and J. M. Vila, Inorg. Chem., 2021, **60**, 3939–3951.

[18] J. Dupont, M. Pfeffer and J. Spencer, Eur. J. Inorg. Chem., 2001, 1917–1927.

[19] R. B. Bedford, 2003, 1787–1796.

[20] M. B. and H. F. W. A. Herrmann, C. Brossmer, K. Öfele, C.-P. Reisinger, T. Priermeier, Angew. Chemie Int. Ed. English, 1995, **34**, 1844.

[21] C. Beller, M.; Fischer, H.; Herrmann, W. A.; Öfele, K.; Brossmer, Angew. Chemie Int. Ed. English, 1995, **34**, 1848–1849.

[22] K. Wang, R. Fan, X. Wei and W. Fang, Green Synth. Catal., 2022, **3**, 327–338.

[23] I. P. Beletskaya and A. V. Cheprakov, J. Organomet. Chem., 2004, **689**, 4055–4082.

[24] N. M. and A. Suzuki, Chem. Commun., 1979, 866.

[25] A. Suzuki, Chem. Commun., 2005, 4759.

[26] K. Karami, M. Ghasemi and N. H. Naeini, Tetrahedron Lett., 2013, **54**, 1352–1355.

[27] I. P. Beletskaya and A. V. Cheprakov, Chem. Rev., 2000, **100**, 3009–3066.

[28] J. Tsuji, Palladium Reagents and Catalysts, Chichester, 2004, vol. 9.

[29] F. Reigosa, P. M. Polo, M. T. Pereira and J. M. Vila, Dalt. Trans., 2024, **53**, 9680–9691.

[30] R. J. Allenbaugh, T. M. Ariagno and J. Selby, RSC Mechanochemistry, 2025, **2**, 30–36.

[31] J. Blanco, E. Gayoso, J. M. Vila and M. Gayoso, 1993, 906–910.

[32] H. Onoue, I. Moritani, J. Organomet. Chem., 1972, **43**, 431.

[33] I. V. B. Y.A. Ustinyuk, V.A. Chertov, J. Organomet. Chem., 1971, **29**, C53.

[34] K. Nakamoto, Infrared Raman Spectra Inorg. Coord. Compd. 5th ed., Wiley, New York.

[35] C. Navarro-Ranninger, F. Zamora, I. López-Solera, A. Monge and J. R. Masaguer, J. Organomet. Chem., 1996, **506**, 149–154.

[36] M. R. Churchill, Perspectives in Structural Chemistry, 1970, vol. 3.

[37] L. Pauling, The Nature of the Chemical Bond, Cornell University Press, Ithaca, New York, 3rd edn., 1960.

[38] W. J. Geary, Coord. Chem. Rev., 1971, **7**, 81–122.

[39] M. Karplus, JACS, 1963, **85**, 2870–2871.

[40] P. S. P. and R. W. Kunz, 31P 13C NMR ofTransition Met. Phosphine Complexes, NMR 16 (Edited by P. Diehl, E. Fluck R. Kosfeld). Springer, Berlín.

[41] J. Vicente, A. Areas, D. Bautista and P. G. Jones, Organometallics, 1997, **16**, 2127–2138.

[42] J. R. Berenguer, J. Forniés, E. Lalinde and F. Martínez, Organometallics, 1996, **15**, 4537–4546.

[43] J. M. Vila, M. T. Pereira, J. M. Ortigueira, J. J. Fernández, A. Fernández, M. López-Torres and H. Adams, Organometallics, 1999, **18**, 5484–5487.

[44] J.Granell, D. Sainz, J. Sales, X. Solans and M. Font-altaba, J. Chem.Soc. Dalton Trans., 1986, 1785–1790.

[45] M. López-Torres, A. Fernández, J. J. Fernández, A. Suárez, M. T. Pereira, J. M. Ortigueira, J. M. Vila and H. Adams, Inorg. Chem., 2001, **40**, 4583–4587.

TRANSLATIONAL CHEMISTRY
AN INTERFACE JOURNAL
HTTPS://WWW.TRANSLATIONALCHEMISTRY.COM/

ORIGINAL ARTICLE | DOI: 10.5584/translationalchemistry.v2i1.256

Determination of four regulated PFASs in drinking water by UHPLC-MS/MS with direct injection: development and validation of a rapid, green analytical procedure

Riccardo Comazzi [1,2,3,#], Michele Protti [4,#], Nicole Canfora [2], Roberto Mandrioli [3,*], Francesco Stante [2], Laura Mercolini [4]

[1]Department for Life Quality Studies (QuVi), Alma Mater Studiorum – University of Bologna, Corso d'Augusto 237, 47921 Rimini (Italy). [2] Laboratori Chimici Stante, Via del Chiù 68-70, 40133 Bologna (Italy). [3] Research Group of Advanced Pharmaceutical Analysis (APA Lab), Department of Pharmacy and Biotechnology (FaBiT), Alma Mater Studiorum – University of Bologna, Corso d'Augusto 237, 47921 Rimini (Italy). [4] Research Group of Pharmaco-Toxicological Analysis (PTA Lab), Department of Pharmacy and Biotechnology (FaBiT), Alma Mater Studiorum – University of Bologna, Via Belmeloro 6, 40126 Bologna (Italy).

Received: June 2026 **Accepted:** June 2026 **Available Online**: June 2026

Abstract

Per- and poly-fluoroalkyl substances (PFAS) are currently being widely used in various industrial applications; however, they represent an environmental and human health concern due to their persistence and bioaccumulation properties. This situation has stimulated the drafting of a European Directive (2020/2184), which regulates PFAS in drinking water. The regulation includes four PFAS of particular concern, whose concentrations must not exceed 20 ng/L as a sum: perfluorooctanoic acid (PFOA), perfluorooctanesulphonic acid (PFOS), perfluorononanoic acid (PFNA) and perfluorohexanesulphonic acid (PFHxS). Aim of this study was to develop and validate an original rapid and sensitive method, without any sample preparation and pre-concentration step, for monitoring the four target analytes in drinking water matrices by UHPLC-MS/MS. Water samples were just diluted 1:1 (*v/v*) with methanol, filtered and directly injected into the analytical system. The method was validated in real drinking water over 0.5-600 ng/L concentration range. Results showed good linearity for all the target analytes ($R^2 > 0.9950$). Accuracy, expressed as recovery and evaluated at three concentration levels, ranged within 96.9-114 % with RSD < 12.9 %. Despite the direct injection, good method detection limits (MDL) were achieved: 0.19 ng/L < MDL < 0.28 ng/L and lower limit of quantification was 0.5 ng/L for all analytes. The validated method was applied to 12 real drinking water samples from North – East Italy. PFOA, PFOS and PFHxS were detected in some samples, while PFNA was never detected. The sum of the four PFAS' concentrations was below the regulatory threshold of 20 ng/L in all samples.

Keywords: direct injection, drinking water, green analytical chemistry, PFAS, UHPLC-MS/MS.

1. Introduction

Per- and polyfluoroalkyl substances (PFAS) constitute a large family of synthetic fluorinated compounds that have been widely employed since the 1950s in industrial processes and consumer products due to their exceptional thermal stability, chemical resistance, and surface-active properties. The extremely stable perfluorinated carbon chain confers to these molecules unprecedented persistence in environmental matrices and in biological systems, leading to the common designation 'forever chemicals' [1]. The environmental persistence of PFAS is accompanied by documented toxicological properties. Several studies have associated chronic exposure to PFAS, particularly long-chained ones, with a range of adverse health outcomes, including hepatotoxicity, thyroid hormone disruption, reproductive toxicity, and increased risk of cancer occurrence [2]. The International Agency for Research on Cancer (IARC) classified perfluorooctanoic acid (PFOA) as carcinogenic to humans (Group 1). Perfluorooctanesulphonic acid (PFOS) has similarly been recognised as a persistent organic pollutant (POP) of global concern and a probable carcinogen for humans (IARC's Group 2) [3]. Both PFOA and PFOS exhibit pronounced bioaccumulation along the food chain and have been detected in human serum, breast milk, liver and kidney tissue across all continents [4-7]. International regulations initially focused on the most extensively studied PFAS. The progressive phase-out of these substances, however, has prompted the widespread industrial adoption of substitute or structurally alternative PFAS, a phenomenon commonly referred to as 'regrettable substitution'. Emerging PFAS such as

***Corresponding author:** Roberto Mandrioli, roberto.mandrioli@unibo.it

perfluorononanoic acid (PFNA) and perfluorohexanesulphonic acid (PFHxS) are now routinely detected in environmental and biological matrices and also display substantial toxicity profiles [8-11]. Among various pathways of human exposure to PFAS, drinking water represents one of the most significant and direct ones, particularly in areas where groundwater or surface water sources have been impacted by industrial discharges or contaminated groundwater. PFAS detection has been reported in water matrices worldwide, including the Arctic [12], ranging from sub-ng/mL to several hundreds of ng/mL in impacted regions [13]. The persistence and mobility of PFAS in aquatic environments, combined with their limited removal by conventional drinking water treatment technologies such as sedimentation and chlorination, render the contamination of finished drinking water a persistent regulatory and public health challenge. Advanced treatment processes, including activated carbon adsorption and nanofiltration or reverse osmosis, can achieve significant PFAS removal [14]. In response to growing evidence of PFAS occurrence in drinking water and their associated health risks, the European Union adopted Directive 2020/2184 [15], which for the first time introduced parametric values for PFAS in drinking water at the European level. The Directive establishes a limit of 100 ng/L for the sum of 20 priority PFAS and a more stringent limit of 20 ng/L for the sum of four substances of particular concern (PFOA, PFOS, PFNA and PFHxS) selected on the basis of their hazard profiles and frequency of detection. The Italian Legislative Decree no. 102/2025, which implements this Directive into national law, reproduces these parametric values. The analytical determination of PFAS in water matrices at the low concentrations required by current and forthcoming regulations poses significant challenges. Reference methods, including EPA Method 537.1 and the European standard UNI EN 17892, typically rely on solid-phase extraction (SPE) using weak anion-exchange (WAX) cartridges followed by liquid chromatography – tandem mass spectrometry (LC-MS/MS) in multiple reaction monitoring (MRM) mode [16-17]. SPE provides high pre-concentration factors and improved limits of quantification (LOQ), but it is often time-consuming, requires large volumes of organic solvents and reagents, and introduces risks of analyte loss, cross-contamination and batch-to-batch variability. In addition, the increasing number of samples required for routine monitoring under the new regulatory schemes calls for high-throughput analytical approaches that minimise labour and solvent consumption while maintaining adequate sensitivity and reliability. Direct injection of filtered water samples into ultra-high performance liquid chromatography coupled to triple-quadrupole tandem mass spectrometry (UHPLC-MS/MS) has been proposed as an alternative to SPE-based workflows for PFAS analysis in water. Direct injection eliminates the SPE step, offering reduced sample preparation time and lower solvent consumption and possibility of contamination, as well as enabling a more sustainable analytical workflow, aligned with the 12 principles of green analytical chemistry (GAC) [18]. However, the number of peer-reviewed studies applying direct injection to PFAS analysis in drinking water remains limited, and the methods reported to date have generally achieved limits of quantification (LOQ) in the range of 10–100 ng/L [19,20] for individual PFAS; these values, while adequate for less stringent regulatory contexts, are insufficient to ensure reliable compliance monitoring against the limit of 20 ng/L imposed by D.Lgs. 102/2025 as the sum of four PFAS, which in turn requires individual LOQs well below 5 ng/L. Furthermore, existing direct injection methods have typically targeted a restricted panel of predominantly long-chain PFAS, without coverage of all the analytes included in the regulatory 'sum of PFAS' parameter, which under D.Lgs. 102/2025 now encompasses a list of approximately 30 compounds subject to a collective limit of 100 ng/L. The development of sensitive, validated direct injection methods capable of simultaneously determining the four priority PFAS, and designed with a view to future extension to the full suite of approximately 30 regulated compounds, therefore represents a pressing analytical need. The present study addresses this gap by developing and validating a rapid, green and reliable UHPLC-MS/MS (QqQ) method for the simultaneous determination of four PFAS explicitly cited in D. Lgs. 102/2025 (PFOA, PFOS, PFNA and PFHxS) in drinking water by direct injection without any pre-treatment other than filtration and dilution. The method is designed to meet the sensitivity requirements for monitoring compliance with the regulatory threshold (20 ng/L as sum). The analytical approach is furthermore conceived as a scalable platform for future extension to the complete panel of approximately 30 PFAS subject to the 100 ng/L collective limit [21], supporting the transition towards comprehensive, high-throughput routine monitoring of drinking water quality in Italy. We report a full validation according to current analytical guidelines [22], including linearity, method detection limits (MDL) and lower limits of quantification, accuracy, precision, recoveries, and we present the application of the method to a set of real drinking water samples collected from drinking treatment plants in North-East Italy.

2. Materials and Methods

2.1. Reagent and standards

Ultrapure water was obtained from a Milli-Q International 10 system (Millipore, Bedford, MA, USA) and used for all solutions. Acetonitrile (ACN) and methanol (MeOH) of MS grade and ammonium formate (NH_4CHOO) and formic acid (FA) of analytical grade were purchased from Merck Sigma-Aldrich (Milan, Italy). Drinking water matrix for calibration was purchased from a commercial brand. Individual standard solutions of PFOA, PFOS, PFNA and PFHxS (≥ 98% purity) and isotopically labelled internal standards of ^{13}C8-PFOA, ^{13}C8-PFOS, ^{13}C9-PFNA and ^{13}C3-PFHxS (≥ 98% atom purity) were purchased from Wellington Laboratories (Guelph, ON, Canada) as 100 µg/mL solutions in methanol. A stock solution containing all analytes at 2 µg/mL was prepared by dilution of the individual standard solutions. Three working standard solutions containing all analytes at 20 µg/L, 1 µg/L and 100 ng/L were prepared in methanol by appropriate dilution of the stock solutions and stored at −20°C. A working internal standard solution containing ^{13}C8-PFOA, ^{13}C8-PFOS, ^{13}C9-PFNA and ^{13}C3-PFHxS at 20 ng/L each was prepared in methanol and used for spiking all samples and calibration solutions.

2.2. Instrumentation and chromatographic conditions

Chromatographic separation was performed using a 1290 Infinity III UHPLC system coupled to a 6495D triple quadrupole mass spectrometer equipped with an electrospray ionisation (ESI) source (both from Agilent, Santa Clara, CA, USA). An Ultra Inert IBD column (2.1 × 100 mm, 3 µm; Restek, Bellefonte, PA, USA) was used for all analyses. The column temperature was maintained at 40 °C. The injection volume was 45 µL for all samples. Mobile phase A consisted of water containing 5 mM ammonium formate (0.1% formic acid), and mobile phase B consisted of acetonitrile. The gradient program was as follows: 0.0 min, 50% B; 0.1-7.0 min, linear increase from 50% to 95% B; 7.0-13.0 min, hold at 95% B; 13.1-13.2 min, decrease from 95% to 50% B; 13.2-18.0 min, hold at 50% B for column re-equilibration. The total run time was 18.0 min and the flow rate was 0.4 mL/min. The instrument setup incorporates a delay column (identical to the main analytical column) between pumps and autosampler to mitigate interference from mobile phase or instrument components. Mass spectrometry was performed in negative ESI mode with the following source parameters: capillary voltage 3.5 kV, source temperature 150 °C, desolvation temperature 180 °C, desolvation gas flow 14 L/min, cone gas flow 11 L/min. Argon was used as collision gas at a pressure of 4.5×10^{-3} mbar in the collision cell. Analytes were quantified using dynamic multiple reaction monitoring (dMRM) of the most intense precursor-product ion transitions. The MRM transitions, collision energy (CE), iFunnel settings and retention times (RT) for all analytes and internal standards are listed in **Table 1**.

Table 1 | Multiple reaction monitoring (MRM) transitions and mass spectrometric parameters for PFHxS, PFOA, PFOS, PFNA and the respective ISs.

Analyte	Molecular formula	Precursor (m/z)	Product [1] (m/z)	CE [1] (eV)	Product [2] (m/z)	CE [2] (eV)	R_t (min)	iFunnel	Polarity
PFHxS	$C_6HF_{13}SO_3$	399	80	48	99	39	4.9	Standard	Negative
PFOA	$C_8HF_{15}O_2$	413	369	6	169	19	5.6	Fragile	Negative
PFOS	$C_8HF_{17}SO_3$	499	99	48	80	52	6.2	Large Molecule	Negative
PFNA	$C_9HF_{17}O_2$	463	419	10	219	16	6.5	Standard	Negative
^{13}C3-PFHxS	$C_6HF_{13}SO_3$	402	80	40			4.9	Standard	Negative
^{13}C8-PFOA	$C_8HF_{15}O_2$	421	376	10			5.6	Fragile	Negative
^{13}C8-PFOS	$C_8HF_{17}SO_3$	507	80	40			6.2	Large Molecule	Negative
^{13}C9-PFNA	$C_9HF_{17}O_2$	472	427	10			6.5	Standard	Negative

[1] Quantifier; [2] Qualifier; CE = collision energy; R_t = retention time.

2.3. Sample collection and preparation

Drinking water samples were collected from 12 different sites of tap water located in North - East Italy, during the November 2025 - January 2026 period. Sampling was performed in pre-cleaned 1 L HDPE bottles according to standard protocols. Samples were transported to the laboratory, stored at 4 °C and analysed within 7 days. Prior to injection, all samples were diluted 1:1 (*v/v*) with methanol and then filtered through 0.45 µm PP membrane filters (Merck Sigma-Aldrich) to remove particulate matter. Filtered samples were then transferred into 2 mL PP vials and spiked with the internal standard solution to give a final concentration of 200 ng/L for each internal standard. Method blank samples (in a 50:50 mixture Milli-Q water:methanol) were processed in the same way to assess background contamination.

2.4. Calibration and quality control

Matrix-matched calibration curves were prepared by spiking drinking water matrix (prepared as described in Section 2.1) with the working standard solution to obtain calibration levels at 0.5, 1, 1.5, 2, 5, 10, 25, 50, 100, 200, 400 and 600 ng/L for each of PFOA, PFOS, PFNA and PFHxS. All calibration solutions were spiked with the internal standard solution at the concentration of 200 ng/L. Calibration curves were set up by plotting the ratio of the analyte peak area to the internal standard peak area against the analyte concentration and fitting by weighted (1/x) linear least-squares regression. Quality control (QC) samples included: (i) method blank (Milli-Q water processed as the samples); (ii) spiked QC samples at low (0.5 ng/L), medium (5 ng/L) and high (400 ng/L) concentration levels for the analytes. QC samples were analysed at the beginning and end of each batch and at a rate of at least one QC *per* ten samples.

2.5. Method validation

Method validation was performed according to Environmental Protection Agency (EPA/537.1) [22] and European (UNI EN 17892) [23] guidelines. The following performance characteristics were evaluated.

- Linearity and calibration range: assessed by the correlation coefficient (R^2), the slope and intercept of the calibration curve, and the residual plot.
- Method detection limit (MDL) and lower limit of quantification (LLOQ): the MDL was estimated from replicate analyses (n = 12) of drinking water samples spiked at low concentration levels, according to the standard deviation approach. The LLOQ was defined as the lowest calibration level meeting predefined acceptance criteria for accuracy and precision [24].
- Accuracy (recovery): evaluated as the percentage of the spiked concentration recovered in spiked drinking water samples at three concentration levels (n = 5 *per* level).

- Precision: intra-day precision (repeatability) and inter-day precision (intermediate precision) expressed as relative standard deviation (RSD %) at the same three concentration levels (n = 5 *per* level, over 3 days).
- Matrix effects: evaluated by post-filtration spiking of authentic drinking water samples at 100 ng/L (n = 12). Since analytes were added directly to the filtered matrix immediately prior to injection, process-related losses were absent; the response of each analyte in the spiked matrix was compared to that obtained from a standard solution in pure solvent at the same nominal concentration, and the matrix effect was expressed as: ME (%) = [(area in matrix − area in solvent) / area in solvent] × 100. Positive and negative values indicate ion enhancement and ion suppression, respectively.

2.6. Data analysis

Chromatographic data were processed with Agilent MassHunter v12.1 software. Quantification was performed using the internal standard method. Statistical analysis was performed using Microsoft Excel 365. Plots were created using GraphPad Prism v 9.5.0.

3. Results and Discussion

3.1. Chromatographic separation and mass spectrometric detection

The selection of the chromatographic column and mobile phase composition was critical to achieve adequate separation of the four analytes within a short run time while maintaining high sensitivity in negative ESI mode. The Restek Ultra Inert column, characterised by a silica-based stationary phase functionalised with a polar (amide) group embedded within an alkyl chain, is specifically designed to minimise secondary interactions with active sites and enhance the formation of hydrogen bonds, optimising the separation of acidic compounds. It provided excellent peak shape and retention for both long-chain (PFOA, PFOS, PFNA) and short-chain (PFHxS) PFAS. All four analytes were well separated within 7 min, with retention times between 4.9 and 6.5 min (**Table 1**). PFHxS (C6 sulfonate), the shortest-chain compound, elutes first at 4.9 min, followed by PFOA (C8 carboxylate) at 5.6 min, PFOS (C8 sulfonate) at 6.2 min, and PFNA (C9 carboxylate) at 6.5 min (**Figure 1**). The MRM transitions were selected based on the most intense precursor-product ion pairs observed in full-scan MS experiments. The sulfonate PFAS (PFHxS, PFOS) showed the characteristic product ion at m/z 80.0 (SO_3^-). Despite the common product ion for the carboxylate series, adequate chromatographic separation prevented cross-talk. The use of isotopically labelled internal standards for all the target analytes compensated for variations in ionisation efficiency.

3.2. Linearity, LLOQ and MDL

Calibration curves for all analytes showed excellent linearity over the investigated concentration ranges. The correlation coefficients (R^2) were ≥ 0.995 for all analytes, and the residuals were randomly distributed around zero, indicating no systematic deviation from linearity (**Table 2**). The calibration model was forced through the origin, as blank samples showed no detectable contamination.

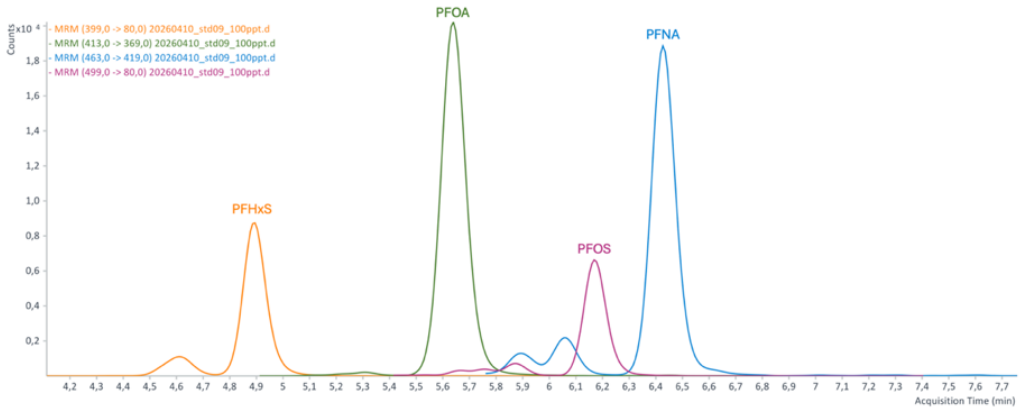

Figure 1 | Chromatographic peaks of four target analytes (PFHxS, PFOA, PFOS and PFNA).

Table 2 | Linearity, lower limits of quantification (LLOQ) and method detection limit (MDL) for PFHxS, PFOA, PFOS and PFNA in drinking water by direct injection UHPLC-MS/MS.

Analyte	Calibration range (ng/L)	R^2	LLOQ (ng/L)	MDL (ng/L)
PFHxS	0.5–600	0.9950	0.5	0.26
PFOA	0.5–600	0.9952	0.5	0.19
PFOS	0.5–600	0.9956	0.5	0.26
PFNA	0.5–600	0.9963	0.5	0.28

The weighted (1/x) regression improved the fit at low concentrations, which is critical for accurate quantification near the LLOQ. The method has shown excellent sensitivity, with MDLs ranging from 0.19 to 0.28 ng/L and LLOQ of 0.5 ng/L for all target compounds (**Table 2**). The LLOQ was established as the lowest calibration level. These values are well below the regulatory limits introduced by D. Lgs. 102/2025 for the sum of PFOA, PFOS, PFNA and PFHxS (20 ng/L) as well as for a presumptive single-compound limit of 5 ng/L, demonstrating that the method is suitable for drinking water compliance monitoring. The LLOQ for PFOA, PFOS, PFNA and PFHxS is also comparable to or better than those reported for SPE-based methods in wastewater, which typically range from 0.5 to 5 ng/L depending on the preconcentration factor [24-26].

3.3. Accuracy, precision and recovery

Accuracy was evaluated as the percentage recovery of spiked analytes in drinking water matrix at three concentration levels (low, medium and high). Recovery values obtained at the three spiking levels (1, 5 and 400 ng/L) ranged from 96.9 % to 114.0 % for all target PFAS, well within the accepted range of 70–130 % according to 2002/657/EC and demonstrating excellent method accuracy across the investigated concentration range. Most recoveries were close to 100 %, indicating negligible systematic bias. Slightly higher recoveries observed at the intermediate concentration level (up to 114.0 % for PFOS) remained within commonly accepted validation criteria, confirming the reliability of the method for quantitative determination of PFAS in water samples. The use of isotopically labelled internal standards improved recovery consistency. Intra-day precision (repeatability) was excellent for all analytes, with RSD values between 2 and 9 % at all concentration levels (**Table 3**). Inter-day precision (intermediate precision) was slightly higher but still within the acceptable limit of 20 %, with RSD values between 4 and 13 %. The highest RSD values were observed for PFNA at the low level (12.8 %).

3.4. Matrix effects

Matrix effects were evaluated by post-filtration spiking of authentic drinking water samples and comparing analyte response in pure solvent (methanol/water 1:1). The results demonstrate negligible to minor matrix effect: ion enhancement for PFOA (+4.80 %), minor ion suppression for PFHxS and PFOS (-6.85 % and -5.09 %, respectively) and negligible effect for PFNA (+1.04 %): see **Figure 2**.

Table 3 | Accuracy (recovery), intra-day precision (repeatability) and inter-day precision (intermediate precision) for the four analytes in drinking water at three concentration levels (n = 5 per level).

Analyte	Level (ng/L)	Recovery (%)	Intra-day RSD (%)*	Inter-day RSD (%)*
PFHxS	1	100.7	5.2	7.7
PFHxS	5	108.6	2.8	8.8
PFHxS	400	96.9	4.0	5.9
PFNA	1	104.1	8.2	12.8
PFNA	5	101.0	3.2	4.6
PFNA	400	104.0	3.8	4.6
PFOA	1	102.1	2.0	6.8
PFOA	5	110.0	3.5	7.2
PFOA	400	102.7	2.2	5.5
PFOS	1	100.3	3.7	8.4
PFOS	5	114.0	5.4	5.6
PFOS	400	100.7	3.3	5.9

*Intra-day precision was assessed on a single day (n = 5); inter-day precision was assessed over 3 days (n = 5 per day).

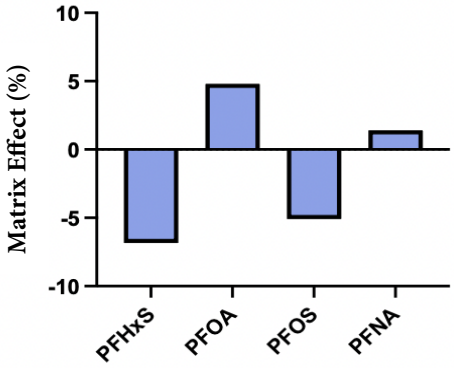

Figure 2 | Matrix effects for the four analytes in drinking water, expressed as percentage ion suppression/enhancement compared to pure solvent.
Note: Matrix effect (%) = [(area in matrix − area in solvent) / area in solvent] × 100. Negative values indicate ion suppression; positive values indicate ion enhancement.

These values are well within the ±20 % acceptance criterion adopted in method validation for environmental water analysis, indicating that the drinking water matrix does not significantly alter the ionisation of the target analytes under the developed UHPLC-MS/MS conditions. The low matrix effects observed are consistent with the use of direct injection of a relatively clean matrix such as drinking water, which contains substantially lower concentrations of co-eluting organic interferents compared to surface water or wastewater matrices. The isotopically labelled internal standards employed (^{13}C8-PFOS, ^{13}C8-PFOA, ^{13}C9-PFNA, ^{13}C3-PFHxS) provided effective compensation for the residual matrix-induced signal variations.

3.5. Application to real drinking water samples

The validated method was applied to the analysis of 12 real drinking water samples collected from tap water sampling sites across North - East Italy. The concentration results are summarised in **Figure 3**. PFOA was the most frequent and most concentrated compound across all sampling sites, with concentrations ranging from 1.36 to 2.0 ng/L and was detected in 6 samples. PFHxS was detected in just 2 out of 12 samples with concentrations of 1.31 and 2.32 ng/L. PFOS was detected in just 1 sampling site, with a concentration of 1.41 ng/L. PFNA was not detected in any sample. In the remaining samples, concentrations were below the LLOQ. The sum of the four regulated PFAS (PFOA + PFOS + PFNA + PFHxS, hereafter PFAS-4 Sum) ranged from 1.36 to 5.73 ng/L across all sites: thus, importantly, all 12 samples displayed PFAS-4 Sum values well below the regulatory limit of 20 ng/L established by D.Lgs. 102/2025 for this parameter, indicating compliance of the monitored drinking water supply with the most stringent PFAS parametric value currently in force in Italy. These concentration levels are consistent with those reported in precedent surveys of PFAS in finished drinking water in northern Italy and other European countries [27]. However, it should be noted that the present method targets exclusively the four PFAS explicitly regulated under the sum-of-four parametric value (PFOA, PFOS, PFNA and PFHxS) and does not provide information on the broader suite of 30 PFAS subject to the collective limit of 100 ng/L under D.Lgs. 102/2025. While the samples analysed here appear compliant with respect to the most critical regulatory threshold, the contribution of the remaining regulated PFAS to the total PFAS burden cannot be assessed from the present dataset. This represents a methodological limitation of the current study, particularly in the context of routine compliance monitoring, where a comprehensive analytical panel covering all regulated compounds is ultimately required. The extension of the developed direct-injection UHPLC-MS/MS platform to the full panel of approximately 30 regulated PFAS represents a feasible next step. Given the sensitivity and throughput advantages demonstrated here, direct injection is a promising candidate approach for this comprehensive monitoring, provided that adequate LOQs (compatible with individual contributions to the 100 ng/L collective limit) can be achieved for all target analytes.

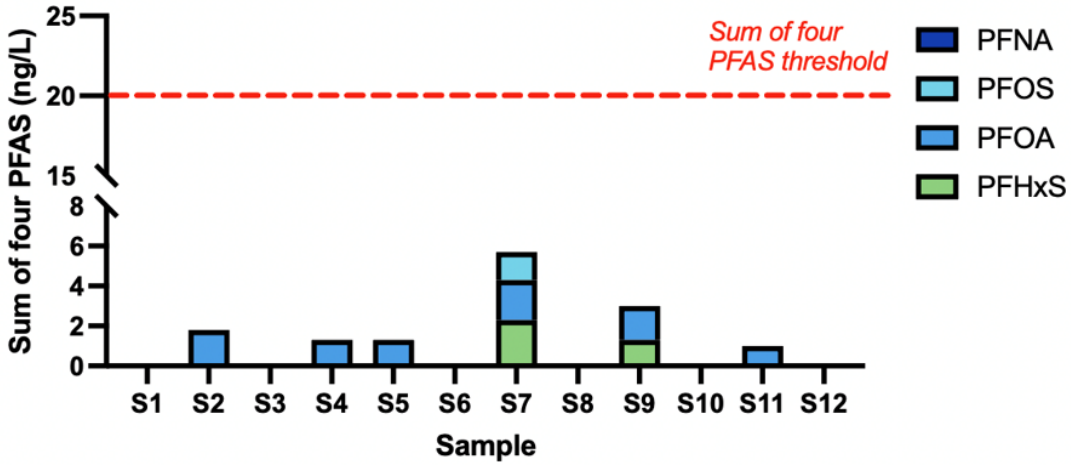

Figure 3 | Concentrations (ng/L) of the four analytes in 12 tap water sampling sites.

3.6. Comparison with SPE-based methods and green analytical chemistry

The method described, based on direct injection, offers different advantages over conventional SPE-based methods for PFAS analysis in drinking water. First, the sample preparation time is reduced from hours to less than 5 min *per* sample, enabling a much higher sample throughput (up to 50 samples *per* day on a single UHPLC-MS/MS system). Second, the method eliminates the use of SPE cartridges, large volumes of organic solvents or other related reagents (typically 10–20 mL *per* sample for SPE elution), reducing both cost and environmental impact of the analytical procedure. Third, the direct injection approach minimises the risk of analyte loss or contamination during sample preparation, which is particularly important for trace analysis of PFAS. In terms of green analytical chemistry, the method aligns with several of the 12 principles: (i) prevention of waste (no SPE waste and less sample waste); (ii) less hazardous chemicals used (only 2 mL of methanol *per* sample); (iii) design for energy efficiency (short run time and no SPE equipment); and (iv) increase in analytical throughput (fewer samples *per* time unit, reducing overall resource consumption). The total solvent consumption *per* sample is reduced from ~15 mL (SPE) to ~0.5 mL (UHPLC mobile phase only), corresponding to a more than 95 % reduction in solvent use. However, the direct injection method has some limitations compared to SPE. The main limi-

tation is the absence of preconcentration factor: SPE methods can achieve LOQ values in the sub-ng/L range (0.1 ng/L) in drinking water. Nevertheless, the LLOQs obtained in this study (0.5 ng/L for PFOA, PFOS, PFNA and PFHxS) are sufficiently low for monitoring compliance with the regulatory limits for drinking water in Italy and the EU, and are comparable to or better than those reported for other direct injection methods in drinking water [20,28,29].

4. Conclusions

A rapid, green and reliable UHPLC-MS/MS (QqQ) method for the simultaneous determination of PFHxS, PFOA, PFOS and PFNA in drinking water by direct injection without pre-concentration has been developed and fully validated. The method provides LLOQs of 0.5 ng/L for each one of the four target compounds. Accuracy (recovery 96-114 %) and precision (intra-day RSD 2.8-8.2 %, inter-day RSD 4.6-12.8 %) meet the requirements of international standard guidelines, and the limited matrix effects are well compensated by isotopically labelled internal standards. The validated method was applied to real samples from twelve drinking water sampling sites in North-East Italy. PFOA was the most frequently detected analyte, PFOS and PFHxS were detected in just a few samples, while PFNA was not detected in any of the analysed samples. The PFAS-4 Sum specifically regulated by the Italian decree did not exceed the limit of 20 ng/L in any of the tested samples. Nevertheless, the sporadic detection of PFOA, PFOS and PFHxS highlights the importance of continued monitoring of these compounds in drinking water, since they may contribute cumulatively to human exposure even at low level contamination. Furthermore, the present method addresses only four of the 30 PFAS compounds subject to regulatory limits under D.Lgs. 102/2025, leaving uncharacterised the potential contribution of the remaining compounds to the collective 100 ng/L threshold. The extension of the developed direct -injection UHPLC-MS/MS platform to the full panel of regulated PFAS therefore represents a priority for future work. The direct injection approach significantly reduces sample preparation time, solvent consumption and risk of contamination compared to SPE-based methods, making it a high-throughput, cost-effective and environmentally sustainable tool for routine monitoring of PFAS in drinking water. The method is suitable for compliance monitoring under D. Lgs. 102/2025 and can be readily adapted for the analysis of drinking water.

Acknowledgements

This research was supported by the National Recovery and Resilience Plan (PNRR), Mission 4, Component 2, Investment 3.3 (D.M. 630/2024) with European Union – NextGenerationEU funds.

References

[1] A. B. Lindstrom, M. J. Strynar, E. L. Libelo, Environ. Sci. Technol. 45 (2011) 7954–7961. DOI: 10.1021/es2011622.

[2] E. M. Sunderland, X. C. Hu, C. Dassuncao, A. K. Tokranov, C. C. Wagner, J. G. Allen, J. Expo. Sci. Environ. Epidemiol. 29 (2019) 131–147. DOI: 10.1038/s41370-018-0094-1.

[3] International Agency For Research On Cancer (IARC), Perfluorooctanoic Acid (PFOA) and Perfluorooctanesulfonic Acid (PFOS). Last accessed: June 24, 2026. Available from: https://publications.iarc.who.int/Book-And-Report-Series/Iarc-Monographs-On-The-Identification-Of-Carcinogenic-Hazards-To-Humans/Perfluorooctanoic-Acid-PFOA-And-Perfluorooctanesulfonic-Acid-PFOS--2025

[4] G. Zheng, E. Schreder, J.C. Dempsey, N. Uding, V. Chu, G. Andres, S. Sathyanarayana, A. Salamova, Environ. Sci. Technol. 55 (2021) 7510–7520. DOI: 10.1021/acs.est.0c06978.

[5] R. R. Worley, S. McAfee Moore, B.C. Tierney, X. Ye, A.M. Calafat, S. Campbell, M.B. Woudneh, J. Fisher, Environ. Int. 106 (2017) 135–143. DOI: 10.1016/j.envint.2017.06.007.

[6] B. C. Kelly, J. M. Sun, M. R. R. McDougall, E. M. Sunderland, F. A. P. C. Gobas, Environ. Sci. Technol. 58 (2024) 17828–17837. DOI: 10.1021/acs.est.4c02134.

[7] B. Khan, R. M. Burgess, M. G. Cantwell, ACS EST Water 3 (2023) 1243–1259. DOI: 10.1021/acsestwater.2c00296.

[8] E. Ivantsova, A. Sultan, C. J. Martyniuk, Toxics, 13 (2025) 436-439. DOI: 10.3390/toxics13060436.

[9] K. P. Das, B. E. Grey, M. B. Rosen, C. R. Wood, K. R. Tatum-Gibbs, R. Daniel Zehr, M. J. Strynar, A. B. Lindstrom, C. Lau, Reprod. Toxicol. 51 (2015) 133–144. DOI: 10.1016/j.reprotox.2014.12.012.

[10] W. Chen, S. Liu, Y. Zhou, B. Liu, W. Wang, C. Chen, Z. Lou, X. Li Shen, Food Chem. Toxicol. 204 (2025) 115657. DOI: 10.1016/j.fct.2025.115657.

[11] K. Schulz, M. R. Silva, R. Klaper, Sci. Total Environ. 733 (2020) 139186. DOI: 10.1016/j.scitotenv.2020.139186.

[12] R. Lohmann, K. Abass, E. C. Bonefeld-Jørgensen, R. Bossi, R. Dietz, S. Ferguson, K. J. Fernie, P. Grandjean, D. Herzke, M. Houde, M. Lemire, R. J. Letcher, D. Muir, A. O. De Silva, S. K. Ostertag, A. A. Rand, J. Søndergaard, C. Sonne, E. M. Sunderland, K. Vorkamp, S. Wilson, P. Weihe, Sci. Total Environ. 954 (2024) 176274. DOI: 10.1016/j.scitotenv.2024.176274.

[13] M. L. Brusseau, R. H. Anderson, B. Guo, Sci. Total Environ. 740 (2020) 140017. DOI: 10.1016/j.scitotenv.2020.140017.

[14]B. C. Crone, T. F. Speth, D. G. Wahman, S. J. Smith, G. Abulikemu, E. J. Kleiner, J. G. Pressman, Crit. Rev. Environ. Sci. Technol. 49 (2019) 2359–2396. DOI: 10.1080/10643389.2019.1614848.

[15] European Parliament and Council, Directive (EU) 2020/2184 of 16 December 2020 on the quality of water intended for human

consumption (recast). Last accessed: June 24, 2026. Available from: http://data.europa.eu/eli/dir/2020/2184/oj

[16] United States Environmental Protection Agency (EPA), Method 537.1: Determination of Selected Per- and Polyfluorinated Alkyl Substances in Drinking Water by Solid Phase Extraction and Liquid Chromatography/Tandem Mass Spectrometry (LC/MS/MS). Last accessed: June 24, 2026. Available from: https://cfpub.epa.gov/si/si_public_record_Report.cfm?LAB=NERL&dirEntryID=343042

[17] M. Mazzoni, M. Rusconi, S. Valsecchi, C. P. B. Martins, S. Polesello, J. Anal. Methods Chem. 1 (2015) 942016. DOI: 10.1155/2015/942016.

[18] A. Gałuszka, Z. Migaszewski, J. Namieśnik, TrAC, 50 (2013) 78-84. DOI: 10.1016/j.trac.2013.04.010.

[19] S. T. Wolf, W. K. Reagen, Anal. Methods 5 (2013) 2444–2454. DOI: 10.1039/C3AY26347A.

[20] M. A. Mottaleb, Q. X. Ding, K. G. Pennell, E. N. Haynes, A. J. Morris, J. Chromatogr. A 1653 (2021) 462426. DOI: 10.1016/j.chroma.2021.462426.

[21] Gazzetta Ufficiale Serie Generale n.153 del 04-07-2025, Suppl. Ordinario n. 24. Last accessed: June 24, 2026. Available from: https://www.gazzettaufficiale.it/eli/id/2025/07/04/25G00106/S

[22] J. Shoemaker, D. Tettenhorst, Method 537.1 Determination of Selected Per- and Polyflourinated Alkyl Substances in Drinking Water by Solid Phase Extraction and Liquid Chromatography/Tandem Mass Spectrometry (LC/MS/MS). U.S. Environmental Protection Agency, Washington, DC, 2020. Last accessed: June 24, 2026. Available from: https://cfpub.epa.gov/si/si_public_file_download.cfm?p_download_id=539984&Lab=CESER

[23] EN 17892:2024, Water quality - Determination of selected per- and polyfluoroalkyl substances in drinking water - Method using liquid chromatography/tandem-mass spectrometry (LC-MS/MS). Last accessed: June 24, 2026. Available from: https://cdn.standards.iteh.ai/samples/72997/b9aa7f9fa0004d269dad14f75b427cf0/SIST-EN-17892-2024.pdf

[24] United States Environmental Protection Agency (EPA), Appendix B to Part 136: Definition and Procedure for the Determination of the Method Detection Limit, Revision 2. Last accessed: June 24, 2026. Available from: https://www.ecfr.gov/current/title-40/appendix-Appendix%20B%20to%20Part%20136

[25] D. Timalsina, B. S. Ramisetty, M. Z. Wang, PLOS Water 5 (2026) e0000501. DOI: 10.1371/journal.pwat.0000501.

[26] B. Huerta, B. McHugh, F. Regan, Anal. Methods 14 (2022) 2090–2099. DOI: 10.1039/D2AY00300G.

[27] J. López-Vázquez, R. Montes, R. Rodil, R. Cela, J. A. Martínez-Pontevedra, M. T. Pena, J. Benito Quintana, Environ. Sci. Pollut. Res. (2024). DOI: 10.1007/s11356-024-34852-z.

[28] L. Ciofi, L. Renai, D. Rossini, C. Ancillotti, A. Falai, D. Fibbi, M. C. Bruzzoniti, J. J. Santana-Rodriguez, S. Orlandini, M. Del Bubba, Talanta 176 (2018) 412–421. DOI: 10.1016/j.talanta.2017.08.052.

[29] J. L. Gray, L. K. Kanagy, C. J. Kanagy, C. A. Anderson, U.S. Geological Survey Techniques and Methods, Book 5, Chapter B13, 121 pages. DOI: 10.3133/tm5B13.